UiT The Arctic University of Norway

Faculty of Health Sciences, Department of Medical Biology

Characterization of extracellular vesicles from U-2OS15E, a human osteosarcoma cell line persistently infected by BK polyomavirus

Aumkar Logendran

Master's thesis in Biomedicine (MBI-3911) May 2021

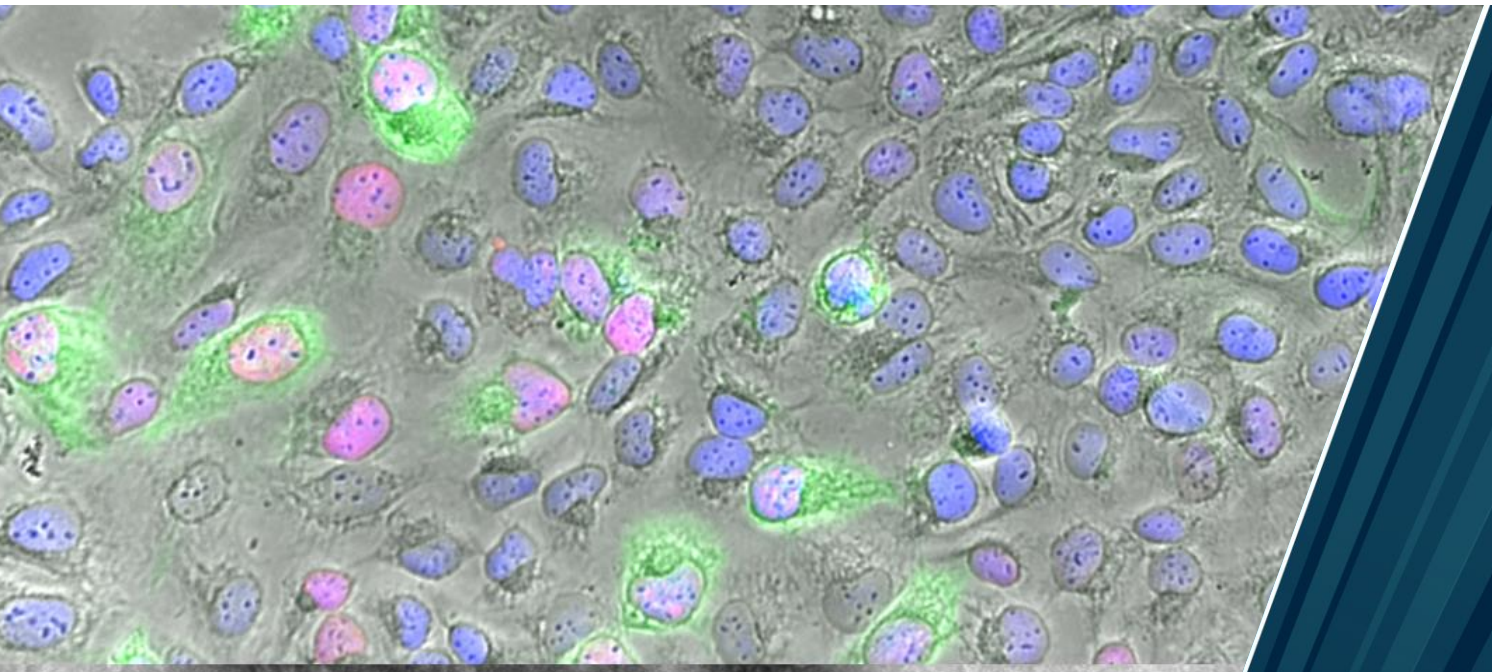

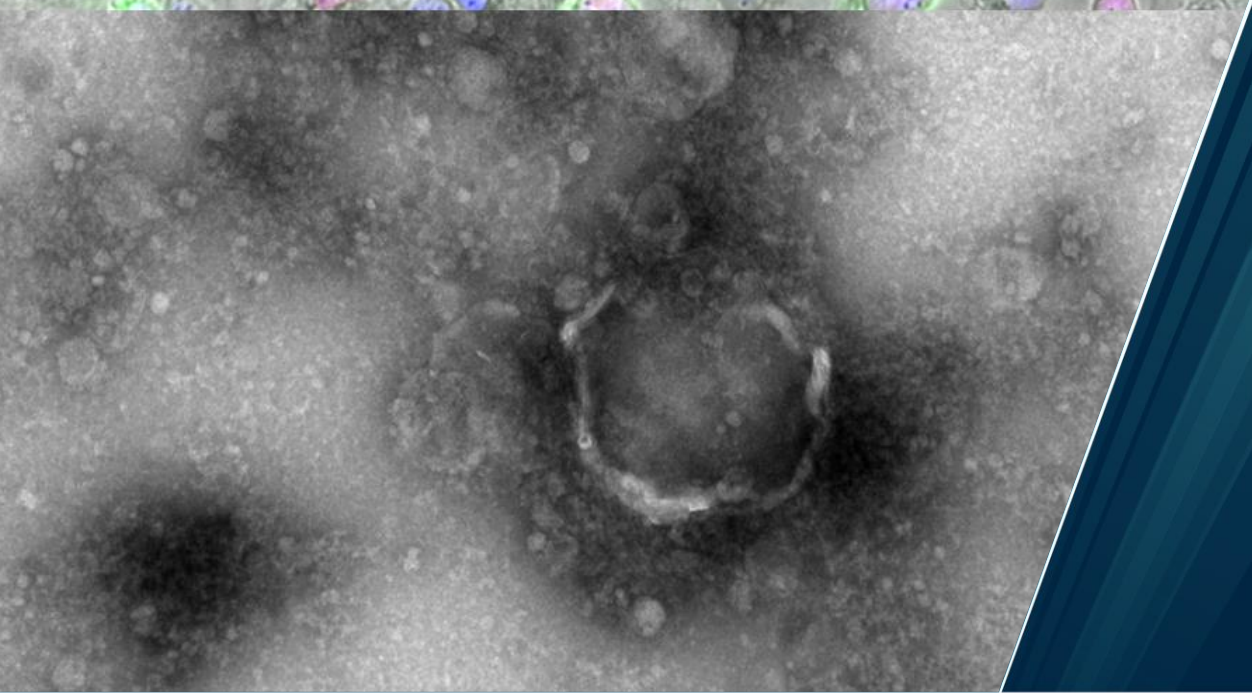

Cover image: immunofluorescence microscopy of U-2OS15E (upper), red and green colors are representing the BK viral proteins LTag and agnoprotein, respectively, and blue is nuclear DNA; negative stain transmission electron microscopy of EVs from U-2OS (lower).

Acknowledgements

The work presented in this thesis was completed at the Department of Microbiology and Infection Control at the University Hospital of Northern Norway from August 2020 to May 2021.

First of all, I want to express my utmost gratitude to my supervisor Professor Christine Hanssen Rinaldo for constant support and for being available to help me every day, including weekends and holidays. Your professional guidance and encouragement is the main reason that I could get through this project. I could never have wished for a better supervisor.

Secondly, I would like to thank my co-supervisor, Stian Henriksen, for all help, ideas and scientific input. It has been a privilege to learn from you. I also want to thank my co-supervisor Karen K. Sørensen from the Vascular Biology Research Group for helping me performing electron microscopy.

Also, I want to thank Jack-Ansgar Bruun and Toril A. Grønset from the Proteomics and Metabolomics Core Facility, Roy A. Lysså from the Advanced Microscopy Core Facility, and all the kind employees at the Department of Microbiology and Infection Control at the University Hospital of Northern Norway for having me.

Last but not least, I want to thank my parents, Logendran Subramaniam and Pathmajothy Murugesu, and my siblings Abirami and Vishnu for the support through this whole year.

Contents

List of Tables

List of Figures

Abstract

The human polyomavirus BKPyV infects most people worldwide and establishes a lifelong persistent infection in the renourinary tract. The virus rarely gives symptoms in healthy people, but it can cause severe disease under certain immunocompromised states. Despite its high prevalence, our knowledge about how the virus evades host immunity and persists still poor. Extracellular vesicles (EVs) are released by all cells and has in the last decade gained recognition as important mediators of cell to cell communication. In recent years, evidence that virus infected cells release EVs containing viral factors and host components related to infection has emerged. Therefore, as an approach to better understand BKPyV persistence, we analyzed the protein content of EVs from U-2OS15E, a persistently BKPyV-infected osteosarcoma cell line, and its ancestral cell line U-2OS. EVs were purified by ultrafiltration combined with size exclusion chromatography and proteomic analysis was performed with LC-MS/MS. We found that 410 proteins were enriched in EVs from U-2OS15E compared to U-2OS, and 183 proteins were deprived. We found enrichment of some proteins involved in increased cell proliferation and cell cycle arrest, and also proteins involved in innate immunity. Some of the enriched proteins in U-2OS15E EVs, such as IKKα, are known to upregulate the innate immune response while other proteins like gasdermin-D can be involved in immune evasion. Our results shed new light on persistent BKPyV infection.

Abbreviations

ABC	ammonium bicarbonate
AMCF	Advanced Microscopy Core Facility
ATP	adenosine triphosphate
BCA	bicinchoninic acid assay
BKPyV	BK polyomavirus
C8B	complement C8 beta chain
CD	cluster of differentiation
CDN	cyclic dinucleotide
CFD	complement factor D
cGAMP	cyclic guanosine monophosphate–adenosine monophosphate
cGAS	cyclic guanosine monophosphate–adenosine monophosphate synthetase
Da	Dalton
ddH2O	double distilled water
dH2O	distilled water
DMEM	Dulbecco's Modified Eagle Medium
DNA	deoxyribonucleic acid
dps	days post seeding
DRAQ5	1,5-bis{[2-(di-methylamino) ethyl]amino}-4, 8-dihydroxyanthracene-9,10-dione
dsDNA	double stranded DNA
DTT	Dithiothreitol
ECM	extracellular matrix
EDTA	ethylenediaminetetraacetic acid
ER	endoplasmic reticulum
ESCRT	endosomal sorting complex required for transport
EVs	extracellular vesicles
EVGR	early viral gene region
FA	formic acid
FBS	fetal bovine serum
FDR	false discovery rate
FSC	forward scatter
GAPDH	glyceraldehyde 3-phosphate dehydrogenase
Geq	genome equivalents
GO	gene ontology
GSDMD	gasdermin D
GTP	guanosine triphosphate
HIV-1	human immunodeficiency virus 1
HSCT	hematopoietic stem cell transplant
HSP	heat shock protein
HSV-1	herpes simplex virus 1
ICP0	herpes virus infected cell polypeptide 0
IFN	Interferon
IgG	immunoglobulin G
IKK	inhibitor of nuclear factor kappa-B kinase

IRF3	interferon regulatory factor 3
ISEV	International society of extracellular vesicles
IAA	Iodoacetamide
JCPyV	JC polyomavirus
kbp	kilo base pairs
kDa	Kilodalton
LC3B	microtubule-associated proteins 1A/1B light chain 3B
LC-MS/MS	liquid chromatography tandem mass spectrometry
LDS	lithium dodecyl sulfate
LTag	large tumor antigen
LTF	Lactotransferin
LVGR	late viral gene region
MAD2L2	mitotic spindle assembly checkpoint protein
MCPyV	Merkel cell polyomavirus
miRNA	micro ribonucleic acid
MISEV	minimal information for studies of extracellular vesicles
mRNA	messenger ribonucleic acid
MS	mass spectrometry
MV	microvesicles
MVB	multivesicular bodies
NCCR	non-coding control region
NF-kB	nuclear factor kappa-light-chain-enhancer of activated B cells
NMWL	nominal molecular weight limit
NOS1	nitric Oxide Synthase 1
NOS3	nitric Oxide Synthase 3
NOSIP	nitric oxide synthase-interacting protein
NTA	nanoparticle tracking
PBS	phosphate buffered saline
PCR	polymerase chain reaction
PEG	polyethylene glycol
PML	progressive multifocal leukoencephalopathy
ppm	parts per million
pRb	retinoblastoma
PRiME	Proteomics and Metabolomics Core Facility
PVDF	polyvinylidene fluoride
PyVAN	polyomavirus associated nephropathy
PyVHC	polyomavirus associated hemorrhagic cystitis
PyVUC	polyomavirus associated urothelial cancer
qPCR	quantitative PCR
RIPA	radioimmunoprecipitation assay
RNA	ribonucleic acid
RPS15	ribosomal Protein S15
RPTEC	renal proximal tubule epithelial cells
rRNA	ribosomal ribonucleic acid
SDS	sodium dodecyl sulfate
SEC	size exclusion chromatography
SSC	side scatter
STING	stimulator of interferon genes

SV40	simian vacuolating virus 40
TBS	tris-buffered saline
TBST	tris-buffered saline with Tween® 20
TCA	trichloroacteic acid
TEM	transmission electron microscopy
TLR	toll like receptor
TNS	trypsin neutralizing solution
TRAF6	tumor necrosis factor receptor associated factors protein 6
TRIM32	tripartite motif-containing protein 32
TRIM56	tripartite motif-containing protein 56
TSG	tumor susceptibility gene
TSP	thrombospondin
UBR4	E3 ubiquitin-protein ligase UBR4
UiT	University of Tromsø
UV	ultraviolet
Å	Ångström

Introduction

BK virus

BK polyomavirus (BKPyV) is a human polyomavirus with a worldwide seroprevalence of 60-100%. Primary infection is typically occurring during early childhood [1,2] and seems to be followed by a lifelong persistent infection in epithelial cells of the renourinary tract.

The family of *Polyomaviridae* is a group of small, naked viruses with circular double-stranded DNA genomes of approximately 5 kilo base pairs (kbp), infecting mammals, birds and fish [3]. The name polyoma comes from the Greek language where *poly* means 'multiple', and *oma-* meaning 'tumor'. The name derives from the first described polyomavirus, identified as murine K virus which was found to induce multiple tumors in mice, such as adenocarcinoma and leukemia [4–6]. However, not all polyomaviruses identified in later years induce tumors in their host. There have been identified 14 human polyomaviruses to date, where five of them are confirmed to cause human diseases mainly affecting immunocompromised patients [6]. In addition to BKPyV, other well-known polyomaviruses are JC polyomavirus (JCPyV) that can cause progressive multifocal leukoencephalopathy (PML), Merkel cell polyomavirus (MCPyV) that causes 80% of Merkel cell carcinoma, and simian vacuolating virus 40 (SV40) which is found in monkeys and has been widely studied as a model eukaryotic virus [6–9].

Virion and genomic structure

The BKPyV virion is icosahedral with a diameter of about 40 to 45 nm. It is constituted of 72 pentameric capsomers of the major structural protein VP1, each having one minor structural protein, either VP2 or VP3, on the internal face.

The genome can be divided in three distinct functional regions: the early viral gene region (EVGR), the late viral gene region (LVGR), and the non-coding control region (NCCR) [6,7,10]. EVGR is expressed in the early state of infection and encodes the non-structural proteins large-Tumor antigen (LTag) and small-tumor antigen (sTag), and also derivates resulting from alternative splicing of the original EVGR transcript [6]. LTag is a nuclear protein and has the ability to bind to and inhibit downstream effects of the tumor suppressor proteins retinoblastoma (pRb) and p53. Additionally, LTag can also function as helicase to unwind DNA

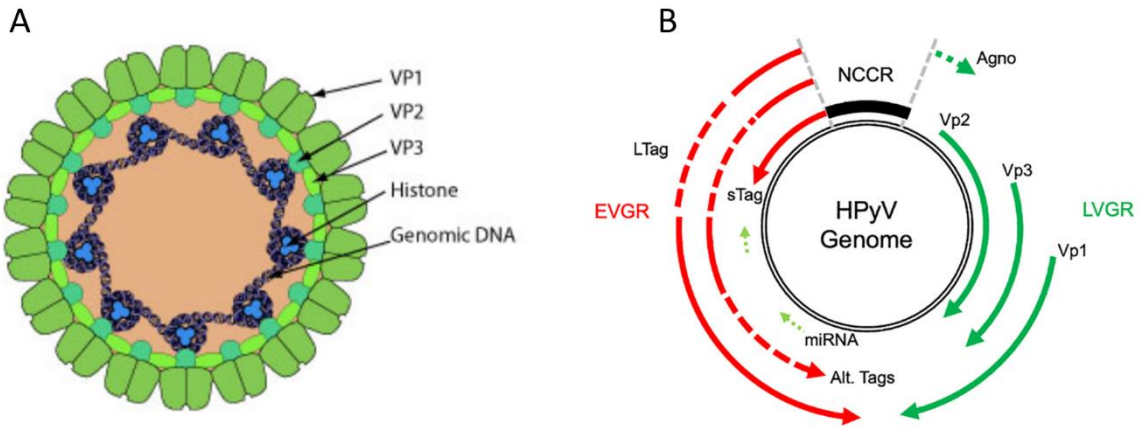

Figure 1.1. *Virion structure and genome organization of human polyomavirus (HPyV).* ***(A)*** *Illustration of the virion structure of HPyV with the major capsid protein VP1 connected with the minor capsid proteins VP2 and VP3. Circular dsDNA is wrapped around histones. Image taken from ViralZone, Swiss Institute of Bioinformatics.* ***(B)*** *Schematic illustration of the HPyV genome. Non-coding control region (NCCR) contains the origin of replication; the early viral gene region (EVGR; red) encoding LTag, sTag, and alternatively spliced Tags; the late viral gene region (LVGR; green) encoding VP1, VP2, VP3, miRNA and/or agnoprotein. Image taken from [6].*

upon replication [11]. LVGR which is transcribed after viral DNA replication encodes the three structural proteins VP1, VP2 and VP3, and the non-structural agnoprotein [10]. VP1 is the major capsid protein that forms the icosahedral capsid, while the minor capsid proteins VP2 and VP3 reside on the inner face of the capsid, and interact with the circular DNA which is organized in nucleosomes i.e. the DNA is wrapped around cellular histones (**Figure 1.1**) [6,10]. Agnoprotein is a small regulatory protein that is expressed by several but not all polyomaviruses. BKPyV agnoprotein which was first detected in Tromsø [12], consists of 66 amino acids and is an abundant cytoplasmic protein. It is essential for efficient replication and interacts with multiple viral and cellular proteins [13]. Recently agnoprotein was found to disrupt the mitochondrial membrane potential and network, thereby facilitating innate immune evasion [14].

The NCCR is a bidirectional regulatory region which contains the origin of replication and promoters/enhancers with numerous transcription factor binding sites regulating EVGR and LVGR expression [6,15]. While most BKPyV strains have well conserved protein coding regions of the genome, the NCCR exhibit considerable variation [16]. The NCCR in BKPyV from urine of healthy people is usually quite similar and is denoted an archetype NCCR. This is thought to be the transmissible form of the virus. BKPyV with archetype NCCR can also be

found in the urine of diseased patients, but in addition they commonly have BKPyV with rearranged NCCR characterized by deletions and duplications compared with the archetype [16,17].

BKPyV also encodes a miRNA on the late strand that is complementary to early transcripts and therefore has the potential to negatively regulate the expression of LTag [18]. The miRNA has been found to limit replication of archetype but not rearranged BKPyV replication [19].

The replication cycle of BKPyV

BKPyV binds to alpha 2,3-linked sialic acid on N-linked glycoproteins and enters cells by caveolae-mediated endocytosis [20]. Following entry, BKPyV is brought to the rough endoplasmic reticulum (ER). Here a fully or partly uncoating takes place before the genome is entering the nucleus [21]. Here the early transcripts are produced, LTag is expressed, and the cell is pushed into S phase. LT-dependent DNA replication begins, followed by activation of the late promoter and expression of the structural proteins of the virus. The newly synthesized genomes and proteins are assembled into progeny virions, which are released from the cell.

While the entry of BKPyV into cells is well described, evidence for the mechanism of viral release are lacking. It is assumed that naked viruses are released through passive strategies, such as host cell lysis. There are reports that BKPyV can follow the lytic replication cycle in renal proximal tubular epithelial cells (RPTECs) [22]. However, strong cytopathic effects of BKPyV infected cells *in vitro* are not seen as frequently as in SV40 infected cells [21]. Moreover, because BKPyV establishes a lifelong persistence, a non-lytic release is also likely, and this was reported to occur in BKPyV infected RPTECs recently [23].

Disease and treatment

The two major diseases caused by BKPyV are polyomavirus associated nephropathy (PyVAN) and polyomavirus associated hemorrhagic cystitis (PyVHC).

PyVAN occurs in 1-15% of kidney transplant patients and is caused by uncontrolled replication of BKPyV in the tubular epithelial cells of the kidney. This leads to interstitial and tubular inflammation, interstitial fibrosis, and eventually tubular atrophy that leads to permanent loss of allograft function and sometimes loss of the allograft [6]. As effective antiviral drugs are

lacking, the treatment strategies are based on reduction of immunosuppression and immune recovery.

PyVHC affects 5-20% of allogenic hematopoietic stem cell transplant (HSCT) patients. Symptoms of PyVHC is a combination of common cystitis symptoms and macrohematuria. The patients have high level BKPyV viruria [6,24]. The pathogenesis of PyVHC is still not completely understood. However, it is suggested to be caused by the combination of several factors. They include damage to urothelial mucosa due to myeloablative conditioning regiments, an uncontrolled replication of BKPyV during immune suppression; and finally, that donor immune cells are attacking cells with viral antigens [25]. Treatment strategies are based on hyperhydration, forced diuresis, bladder irrigation, erythrocyte and platelet transfusion, and urologic intervention [6].

Emerging evidence indicates that BKPyV replication in the kidney and urothelial tract of kidney transplant patients may lead to polyomavirus associated urothelial cancer (PyVUC) [26]. Different from other urothelial cancers, PyVUC lacks evidence for mutations in some common cancer associated genes, while harbouring chromosomally integrated BKPyV genome [27]. Along with rearrangements in the viral NCCR activating expression of EVGR, the encoded LTag and stag promote cell progression to S-phase, cell transformation and PyVUC [6,26]. Reducing immunosuppression to cause immune recovery along with regular cancer treatment may be essential to obtain a lasting cure of metastasizing PyVUC [6].

Viral persistence and immune evasion

Although discovered 50 years ago, the primary mode of transmission, viral persistence and reactivation of BKPyV is still not completely understood [28,29]. Respiratory or oral transmission has been strongly implicated. Following the primary infection of a mucosal surface, BKPyV is probably spread with the blood to the urinary tract as 30 to 50 percent of humans without kidney disease have detectable BKPyV DNA sequences in kidney tissue obtained at surgery or autopsy [30], and shedding of BKPyV in the urine of healthy adults is frequently reported [31,32].

During immunocompromised states, like under pregnancy, systemic lupus erythematosus, post organ transplantation or human immunodeficiency virus 1 (HIV-1) infection, BKPyV shedding

in urine is increased and increased replication sometimes cause severe diseases as described above [33].

Since BKPyV DNA is associated with cellular histones and forms so-called minichromosomes, the switch between persistent and reactivated infection could theoretically be regulated at the epigenetic level similar to the epigenetic control of herpesvirus latency [34]. However, it has been challenging to investigate this question as it is difficult to access healthy human specimens.

The proximal tubular epithelial cells are thought to be key mediators of the inflammatory response in the kidney. The possibly lifelong persistence of BKPyV in these cells therefore is an enigma. Most of the time, the virus is probably in a latent state where few or no viral genes are transcribed, keeping the virus protected from the immune response [32]. BKPyV miRNA may play an important role in this regulation. BKPyV mutants that did not express miRNA, were found to express higher levels of LTag than wild type virus [19]. This made them replicate significantly better than wild type virus. On the other hand, the cells containing high levels of LTag were probably more visible for the immune system. Therefore, a balanced level of LTag may be important for the persistent infection. The BKPyV miRNAs has also been reported to target the cellular stress-induced ligand ULBP3 to allow the virus to escape detection by the immune system [35].

Another way that BKPyV can evade immune detection is via the agnoprotein. As earlier mentioned, BKPyV agnoprotein is disrupting the mitochondrial membrane potential which is causing innate immune evasion [14]. Moreover, the related SV40 LTag has been reported to block the cGAS-STING pathway, a component of the innate immune system that detects intracellular DNA [36]. In addition, MCPyV and BKPyV LTag has been reported to inhibit Toll-like receptor 9 (TLR9) gene expression, which might serve as another approach for the viral genomes to evade host immune detection [37].

Stimulator of interferon genes

Innate immunity against viruses is largely dependent on a variety of pattern recognition receptors (PRRs) detecting viral particles such as DNA, RNA and viral proteins, termed as pathogen associated molecular patterns (PAMPs). PRRs involved in anti-viral immunity include Toll like receptors (TLRs) 3, 7, 8, and 9, RIG-I-like receptors MDA5 and RIG-I, and cytosolic DNA sensors such as cyclic GMP-AMP synthase (cGAS) [38]. The DNA sensing pathway through cGAS and its downstream effector, stimulator of interferon genes (STING) has emerged in recent years as an important mechanism in immunity against dsDNA viruses [38,39]. STING is a transmembrane protein on the endoplasmic reticulum (ER), and it resides here in an inactive state. Upon detection of foreign cytoplasmic DNA, STING is activated, leading to transcription of type 1 interferon (IFN) and proinflammatory cytokines through the IRF3 or NF-κB pathways [38].

The cGAS-STING cytosolic DNA sensing pathway

Briefly described, cGAS binds to cytosolic dsDNA upon detection and undergoes a conformational change in which ATP and GTP is converted into the cyclic dinucleotide (CDN) 2'3-cyclic GMP-AMP (cGAMP) [38,39]. CDNs are the natural ligand of STING, and upon binding to cGAMP, STING becomes active and translocates to the intermediate compartments between the ER and Golgi. During translocation, STING undergoes a conformational change in which the C-terminus is exposed, and it oligomerizes. cGAMP then recruits TANK-binding kinase 1 (TBK1) which phosphorylates the C-terminal tail of STING. Phosphorylation of STING by TBK1 then provides a docking site for interferon regulatory factor-3 (IRF3). TBK1 phosphorylates IRF3, causing it to dimerize and translocate to the nucleus where it induces transcription of genes encoding various cytokines, chemokines and IFNs, including type I IFNs.

In addition to IRF3 activation, another transcription factor, NK-κB, is activated in this DNA sensing pathway [39]. A number of proteins are thought to be involved in this process, including the E3 ligases TRIM32, TRIM56, TRAF6, the kinases TBK1 and the inhibitor of κB kinase (IKK) complex proteins IKKα and IKKβ, and finally the ubiquitin binding protein NK-κB

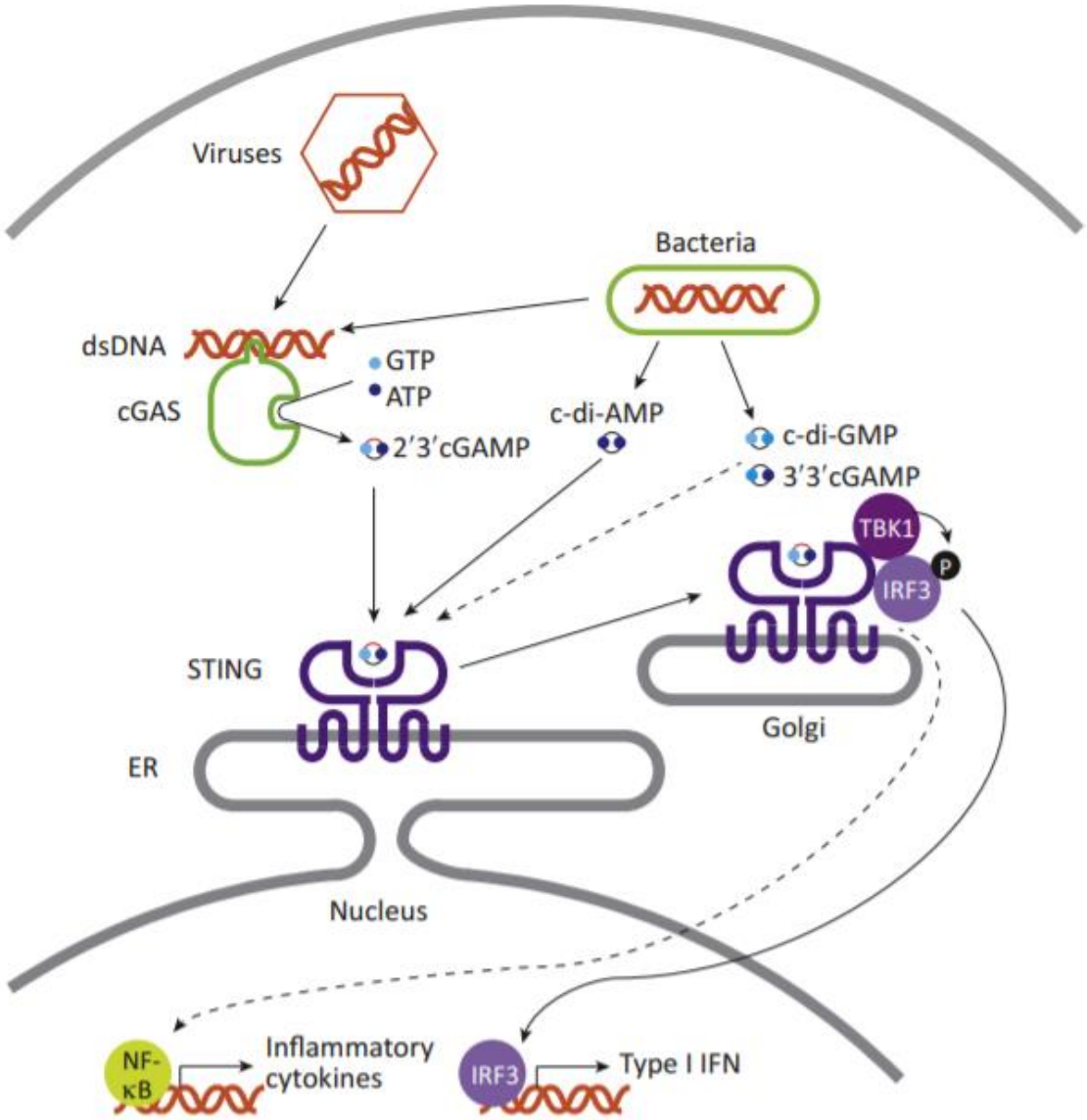

Figure 1.2 *Schematic representation of the cGAS-STING pathway. Upon detection of dsDNA in the cytosol, cGAS synthetizes cGAMP. cGAMP binds to and activates STING which translocates to the Golgi where TBK1 is recruited to phosphorylate the C-termini of STING. This recruits IRF3 for phosphorylation by TBK1, which in turn leads to IRF3 translocation to the nucleus and transcription of target genes including IFN-α/β. NF-κB activation is also observed downstream of STING activation, however, the mechanism is not completely understood. Figure is taken from* [122].

essential modulator (NEMO; also known as IKKγ) [38]. Although, the molecular processes in NK-κB activation downstream of cGAS-STING is poorly understood, its activation in the TLR pathways is well documented. TRAF6 generates ubiquitin chains that bind to IKKγ, which in turn triggers IKKα and IKKβ phosphorylation. Phosphorylation of IKKα and IKKβ leads to the subsequent phosphorylation and proteasomal degradation of inhibitor of κB (IκB). Degradation

of IκB allows NF-κB to translocate to the nucleus and regulate transcription of proinflammatory cytokines and IFNs in cooperation with IRF3 [38].

Evasion of the cGAS-STING pathway by DNA viruses

The production of IFNs in response to cytosolic viral DNA through this pathway is important for immunity against DNA viruses. Unsurprisingly, DNA viruses have evolved mechanisms to avoid or inhibit this signaling system, to be able to successfully infect cells.

A virus that has been shown to target the cGAS-STING pathway is herpes simplex virus 1 (HSV-1) [40]. The immediate early protein, ICP0, of HSV-1 is thought to block the pathway by degradation of hostile factors through its E3 ligase activity. An ΔICP0-mutant HSV-1 could successfully replicate in STING deficient cells, however, by transiently activating the STING pathway, the viral replication was reduced by up to 90% [41]. Additionally, the HSV-1 tegument protein UL46, and the regulatory protein ICP27 have both been shown to interact with TBK1, leading to a reduction in the phosphorylation and translocation of IRF3 [42]. Furthermore, HSV-1 infected cells were shown to secrete extracellular vesicles (EVs) containing STING in order to block viral replication in recipient cells [43].

Other DNA viruses that have been shown to interact with the cGAS-STING pathway to evade DNA sensing are adenovirus (AdV) and human papillomavirus (HPV) [36,40]. The oncogenes E1A and E7, from AdV and HPV, respectively, are reported to inhibit cGAS-STING by directly binding to STING. Silencing of the mentioned oncogenes resulted in restoration of the cGAS-STING pathway which was measured by type I IFN production. As mentioned earlier, SV40 LTag is also suggested to interact with the cGAS-STING pathway, however, the molecular mechanism remains unclear [36].

Characterization of extracellular vesicles

Cell to cell communication is essential for all multicellular organisms in order to maintain their physiology and to function as a system. Cells communicate through direct interactions (juxtacrine signaling) with neighboring cells, or the cells can release soluble factors, such as hormones, growth factors and cytokines. The soluble factors released by a cell can act on the cell itself (autocrine signaling), or it could have an impact on an adjacent (paracrine signaling) or a distant (endocrine signaling) cell. Over the past decade, EVs has earned recognition as important mediators of cell to cell communication [44].

EVs were first time described in 1983 when multivesicular bodies in reticulocytes were found to release EVs into the extracellular space [45]. Since then, nearly all mammalian cells, lower eukaryotes and prokaryotes have been found to produce EVs [46]. EVs are heterogenous when it comes to size, sedimentation rates and surface proteins and this seems to depends on cell type, intracellular origin, isolation method or enrichment techniques [44]. This has not only caused confusion about the nomenclature of different subtypes of EVs, but also in defining an EV. Common for all EVs is that they are lipid bilayer structures released from cells, in which they contain information in the form of proteins, nucleotides or lipids. In 2018 the international society for extracellular vesicles (ISEV) released MISEV2018: minimal information for studies of extracellular vesicles [47]. Their definition of EVs is:

"*EV's are the generic term for particles released from the cell that are delimited by a lipid bilayer and cannot replicate, i.e. do not contain a functional nucleus."*

Enveloped viruses, in particular retroviruses have been referred to as EVs, as they resemble EVs in both structural and functional aspects [48]. However, retroviruses do not fulfill the criteria of ISEVs definition of an EV, since viruses can replicate.

Nomenclature of EV subtypes

In the early years of EV studies, the term 'exosome' was used to define all EVs with a size range from 40 nm up to 1000 nm [49,50]. Today, EVs are divided into three main subgroups: apoptotic bodies, microvesicles (MVs) and exosomes. Apoptotic bodies are the largest group of EVs with a size range of 500-4000 nm. They are created during apoptosis and have a heterogenous shape and density. Apoptotic bodies differ from other EVs as they carry

fragmented genomic DNA and cell organelles [51]. Exosomes on the other hand are uniform, spherical structures with a size range of 30-150 nm. Exosomes are of endosomal origin, contained within multivesicular bodies (MVB) and released into the extracellular space upon fusion of MVBs with the plasma membrane. MVs are EVs of various shape with a size range of 50-1000 nm. They are formed by budding from the plasma membrane [44,50,51].

There have been variations in EV subgroup definitions. For example, 'exosomes' have been defined [49] as vesicles that bud into endosomes which forms MVBs and then are released into the extracellular space through fusion with the plasma membrane; vesicles that sediment only after centrifugation at ~70,000-100,000g; and as EVs with a size around 30-150 nm and a buoyant density of 1.13-1.19 g/ml [51]. There are challenges in defining EVs according to their sedimentation rate and buoyant density. Both sedimentation rates and buoyant densities are largely dependent on sample origin, rotor type used during isolation, and sample viscosity. These factors are discussed later under the section "Isolation methods". Also, because of the overlap in sizes between the different subgroups of EVs, it may seem more precise to characterize EVs by their intracellular origin.

Composition of EVs

The composition of EVs is based on recent studies that have been characterizing EV protein, lipid, and nucleic acid content. Common methods used are western blot, proteomic studies, immune gold labeling combined with electron microscopy, antibody coupled flow cytometry, lipidomic studies, and PCR. Proteins that are enriched in EVs can be used as markers to verify the isolation, however, there have been some challenges in finding specific markers for certain subpopulations of EVs. The most commonly used EV markers are tetraspanins, annexins, flotillins, endosomal sorting complex required for transport (ESCRT) complexes, and heat shock proteins, as those proteins are abundant in EVs [51]. Major histocompatibility complex (MHC) molecules have been detected in EVs >100 nm, however they have not been associated with a certain subgroup of EVs [50]. The tetraspanins CD9, CD63 and CD81 were thought to be specific markers of exosomes, but these proteins have also been observed in apoptotic bodies and MVs [44,52]. One study claimed that annexin A1 is a specific marker of MVs, but there have also been observations of annexin A1 in exosomes [53–55]. In these last-mentioned studies, the exosomes were isolated by sedimentation at 100,000g. By this method

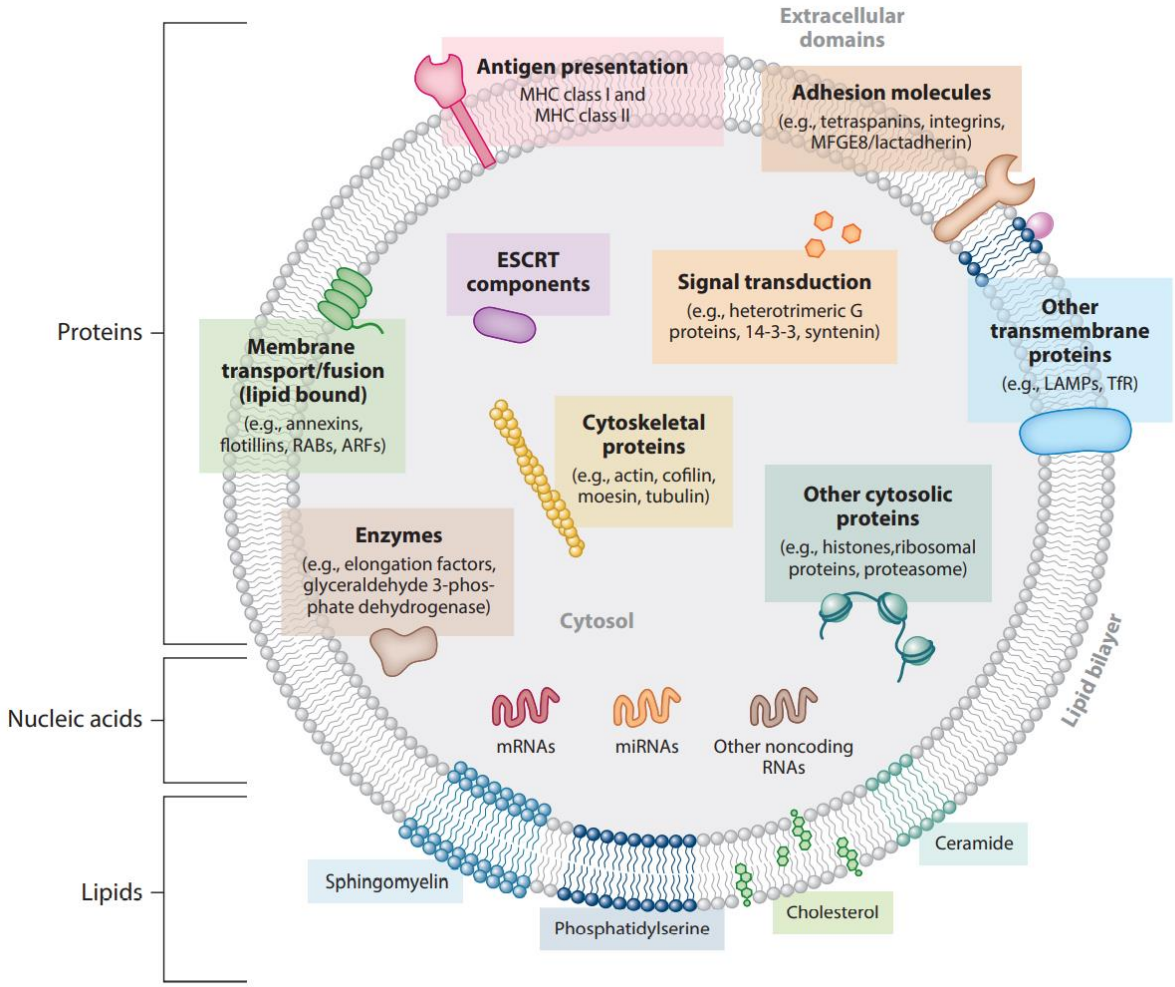

***Figure 1.3**. Schematic representation of the overall composition and membrane orientation of the EVs. Each of the listed components may be present in some subtype of EVs and not in others. Image is taken from [50].*

contaminants will also sediment and it is not an optimal method to separate exosomes from MVs. This will be discussed in more detail later.

Although they are not specific for MVs, the most common markers used to detect MVs are integrins, selectins and CD40. MV membranes also contain more cholesterol, diacylglycerol, phosphatidylserine compared to exosome membranes [51]. Markers commonly used to detect exosomes are CD9, CD63, CD81, and the heat shock proteins HSP60, HSP70, HSPA5, HSP90, and CCT2. ALIX which is involved in ESCRT complex is also used to detect exosomes. Markers used to detect apoptotic bodies are C3b, thrombospondin (TSP), and histones [51]. It is relatively easy to distinguish apoptotic bodies from the other two subgroups, as apoptotic bodies carry many cellular components such as mitochondria, ER complexes, Golgi complexes,

ribosomes, and proteasomes. Thus, certain exosome and MV negative markers, like GAPDH can be used to detect apoptotic bodies.

The biological function of EVs

The main function of EVs is to transport information. The lipid membrane of EVs encapsulates the information and protects it from degrading enzymes present in the extracellular space. Thus, the information can be delivered to distant sites. EVs can bind to cell surface receptors via its surface proteins and lipids to merge its membrane with the recipient cell plasma membrane and deliver information [46]. Such information can be transcription factors, infectious particles, signal molecules, mRNA, non-coding RNAs and growth factors. Since EVs carry a wide range of biological information, it participates in maintenance of normal physiology, such as tissue repair, immune surveillance, stem cell maintenance and blood coagulation [44,46].

In addition to maintaining normal physiological function, EVs have also been shown to participate in viral reproduction and cancer progression. Studies have shown that tumor derived EVs secrete molecules that contributes to angiogenesis, tumor growth, and suppression of antitumor immune response [56]. On the other hand, tumor derived EVs have also shown to be involved in immune regulatory functions, such as antigen presentation and activation of immune cells. In this way, tumor derived EVs, both contributes to tumor progression as well as they are involved in tumor suppression [56]. Similarly, EVs during viral infections have been shown to play dual roles. EVs of virus infected cells can function as transport of viral and cellular particles that facilitate infection in recipient cells, and they can transport molecules promoting immune response in recipient cells prior to infection [43,57].

Finally, EVs have emerged as therapeutic drug delivery vehicles [58]. Because of their ability to stay stable in the circulation and overcome natural barriers such as the blood-brain barrier, and since they possess intrinsic cell targeting properties, EVs can be engineered to deliver drugs to specific tissues or organs in the body [59]. However, development of EVs as drug delivery vehicles has been limited due to lack of scalable EV isolation and efficient drug loading.

Isolation methods of EVs

Over the years, there have been developed several methods to isolate EVs. Common ways to isolate EVs are focused either on the physical properties of EVs, such as buoyant density and size, or based on chemical properties, like interactions with specific surface molecules on EVs [51]. In the previous decade, differential centrifugation was considered the gold standard of EV isolation [60]. However, new methods have gained credibility in isolating more purified and a higher yield of EVs.

In most studies of EVs, the first step after harvesting samples is a step of ultrafiltration [47,51,60–62]. There are commercial centrifuge filters with different pore sizes, allowing isolation of particles with a selected size range. A filter cup with a pore size of 0.22 µm has been the most commonly used filter for EV isolation. It retains all components with a diameter exceeding 220 nm [62]. In some studies, ultrafiltration has been executed after differential centrifugation, while in other studies, it has been the first step [51,62].

Post isolation of EVs, the yield is often verified by different experimental methods. Western blot with specific EV markers, nanoparticle tracking analysis (NTA) which is a method for visualizing and analyzing particles in liquids, or transmission electron microscopy (TEM) are the most common methods to verify EVs.

Ultracentrifugation

In a worldwide survey of members of ISEV, published in 2015, 81% of the participants reported that ultracentrifugation was used as the primary method of EV isolation [60]. In order to reduce the amount of non-EV particles that co-isolates with EVs, many uses differential centrifugation. This method consists of successive centrifugation steps with increasing centrifugation forces and durations, generally aimed at isolating smaller from larger objects.

In principle, differential centrifugation is based on sedimentation rates of particles in biofluids depending on their buoyant density. Biofluids, such as conditioned cell media, urine and blood plasma are complex mixtures of particles that differs in size and densities, in which they can be separated according to their sedimentation rates by successive increases in centrifugation forces and time [62,63]. Large particles, such as cells and apoptotic bodies are pelleted and removed during the first centrifugation steps, leaving most of the smaller particles in the supernatant. By successive increase in centrifugation force and duration, smaller particles are pelleted.

Differential centrifugation works well only when the sedimentation rates between particles differ significantly. Microvesicles are pelleted at 10,000-20,000 g, while exosomes are pelleted at 100,000-200,000g making it possible to separate MVs from exosomes by ultracentrifugation [62].

There are some challenges with this method for isolation of EVs. The first one being that although the steps of differential centrifugation are similar in most protocols, there are many detailed differences, such as run time and centrifugation force. As EVs from different biofluids may have different sedimentation rates, isolation steps have to be modified according to the sample origin [62,63]. In a proteomic study of EVs derived from blood plasma, Whitham *et al.* compared the EV yield after centrifugation at 20,000g to the one from centrifugation at 100,000g [64]. Interestingly, there were no significant quantitative differences in the EV markers TSG101, ALIX, CD63 and CD9 between samples subjected to 20,000g or 100,000g centrifugation. The authors claimed that quantitative proteomic analysis on EVs is possible to do by sedimentation of EVs at 20,000g for 1 h, rather than prolonged high-speed ultracentrifugation [64]. In a different study of EVs isolated from human serum, centrifugation at 40,000g and 110,000g were compared, in which the authors suggested that centrifugation at 40,000g could provide comparable or even improved results [62,65]. The results from the two studies described above can indicate that there is a significant loss of EVs, during centrifugation at 10,000-20,000g prior to the 100,000g centrifugation step.

The usage of different centrifuge rotors can also cause problems for reproducibility. Sedimentation is not only dependent on centrifugation force and time, but also the sedimentation path-length, radius of rotation and the *k*-factor of the rotor. The *k*-factor is the pelleting efficiency of the rotor at max speed and varies between rotors depending on the maximum and minimum radius of the rotor. Differences in *k*-factor can be one of the reasons why there are so large differences in protocols for EV isolation with this method [51,62,63]. There have been developed calculators that can be used to modify protocols to the available rotor model, however, frequently the *k*-factor and rotor model are not described.

Density gradient centrifugation

Similar to differential centrifugation, the principle of density gradient centrifugation is based on sedimentation rates and buoyant densities of the sample. However, the method is different

since it involves applying a density gradient to the sample. During high-speed centrifugation, particles of different densities are separated according to their buoyant density and size. The result is a more pure, and a higher yield of EVs compared to isolation by ultracentrifugation [66]. The two most common reagents used in this method is sucrose and iodixanol (OptiPrep™). OptiPrep is usually preferred as it is capable of forming iso-osmotic solutions at all densities, and therefore can maintain the size of vesicles and other membrane organelles in the gradient, allowing better separation [51,62,67].

Since both ultracentrifugation and density gradient separation are based on sedimentation under high-speed centrifugation, they face some of the same challenges. Variations in rotor types, *k*-factors, duration, sample origin and centrifuge forces have caused low reproducibility. There have been difficulties in defining an MVs buoyant density, however, exosomes usually are found in fractions with Optiprep densities between 1.05-1.26 g/ml, (**Table 1**). It may be difficult to find EVs without further analysis, such as WB, NTA or TEM [51,62].

Table 1. *Results from studies isolating EVs, a human polyomavirus, or both with Optiprep*

Sample origin	EV density (g/ml)	Virus density (g/ml)	xg_{avg}	Duration	*k-factor*	Reference
Blood plasma	1.06-1.16	-	178,000	2 h	143.9	[68]
Cell lysate	-	1.24	234,000	3h 30 m	-	[69]
Conditioned medium	1.10-1.17	-	160,000	17 h	173	[70]
Saliva	1.24-1.26	-	160,000	17 h	173	[70]
Blood plasma	-	1.19-1.20	234,000	3 h 30 m	59	[71,72]
Conditioned medium	1.06-1.11	1.20	237,000	3 h 30 m	59	[73]
Blood plasma	1.12-1.24	-	100,000	18 h	-	[74]
Blood plasma	1.06-1.10	-	100,000	18 h	-	[74]
Conditioned medium	1.11	-	100,000	18 h	-	[75]
Conditioned medium	1.13	-	100,000	18 h	-	[75]

As shown in table 1, sample origin can also impact the outcome of density gradient centrifugation. For instance following the same protocol, EVs from conditioned cell media was detected with a buoyant density of 1.10-1.17 g/ml, while EVs from saliva was detected at 1.24-1.26 g/ml [70].

Overall, this method is preferred over ultracentrifugation because it yields EV preparations with higher purity. Using density gradient centrifugation, blood plasma-derived EVs were successfully separated from lipoproteins [68]. This has been challenging using other isolation methods based on size or ultracentrifugation. It has also been reported that density gradient centrifugation can separate EVs from virions that are in the same size range [51,73,76].

Size exclusion chromatography

Size exclusion chromatography (SEC) is a method that separates particles based on size. SEC columns are tightly packed with polymers such as agarose or polyacrylamide with pores of different sizes. Smaller particles will be trapped in the pores for longer time, allowing the larger particles to come through the column first, and the smallest at last [51,68,77]. By collecting fractions of a certain volume, it is possible to isolate EVs from other particles of different sizes. There are commercial SEC kits that are specifically designed to isolate EVs, in which one can expect a consistent result that makes SEC a reliable method for EV isolation. SEC is also a more rapid method compared to the two methods described above. While SEC can be performed within an hour, centrifugation methods usually take several hours if not days.

One disadvantage with SEC is that the size of the sample to be analyzed is much smaller than for density gradient- or ultracentrifugation. The most common commercial SEC columns take a sample size of 2 ml. There are also commercial kits that can take larger sample size, however, they can be unfavorable due to increased cost. Another challenge with SEC is that this method can co-isolate particles of the same size as EVs, such as larger protein aggregates, virus, organelles and lipoproteins. An advantage of SEC is that it is insensitive to high viscosity, and it preserves the particles integrity and biological activity [51,61].

Over the years, SEC has gained recognition as an isolation method with high reproducibility, high purity of the yield, as well as a rapid method for EV purification.

Precipitation based isolation

Precipitation based EV isolation methods are widely used and there are many commercial kits developed. The principle of these methods is to precipitate EVs by addition of an appropriate volume of a polymer solution, followed by recovering EVs through low-speed centrifugation

[62]. Polyethylene glycol (PEG) has been the most commonly used polymer solution besides the commercial kits with secret polymer solutions.

The size distribution of EVs isolated by precipitation is similar to the ones isolated by the three methods described above, but the yield of EVs is significantly larger. However, co-precipitation of non-EV nucleoproteins, proteins, virus, immunoglobulins and immune complexes has been reported. Another disadvantage is that various commercial kits vary in efficiency and quality [51]. Also, PEG is known for interfering with downstream mass-spectrometry (MS) based proteomic analysis, therefore, it is necessary to remove those polymers in order to do MS based analysis [62].

The advantage of this method is that unlike centrifugation or size-based methods, precipitation makes it possible to process a large number of samples. The method is simple and fast, in which this method is attractive in clinical research [51].

Affinity purification

Affinity based isolation of EVs is based on the interaction of certain EV surface components with other molecules, such as antibodies, lectins and lipid-binding proteins [51,62]. Among these are antibody-based isolation of EVs the most widely available and most used. Some surface markers that are widely used to capture EVs are the tetraspanins CD9, CD63, CD81, or other proteins such as heat shock proteins and annexins. One way of extracting EVs from a complex mixture of particles is immunocapturing by coupling antibodies to magnetic beads [51,62].

The advantage of this method is that it is rapid and simple, it has a high reproducibility and there is a possibility of automation which can be useful for clinical research [51]. One major disadvantage of this method is that immunocapturing discriminates between EVs that carry the antibodies and excludes EVs without the target proteins. EVs are heterogenous populations, and presence of certain EV markers can vary depending on cell type, culture conditions, and treatment during extraction.

U-2OS and U-2OS15E

U-2OS (ATCC® HTB96) is an immortalized human cell line that was established from the tibia of a 15-year-old female patient suffering from osteosarcoma. The cell line is of epithelial origin and is anchorage dependent *in vitro* [78]. Since this is a cancer cell line, U-2OS is altered in chromosome counts and there are also defects in different biological pathways.

In Tromsø more than 20 years ago, U-2OS cells were experimentally infected by BKPyV. Several subclones were isolated and one of them, denoted U-2OS15E, was later shown to be persistently infected by BKPyV, producing infectious virions for more than 300 generations [79]. This persistent BKPyV-infection has similarities to the *in vivo* infection of kidney epithelial cells and it is therefore highly interesting to study U-2OS15E cells in more detail.

Aim of the study

The aim of this study is to learn more about persistent BKPyV-infection by comparing the protein content of EVs from U-2OS and U-2OS15E, an osteosarcoma cell line persistently infected by BKPyV.

Methods

Cell culturing

Human osteosarcoma cells U-2OS (ATCC® HTB-96™, Manassas, VA, USA) and U-2OS15E [79] were cultured in Dulbecco's Modified Eagle Medium (DMEM; 11965-092, Gibco, Thermo Fisher, Waltham, MA, USA) with 10% (v/v) Fetal Bovine Serum (FBS; A31604-01, Gibco) at 37 °C with 5% CO_2. For maintenance, cells were seeded in T25 cell culture flasks and passaged every 3-4 days when the cells were about 90% confluent. Cells were washed once with room tempered phosphate buffered saline (PBS; 14190-094, Gibco) and detached by trypsinization (0.05% Trypsin EDTA; 25300-054, Gibco) followed by resuspension of cells in DMEM with 10% (v/v) FBS. When counting of cells were needed, an automatic cell counter (Countess™, Thermo Scientific) was used. All experiments were performed with cells in passage 25-50.

Isolation of EVs

U-2OS and U-2OS15E cells were seeded into three T175 flasks, each containing 35 ml DMEM with 10% (v/v) FBS and grown to about 90% confluence at 37 °C with 5% CO_2. When cells reached the desired confluence, they were washed with room tempered PBS once, and then DMEM containing 2% (v/v) exosome depleted FBS (A27208-03, Gibco) was added and cells were incubated at 37 °C with 5% CO_2 for 2 days. On day two, conditioned media was harvested, and cells and debris were removed by centrifugation at 300g, for 10 min at 4 °C. This was followed by centrifugation of the supernatant at 2000g, for 10 min at 4 °C. Next, the supernatant was added to a centrifugal filter cup (Centricon® Plus-70, Merck Millipore, Billerica, MA, USA) with a cellulose filter with a 10,000 NMWL cut off, and centrifuged in a swinging bucket rotor at 25 °C and 3,500g for 45 min. Since the filter cup only takes 70 ml, we first added 70 ml and centrifuged for 10 min as described above, followed up by refilling the remaining ~30 ml and centrifugation for 45 min. The residue from filtration was collected by turning the filter upside down in a collection cup before it was centrifuged at 1000g for 1 min. The yield was then resuspended in PBS to a total volume of 2 ml and stored at 2-8 °C until further, but no longer than 24 h.

Purification of EVs by size exclusion chromatography

In order to remove contaminating proteins from the isolated EVs, size exclusion chromatography (SEC) can be used. The ready-made SEC columns (PURE EVs, HansaBioMed Lifesciences, Tallin, Estonia) were washed with 30 ml room tempered PBS. Next, 2 ml of the pre-isolated EV sample was loaded on the column and immediately when the sample had passed through the filter and into the gel, the first fraction of 500 µl was collected. In total, 24 fractions of 500 µl were collected using PBS as eluent. The presence of EVs in selected fractions was identified by western blotting with antibodies directed against CD63 and CD9 (see the section for western blotting). Fractions containing CD63 and CD9 were pooled and concentrated with a cellulose centrifugal filter (Amicon® Ultra-15; Merck Millipore) with 10,000 NMWL cut-off by centrifugation at 4000g, for 40 minutes at 25 °C. Protein content was determined by BCA protein assay (Pierce™ Rapid Gold BCA Protein Assay, Thermo Scientific™, Wilmington, DE, USA) according to the manufacturer's instructions. The concentrated EVs were stored at -80 °C until further use.

Density gradient ultracentrifugation

In order to try to separate EVs from BKPyV, an iodixanol density cushion (OptiPrep™, D1556, Sigma-Aldrich, MO, USA) was used on the pre-isolated EV samples after filtration. Frist, a 50% OptiPrep solution diluted in 1x PBS was made by mixing 10 ml 60% OptiPrep solution with 1.2 ml 10x PBS (Gibco) and 0.8 ml ddH_2O. Next, 10% and 30% solutions were made by dilution of 50% OptiPrep with PBS. The 40% solution was made by mixing 2 ml 50% OptiPrep with 500 µl of the sample. Using a 5 ml syringe and an 80 mm needle, 1 ml 10% OptiPrep was loaded into a 5 ml open-top Thinwall tube (Beckman Coulter, CA, USA), followed by layering 1 ml 30%, 2.5 ml 40%, and 0.4 ml 50% OptiPrep underneath the previous, creating a discontinuous gradient.

Density gradient centrifugation was performed at 192 000g_{avg} for 18h at 4 °C (SW 50.1 rotor, *k*-factor 78, Beckman Coulter). After centrifugation, ten 500 µl fractions were collected and the buoyant density of OptiPrep in each fraction was determined by diluting the fractions 1:10,000 in water and measuring absorbance at 244 nm with NanoDrop™ One (Thermo Scientific™).

Western blot

As controls, cell lysates of U-2OS and U-2OS15E were prepared from T25 cell culture flasks. The cells were first washed once with room tempered PBS, before 1 ml in-house made RIPA (radioimmunoprecipitation assay; **Appendix A**) buffer with 10 µl Halt™ Protease Inhibitor (#78430, Thermo Scientific™) was added to each flask. After 10 min incubation at room temperature, lysates were collected into centrifuge tubes by the use of a cell scraper and centrifuged at 10,000g for 10 min. Protein content of the supernatant was determined by BCA protein assay as mentioned above, and aliquots of 75 µl were stored at -80 °C until further use.

Samples of cell lysates, isolated EVs, SEC fractions, and OptiPrep fractions were prepared for gel electrophoresis under either reducing or non-reducing conditions, depending on the subsequently used primary antibodies. For running SEC- and OptiPrep fractions on gel, 45 µl was loaded per well, while for EVs and whole cell lysates, 5 µg protein and 15 µg protein, respectively, was used. Chameleon Duo 928-60000 (LI-COR) was used as protein standard. For reducing conditions, samples were prepared in lithium dodecyl sulfate (LDS) sample buffer (NuPage™, NP0007, Invitrogen™, CA, USA) and sample reducing agent (NuPage™, NP0004, Invitrogen™), heated to 70 °C for 10 min before loading on Bolt 4-12% SDS-PAGE Bis-Tris Plus gels (NW04120BOX, Invitrogen™). The gel cassette was mounted in a minicell and filled with 1x NuPage™ MES SDS Running Buffer (NP0002, Invitrogen™) and 500 µl antioxidant (NuPage™, NP0004, Invitrogen™) in the inner chamber, and electrophoresis was run at 200 V for 35 min. For non-reducing conditions, samples were prepared similarly to reducing gel, only without the addition of reducing agent and antioxidant.

After electrophoresis, proteins were transferred from the gel to a 0.45 µm PVDF membrane (Invitrolon™, LC2005, Invitrogen™) in an in-house made blotting buffer (**Appendix A**) at 30 V for 1 h. After blotting, membranes were blocked in 3 ml blocking buffer (Intercept™, LI-COR Biosciences, Lincoln, NE, USA) diluted 1:2 in PBS for 1 h before 3 µl Tween® 20 (P9416, Sigma-Aldrich) and primary antibodies were added and incubated over night at 4 °C on a spinning wheel at 13 rpm. Primary antibodies used on membranes are shown in **Table 2**.

Table 2. *Primary antibodies used in western blot analysis.*

Antibody	Name	Host/Clonality	Dilution	Manufacturer
ALIX	Ab117600	Mouse monoclonal	1:1000	Abcam, Cambridge, UK
Annexin A1	Ab214486	Rabbit monoclonal	1:2000	Abcam
BKPyV-agno	81038	Rabbit polyclonal	1:10,000	[12]
BKPyV-VP1	21292	Rabbit polyclonal	1:10,000	[79]
BKPyV-VP1	MAB3204	Mouse monoclonal	1:1000	Abnova, Taipei, Taiwan
CD9	Ab92726	Rabbit monoclonal	1:2000	Abcam
CD63	10628D	Mouse monoclonal	1:250	Invitrogen™
CD81	10630D	Mouse monoclonal	1:250	Invitrogen™
Flotillin-1	D2V7J	Rabbit monoclonal	1:1000	Cell Signaling Technology, MA, USA
GAPDH	Ab8245	Mouse monoclonal	1:2000	Abcam
LC3B	Ab51520	Rabbit polyclonal	1:3000	Abcam
Phospho-STING	E9A9K	Rabbit monoclonal	1:1000	Cell Signaling
STING	NBP2-24683	Rabbit polyclonal	1:1000	Novus Biologicals, Centennial, CO, USA
SV40 Tag	Pab416	Mouse monoclonal	1:1000	Merck Millipore

Following overnight incubation with primary antibodies, membranes were washed 4 x 5 min with in-house made TBST (**Appendix A**) on a spinning wheel at 13 rpm. For infrared detection of proteins, secondary antibodies diluted in 3 ml TBST with 3 µl 10% sodium dodecyl sulphate (SDS) was added to the membrane and incubated in room temperature for 1 h. The antibodies used were: IRDye® 680LT anti-mouse IgG (1:20,000 dilution, LI-COR) and IRDye® 800CW anti-rabbit IgG (1:15,000 dilution, LI-COR). Membranes were again washed 4 x 5 min with TBST and 1 x 5 min with TBS (**Appendix A**). Infrared signals were detected with an Odyssey CLx Imager (LI-COR) and images were acquired with Image Studio software version 5.2 (LI-COR).

Immunofluorescence staining

For immunofluorescence staining 15,000 U-2OS and U-2OS15E cells were seeded in 48-well cell culture plates. Two and four days post seeding (dps), cells were washed 2 times in 1 x PBS at 37 °C and then fixed in 100% methanol for 10 min at room temperature, followed up by washing twice with 1 x PBS. Cells were then blocked with 5% (v/v) goat serum in 1 x PBS for 30 min at room temperature. Primary antibodies diluted in 1% (v/v) goat serum in PBS were added to the respective wells and incubated for 30 min at 37 °C.

Antibodies used were: BKPyV-agno (rabbit polyclonal, 1:1000 dilution; 81038 [12]), BKPyV-VP1 (rabbit polyclonal, 1:500 dilution; 21292 [79]), BKPyV-VP1 (mouse monoclonal, 1:50 dilution; MA5-33242, ViroStat, Westbrook, ME, USA), and SV40 LT-ag (mouse monoclonal, 1:100 dilution; PAb416, Merck Millipore). Post incubation with primary antibodies, cells were washed 4 times with 1 x PBS and secondary antibodies, goat-anti-rabbit 488 (1:500 dilution; Alexa Fluor™, Invitrogen™) and goat-anti-mouse 568 (1:500 dilution; Alexa Fluor™, Invitrogen™), diluted in 1 x PBS with 1% goat serum was added and incubated in room temperature for 30 min covered from light. Cells were again washed 4 times in 1 x PBS, and nuclear DNA staining was performed by addition of DRAQ5™ (Invitrogen™) at 1:1000 dilution in 1 x PBS for 5 min in room temperature. Finally, the cells were washed twice in 1 x PBS and stored at 2-8 °C protected from light until microscopy.

Immunofluorescence imaging was done with Nikon TE2000 microscope, and images were acquired and processed with Nikon-Qi2 camera and NIS-Elements BR software version 5.21.03. Further processing and analysis was performed in ImageJ.

BKPyV quantitative PCR

To examine the release BKPyV in supernatants from U-2OS15E cells, 50 µl of the conditioned media was harvested for seven consecutive days. Samples were diluted 1:100 in ddH_2O and boiled for 5 min to reduce PCR inhibitors and inactivate the virus, and 5 µl of the sample was used as template for BKPyV quantitative PCR (qPCR) using TaqMan™ Fast Universal PCR Master Mix (Applied Biosystems®, Foster City, CA, USA) [80]. PCR was performed in 25 µl of reaction mix containing 75 pmoles of forward and reverse primers. Primers used were: BKfor: 5'-ACGAGGCAAGDGTTCTATTACTAAAT-3', and BKrev: 5'-GARGCAACAGC AGATTCYCAACA-3'. The target probe was: 5'-6-FAM-AAGACCCTAAAGACTTTCCYT CTGATCTACACCAGTTT-TAMRA-3'. qPCR was carried out in triplicates using ABI 7500 Fast System (Applied Biosystems®) with the following conditions: 95 °C for 20s and 45 cycles of 95 °C for 3s and 60 °C for 30s. OptiPrep fractions were prepared and analyzed by the same protocol.

Mass spectrometry

Isolated EVs after SEC were diluted in 1 x PBS to a final volume of 200 µl. Protein precipitation was performed by the addition of 1 ml acetone containing 10% (v/v) TCA (Sigma-Aldrich) and 20 mM DTT to 200 µl sample, and overnight incubation at -20 °C. The solution was centrifuged at 16 000g for 10 min at 4 °C, and the protein pellet was washed with ice cold acetone. The following steps were performed at the Proteomics and Metabolomics Core Facility (PRiME) at the University of Tromsø.

TCA precipitated protein pellets were resolved in 20 µl 2 M Urea and 100 mM ammonium bicarbonate (ABC) and sonicated for 25 cycles (1 min on and 30 s off) with 100 % amplitude in a Cup Horn sonicator with watercooler (CupHorn/watercooler: Qsonica. Sonicator: Fisherbrand FB705, Fisher Scientific, Hampton, NH, USA). Disulfide bridges were reduced with 1,4-dithiothreitol (DTT) to a final concentration of 5 mM by incubation at 54 °C for 30 min. Cysteines were alkylated with 15 mM iodoacetamide (IAA) and incubation for 30 min at room temperature covered from light. To remove excess IAA, DTT solution corresponding to a final concentration of 5 mM was added. Pre-digestion with Lys-C (125-05061 FUJIFILM Wako Pure Chemical Corporation) was performed under gentle agitation for 5 h at 37 °C, with enzyme-to-protein ratio 1:30 (w/w) in a buffer containing 1 mM calcium chloride, 2 M urea, and 100 mM ABC. Trypsin (V511A; Promega) digestion was performed with enzyme-to-protein ratio 1:20 (w/w). Calcium chloride solution, water, and 1 M ABC were added to the sample to a final concentration of 1 mM calcium chloride, 1 M urea, and 100 mM ABC. The digestion was done under gentle agitation for 16 h at 37 °C. Omix C18 (A57003100, Agilent, Santa Clara, CA, USA) was used for sample concentrating and cleanup. Purified peptide samples were dried in a vacuum concentrator and dissolved in 15 µl 0.1% formic acid (FA). Protein concentration was measured with 205nm, 31 method with baseline on a NanoDrop™ ONE (Thermo Scientific™).

The peptide mixtures were loaded into a Thermo Fisher Scientific EASY-nLC1200 system and EASY-Spray column (C18, 2µm, 100 Å, 50µm, 50 cm). Peptides were fractionated using a 5-80% acetonitrile gradient in 0.1 % formic acid over 60 min at a flow rate of 300 nl/min. The separated peptides were analysed using a Orbitrap Exploris 480 mass spectrometer (Thermo Scientific™). Data was collected in data dependent mode using a Top15 method. The raw data was processed using the Proteome Discoverer 2.5 software (Thermo Scientific™). The fragmentation spectra was searched against the UniProt human database from 2020 and NCBInr

polyomavirus database. Peptide mass tolerances used in the search were 10 ppm, and fragment mass tolerance was 0.02 Dalton (Da). Peptide ions were filtered using a false discovery rate (FDR) set to 5 % for peptide identifications. Proteomic analysis was done in FunRich version 3.1.3 by searching proteins against the Gene Ontology (GO) database which was downloaded 10/01/2021. Enrichment analysis was done in Proteome Discoverer version 2.5.

Flow cytometry

U-2OS and U-2OS15E were seeded in T75 flasks and grown to ~90% confluence. The cells were detached by addition of 3 ml 0.05% trypsin EDTA (Gibco), and trypsinization was stopped by addition of 6 ml trypsin neutralization solution (TNS; 0113, ScienCell Laboratories, Carlsbad, CA, USA). Cells were transferred to 14 ml tubes and centrifuged at 300g for 10 min at 4 °C. Pellets were washed with ice-cold 1 x PBS, and cell concentration was determined by automatic counting. About 1 million cells was added per 14 ml centrifuge tube and pelleted as described in the previous steps. The cells were then fixed by addition of methanol at -80 °C under constant high-speed vortexing. The fixed cells were stored in methanol at -80 °C until staining.

Samples were stained one day prior to analysis. Methanol was removed from the cells by centrifugation at 600g for 10 mins at 4 °C, and 5 ml 1 x PBS was added to each tube to rehydrate the cells. Cells were again pelleted, and excess PBS was removed before cells were resuspended in 100 µl 1 x PBS with 5% (w/v) Bovine Serum Albumin (BSA; Sigma Aldrich), and 1 µl anti-SV40 LT-ag (PAb416, Merck Millipore), and incubated for 1 h at room temperature. After incubation, the tubes were added 5 ml PBS and cells were pelleted at 600g as described above. The cell pellet was resuspended in secondary antibody, 0.5 µl goat-anti-mouse (Alexa Fluor™ 488, A11029, Invitrogen™) diluted in 100 µl 1 x PBS with 5% (w/v) BSA and incubated for 1h in room temperature covered from light. Cells were washed in 5 ml 1 x PBS as described above and resuspended in 500µl 1 x PBS 5% (w/v) BSA until analysis. Controls are shown in **table 3**.

Table 3. *Controls for flow cytometry to detection of BKPyV infected U-2OS15E cells.*

Cell line	Primary antibody	Secondary antibody	Purpose
U-2OS	No	No	Autofluorescence of U-2OS
U-2OS	No	Yes	Unspecific binding of Alexa Fluor™ 488
U-2OS	Yes	Yes	Unspecific binding of PAb416
U-2OS15E	No	No	Autofluorescence of U-2OS15E
U-2OS15E	No	Yes	Unspecific binding of Alexa Fluor™ 488

Flow cytometry was performed using a LSRFortessa™ (BD, Franklin Lakes, NJ, USA) with the excitation laser set to 488 nm. Data was acquired in FACSDiva™ (BD) version 8.0.1.

Negative staining and transmission electron microscopy

Before negative staining of samples from OptiPrep density gradient, iodixanol was removed from each fraction by multiple cycles of diluting sample in PBS and passing through a 10 NMWL centrifugal filter (Amicon® Ultra-0.5, UFC501024, Merck Millipore) according to the manufacturer's instructions. Finally, washed samples were diluted in 30 µl PBS and negative staining performed. For SEC fractions, no additional purification was done before negative staining.

For negative staining, formvar coated 400 mesh copper grids were glow discharged for 10 s at 10mA. The grids were then placed on 5 µl droplets of samples and incubated for 20 min in a moist chamber. Next, the grids were washed 4 times with ddH_2O and incubated in 1% uranyl acetate for 20s. Grids were dried for 15 mins, and the grids were examined using transmission electron microscopy (TEM) HT7800 (Hitachi, Tokyo, Japan). Images were acquired with RADIUS software version 2.1, and further processing was performed in ImageJ.

Results

Characterization of U-2OS and U-2OS15E

In order to characterize the expression of BKPyV viral proteins in U-2OS15E cells, cells were seeded in 48 well plates and fixed with methanol 2 and 4 days post seeding (dps). As a negative control U-2OS cells were included and treated the same way. Although approximately 15 000 cells per well had been seeded, phase contrast microscopy at 2 dps showed that U-2OS cells were somewhat more confluent than U-2OS15E cells (**Figure 4.1**). However, at 4 dps U-2OS15E had become fully confluent (**Figure 4.1**). Immunofluorescence staining with rabbit sera directed against BKPyV VP1 and agnoprotein, respectively, and a mouse monoclonal antibody against SV40 LTag (PAb416) known to cross react with BKPyV LTag, or a mouse monoclonal antibody directed against BKPyV VP1 (MA5-33242) was performed. As secondary antibodies, goat anti-rabbit Alexa Fluor™ 488 and goat anti-mouse Alexa Fluor™ 568 were used. In addition, nuclear DNA was stained with DRAQ5™. The cells were then analyzed with phase contrast and immunofluorescence microscopy.

Immunofluorescence microscopy of U-2OS15E cells at 2 and 4 dps revealed that only some of the cells expressed LTag, or LTag and agnoprotein (**Figure 4.1**), LTag and VP1, or VP1 and agnoprotein (**Figure 4.2**). Since agnoprotein is a cytoplasmic protein, agno-staining allowed visualization of the complete BKPyV-infected cells. On the other hand, LTag and VP1 was mainly present in the nuclei and showed enlarged nuclei. While some cells had strong staining, others were weaker stained. In U-2OS cells, no staining was seen.

That some cells only showed nuclear LTag staining, probably reflected that they were recently infected and only expressed the early genes (**Figure 4.1**). Agnoprotein and VP1 are both expressed in the late phase of the BKPyV replication cycle and these proteins were observed in the same cells at 4 dps (**Figure 4.2**). Interestingly, in cells 2 dps, VP1 expression was only seen when the polyclonal rabbit serum and not when the mouse monoclonal VP1 antibody was used (**Figure 4.2**).

In order to investigate how large share of the U-2OS15E cells were infected by BKPyV, approximately 15 000 U-2OS15E cells were seeded into 48 well plates and cells were methanol fixed at 4 dps. Immunofluorescence staining using PAb416 as primary antibody and goat anti-mouse Alexa Fluor™ 488 as secondary antibody was performed, and nuclear DNA was stained

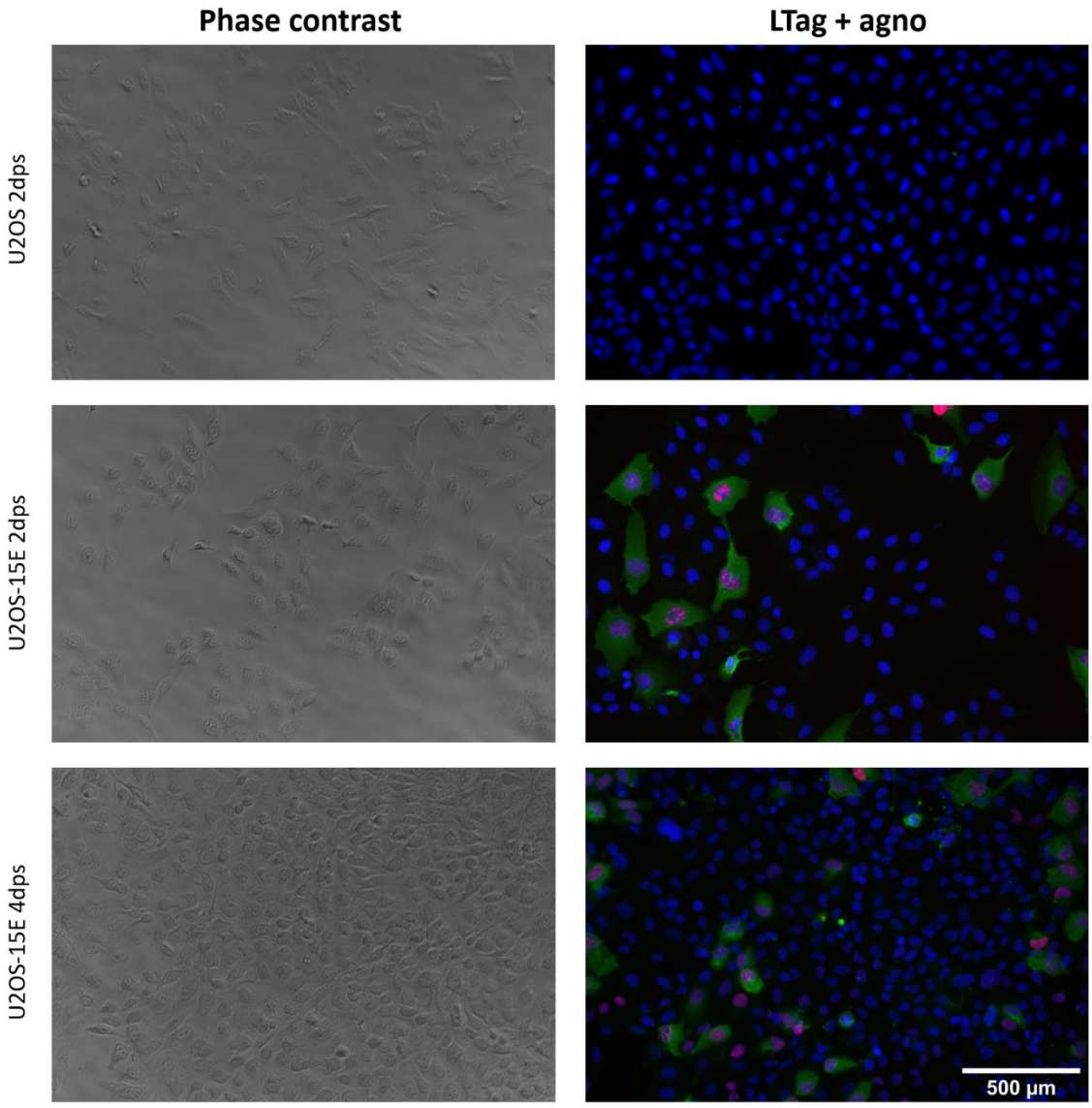

Figure 4.1. *Phase contrast and immunofluorescence microscopy of U-2OS and U-2OS15E. Cells were seeded in a 48-well plate and fixed with methanol 2 or 4 days post seeding (dps). Rabbit polyclonal anti-agno serum (81038) and mouse monoclonal anti-SV40 LTag antibody (PAb416) were used as primary antibody to stain BKPyV infected cells. As secondary antibodies, goat-anti-rabbit Alexa Fluor 488 (green) and goat-anti-mouse Alexa Fluor 568 (red) were used. Nuclear DNA was stained with DRAQ5™ (blue).*

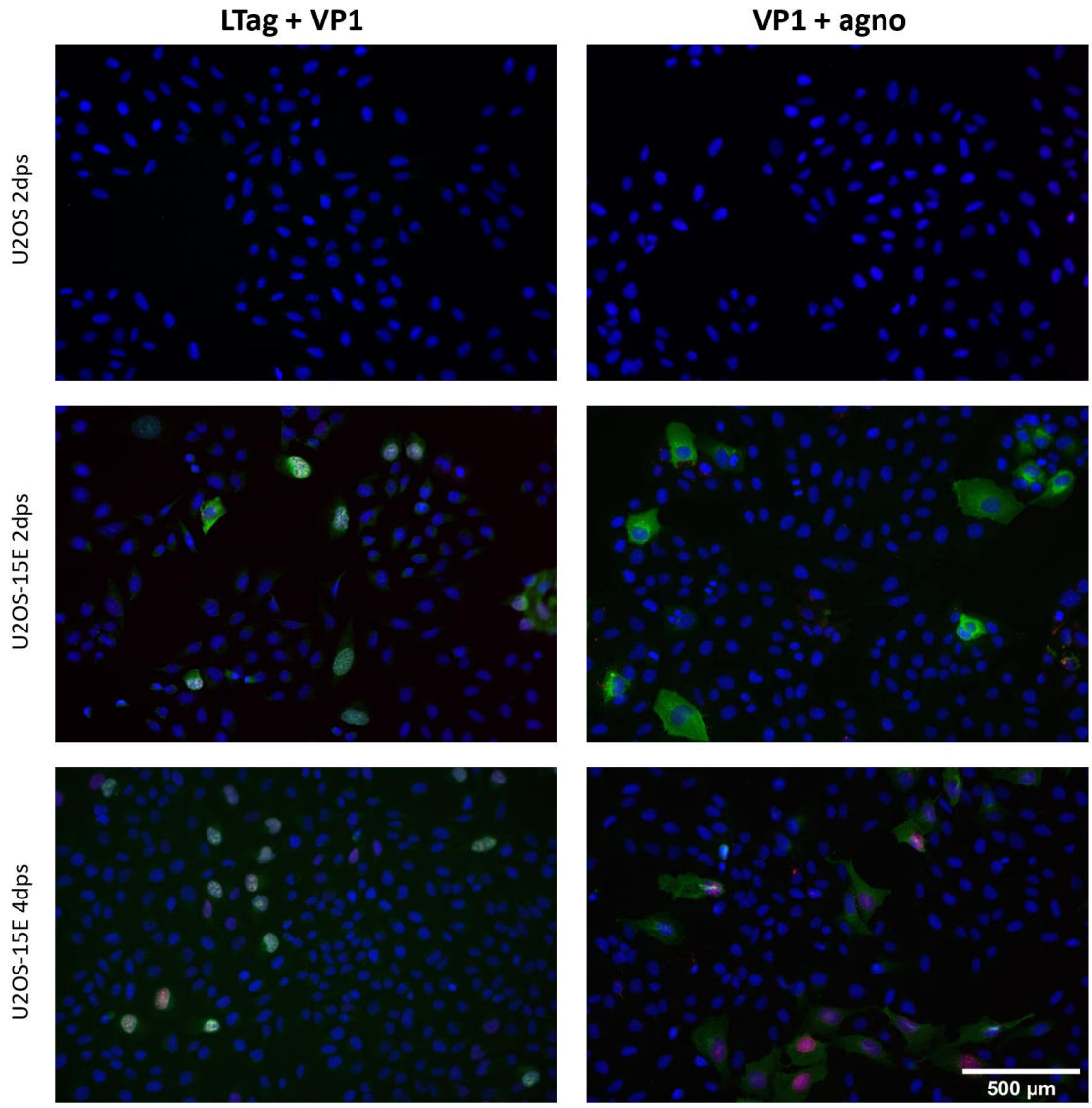

Figure 4.2. *Immunofluorescence microscopy of U-2OS and U-2OS15E. Cells were treated similarly as in* ***Figure 4.1****. As primary antibody, mouse monoclonal anti-SV40 LTag antibody (PAb416) was combined with rabbit polyclonal anti-BK VP1 (V21292) serum (left), while rabbit polyclonal anti-agno serum (A81038) was combined with mouse monoclonal anti-BK VP1 (MA5-33242) (right). As secondary antibodies goat-anti-rabbit Alexa Fluor 488 (green) and goat-anti-mouse Alexa Fluor 568 (red) was used. Nuclear DNA was stained with DRAQ5™ (blue).*

by DRAQ5 (results not shown). Images were acquired, uninfected and BKPyV-infected cells were counted by creating a binary threshold in Image-J. In more detail, the two wells with U-2OS15E were divided into five pre-decided fields of view, and images were acquired at 200x magnification. In total, 1869 cells were counted in which 535 i.e. 29% of the total number of counted cells expressed LTag. Since we cannot exclude that some infected cells did not express BKPyV protein, the result suggested that at least 29% of U-2OS15E cells were infected with BKPyV.

In order to analyze the percentage of BKPyV-infected cells in U-2OS15E with an apparently more sensitive and more quantitative method, a flow cytometric indirect immunofluorescence assay was used [81]. U-2OS15E cells were collected by trypsinization and fixed in methanol. Again, cells were labeled with PAb416 as primary antibody, and the secondary antibody goat-

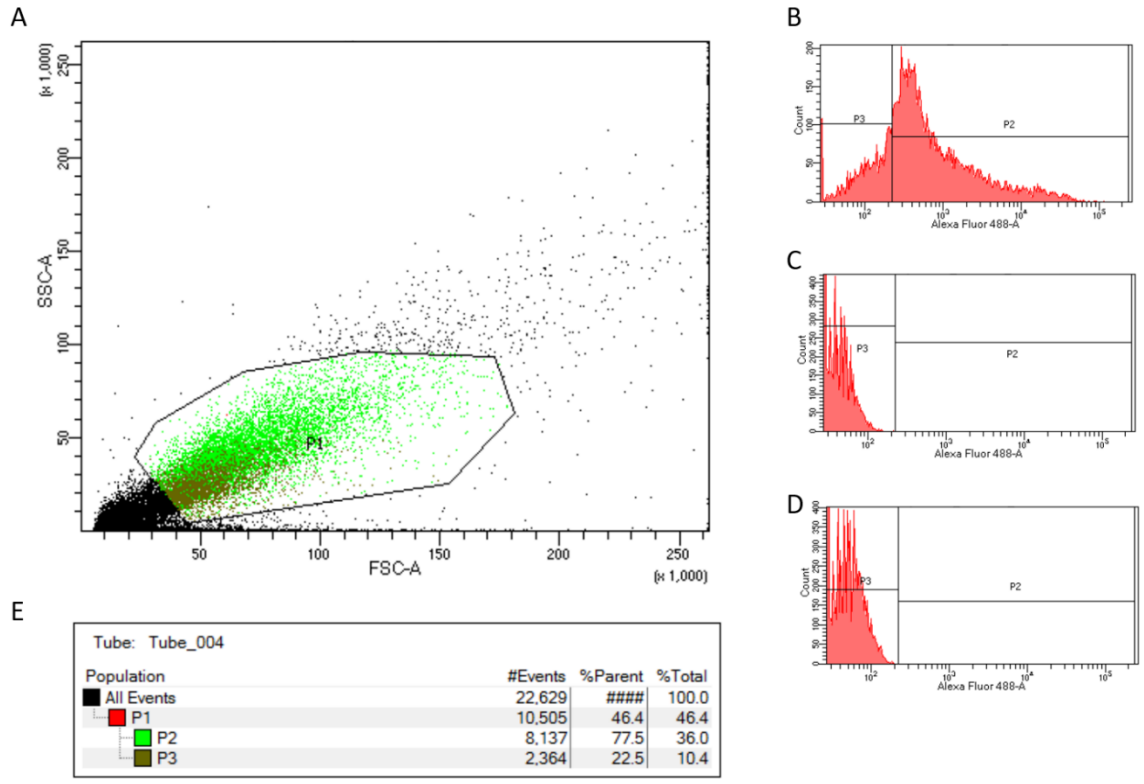

Figure 4.3. *Flow cytometric analysis of U-2OS15E stained with mouse monoclonal anti-LTag (PAb416) as primary antibody, and goat anti-mouse Alexa Fluor 488 as secondary antibody.* ***(A)*** *The plot shows 10,000 events occurring within P1 in which forward scatter (FSC) is plotted against side scatter (SSC). P1 represents the population of cells that are analyzed. All the green dots are representing cells that are LTag positive, and the brown dots are U-2OS15E cells that are LT-ag negative.* ***(B-D)*** *Histogram shows distribution of cells plotted against fluorescence. A threshold was made in which population P3 is representing autofluorescing cells, and P2 is representing cells that are fluorescing AlexaFluor 488, and hence are infected by BKPyV.* ***(B)*** *U-2OS15E stained with primary and secondary antibody.* ***(C)*** *Distribution of U-2OS15E cells stained with only secondary antibody (AlexaFluor™ 488).* ***(D)*** *Distribution of U-2OS15E without staining to measure autofluorescence.* ***(E)*** *Statistical analysis of flow cytometric run.*

anti mouse Alexa Fluor™ 488. U-2OS cells were included as a negative control and were treated the same way. Fluorescence was measured with a BD LSRFortessa™ using a 488 nm excitation laser.

Forward scatter (FSC) and side scatter (SSC) gating was used to exclude clogged and damaged cells, cells outside the desired size range, and debris. FSC is measuring the size of the cell analyzed, and SSC measures the cell surface granularity or internal complexity. A gate, P1, was made by using unstained U-2OS to include cells of desired size and surface granularity (**Figure 4.3 A**). Due to large sample loss during staining and filtration with cell strainers, only one run of each sample in which 10,000 events recorded was performed. A gate P2 was made to discriminate between autofluorescing cells (P3) and cells that are labeled with PAb416 and Alexa Fluor™ 488 (P2) (**Figure 4.3 B-D**). As controls unlabeled U-2OS, unlabeled U-2OS15E, U-2OS labeled with both primary and secondary antibodies, U-2OS labeled with only secondary antibody, and U-2OS15E labeled with only secondary antibody were prepared. However, due to recommendation from the person working at the Advanced Microscopy Core Facility (AMCF) at UiT, U-2OS stained with both primary and secondary antibodies were not analyzed. The statistical analysis of the flow cytometric run showed that 77.5% of U-2OS15E were expressing LTag, and hence were infected by BKPyV (**Figure 4.3 E**). Since many cells cluster in the left corner, the voltage should probably have been increased (**Figure 4.3 A**). Scatter plots and histograms of all included controls are shown in **Appendix B**. This experiment needs to be repeated with all controls and with several parallels.

Since clearly not all cells in the U-2OS15E cell culture were BKPyV-infected, we wanted to investigate if extracellular BKPyV was present in the supernatant. As an approximation to this we decided to measure the amount of extracellular BKPyV DNA present. Briefly described, U-2OS15E cells were seeded in a T25 culture flask and a 50 µl sample from the culture supernatant was collected 1 h post seeding. Thereafter, a sample was collected every 24 h for seven days and stored at 2-8 °C to the end of the experiment. The supernatants were diluted 1:10,000 in dH_2O and boiled shortly, before they were analyzed by BKPyV qPCR. The result that was presented as genome equivalents (Geq) per ml supernatant, showed that there was a 10-fold increase in extracellular BKPyV DNA from day 0 to day 1, followed up by a slower increase up to day five (**Figure 4.4 A**). To analyze if there was a significant increase in BKPyV load from day to day, the change in BKPyV load was log transformed. The plot showed that there only was a significant increase ($log_{10}>0.5$) from day 0 (1h) to day one (24h) (**Figure 4.4 B**).

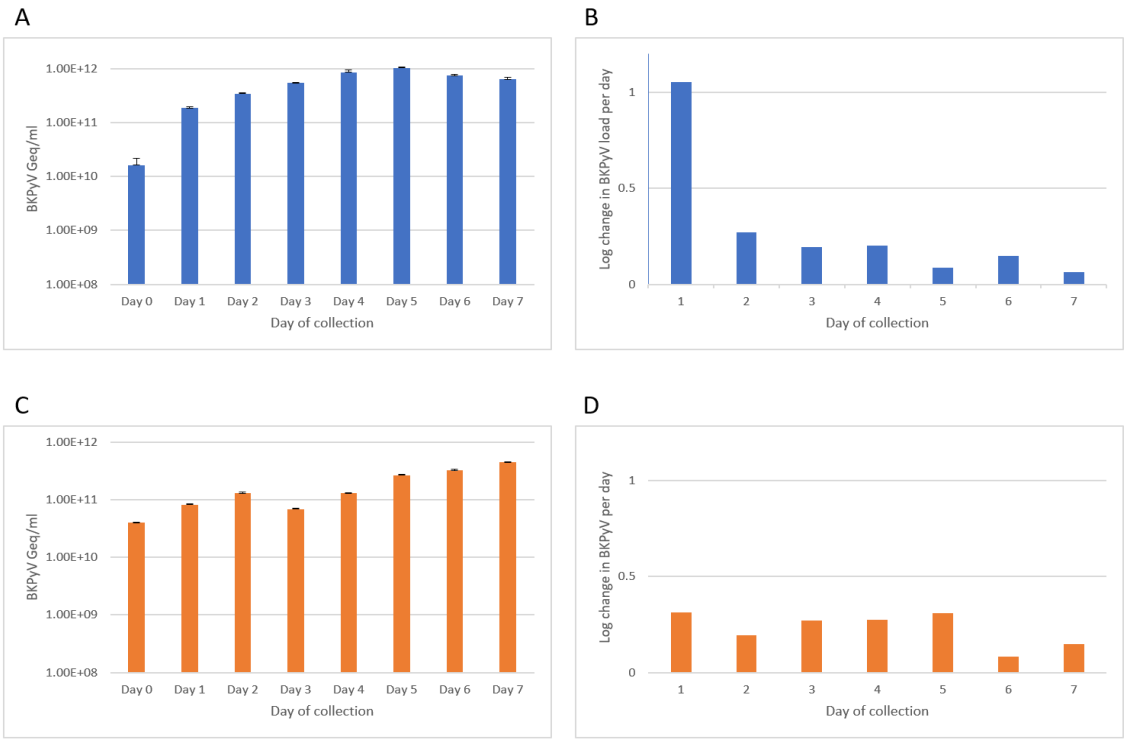

Figure 4.4. *qPCR of extracellular BKPyV DNA in U-2OS15E culture flasks.* ***(A-B)*** *Cells were seeded out on day 0. A sample was collected 1 h after seeding and a new sample was collected every 24 h for seven days. Change in extracellular BKPyV DNA was log transformed. Log_{10} > 0.5 indicates a significant increase in BKPyV.* ***(C-D)*** *Cell culture media was replaced on day 0. Samples were collected in the same manner as described for* ***(A-B)****. The standard deviation in* ***(A)*** *and* ***(C)*** *is calculated from the PCR run with three triplets of each sample.*
Optimally, these experiments should be repeated at least twice each.

Because the largest release of BKPyV DNA was found from day 0 to day one, i.e. directly after trypsinization of the cells, we decided to investigate the extracellular BKPyV load differently. Again, the cells were seeded in a T25 flask, but this time grown to >80% confluence. The culture supernatant was discarded, and cells were washed once in PBS before new media was added. Similar to the previous experiment, the first sample (day 0) was collected 1 h after addition of new media, and a new sample was collected every 24 h for seven days. This time BKPyV qPCR found no significant increase in BKPyV load from day 0 to day one, but the viral load increased slowly and was about 10 -fold increased by day 7 (**Figure 4.4 C** and **4.4 D**).

We concluded that somewhere between 29% and 78 % of U-2OS15E cells were infected with BKPyV depending on the method used. Trypsinization of the cells seemed to cause the largest release of BKPyV DNA. The extracellular BKPyV load was slowly but continuously increasing, suggesting a non-synchronized replication cycle of the infected cells.

Isolation of EVs from U-2OS and U-2OS15E by size exclusion chromatography and density gradient centrifugation

Viruses that establish persistent and chronic infections may use EVs to enhance establishment and maintenance of the infection [82]. We therefore wanted to investigate and compare the EVs released from U-2OS and U-2OS15E cells. Purification of EVs from U-2OS and U-2OS15E cell cultures was performed as shown in **Figure 4.5**. In brief, cells were grown to 90-100% confluence and incubated in exosome depleted growth medium for 2 days. On day two, conditioned medium was collected in 50 ml centrifuge tubes. Cells and debris was removed by a first centrifugation step at 300g. The supernatant was transferred to a clean vial and this was followed by centrifugation at 2000g. Again, the pellet was discarded. Next, approximately 100

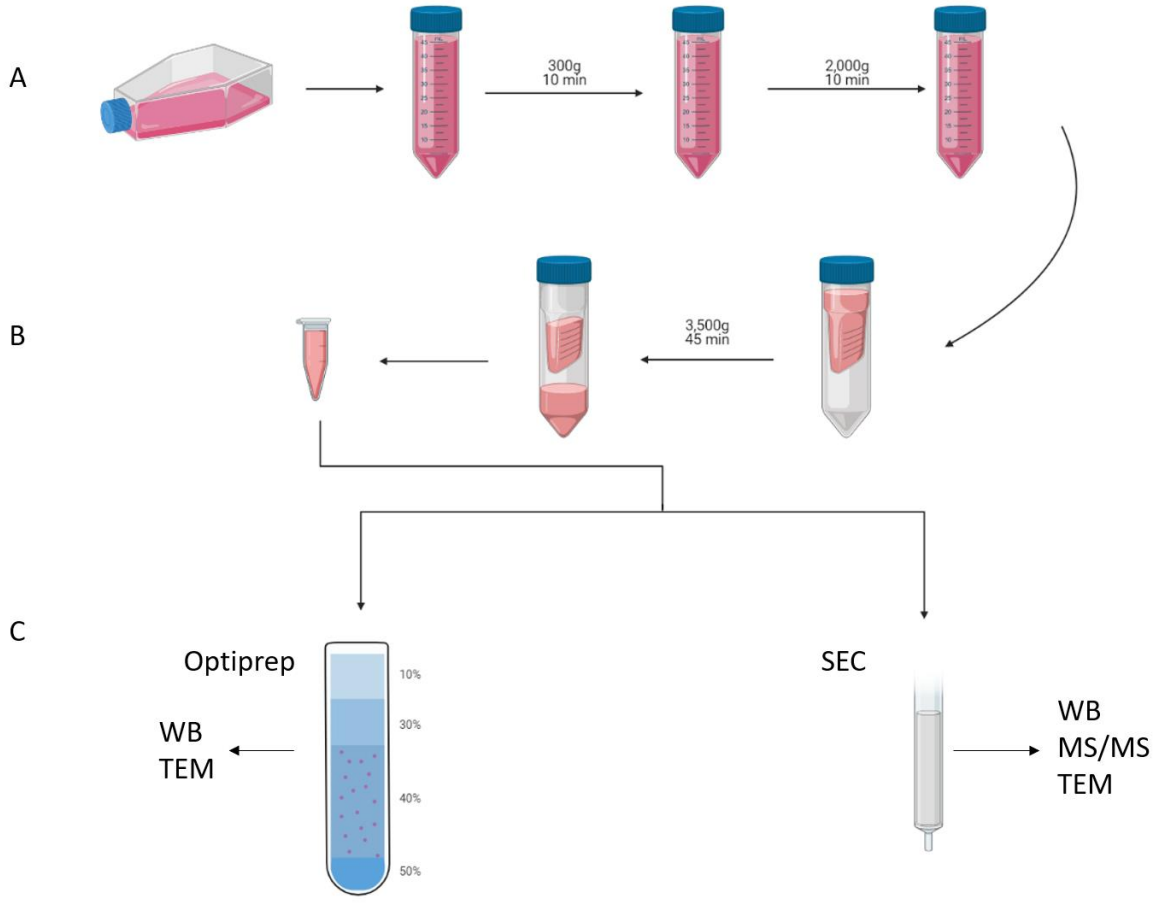

Figure 4.5. *A graphical presentation of the experimental workflow to purify vesicles from U-2OS and U-2OS15E.* ***(A)*** *After collection of cell culture media, cells, debris, and large vesicles were removed by low-speed differential centrifugation.* ***(B)*** *Ultrafiltration to concentrate vesicles. Supernatant from (A) was filtered with a 10 kDa cellulose filter to concentrate EVs.* ***(C)*** *Isolation of EVs. Density gradient centrifugation with OptiPrep™ and size exclusion chromatography were performed to purify the vesicles and do further analysis of EVs. Image is generated in BioRender.*

ml supernatant, from each respective cell culture, was concentrated to ~2 ml by ultrafiltration with a 10 kDa filter at 3,500g. Purification of EVs from the concentrate was done either by SEC or by density gradient centrifugation using OptiPrep. Purified EVs were further analyzed by performing western blot, TEM and mass-spectrometry.

For isolation of EVs by SEC, we used commercial SEC-columns. In total 24 fractions of 0.5 ml each were collected. According to the manufacturer, EVs were expected to mainly be in fraction 7 to 11. Following SEC on concentrated supernatants from U-2OS15E and U-2OS, fractions 5 to 13 were therefore analyzed by western blot. In short, the proteins were separated on a non-reducing gel, blotted onto a membrane and incubated with antibodies directed against the tetraspanins CD63 and CD9, which are commonly used as markers for exosomes. The antibodies only work properly on proteins that have not been reduced. CD63 has an expected molecular weight of 25 kDa, but typically gives smeared bands between 25 and 70 kDa due to post-translational modifications. We could detect CD63 with the expected size in fraction 6 to 11 from U-2OS (**Figure 4.6 A**), and fractions 5 to 11 from U-2OS15E supernatants (**Figure 4.6 B**). Using supernatant from U-2OS, CD63 peaked in fractions 6 to 9, but when using supernatants from U-2OS15E, CD63 peaked in fractions 5 to 8 i.e. being one fraction shifted. CD9 has an expected molecular weight of 25 kDa. There was no signal for CD9, even when the signal in the green channel was increased to maximum. In order to investigate if U-2OS cells express CD9, western blot was performed on whole cell lysates from U-2OS cells. In addition, 45 µl combined SEC-fractions (fraction 6 to 9) from another EV experiment with U-2OS and U-2OS15E were included. A strong CD9 band with the expected molecular weight was detected in the lane of the U-2OS lysate (**Figure 4.6 D**), clearly demonstrating that U-2OS express CD9. This time there was also a weak CD9 band in the lane with the combined U-2OS EV fractions after maximizing the signal of the green channel, and a barely detectable signal in U-2OS15E fractions (**Figure 4.6 D**).

Although CD63 is commonly used as a marker of exosomes, it is probably not expressed on all different EVs. We wanted to investigate the isolation method for all EVs, including MVs and apoptotic bodies. We therefore decided to investigate the fractions with an alternative method. The relative protein content in SEC fractions from U-2OS was determined by measuring absorbance at 280 nm. Determination of protein content by measuring A280 is based on absorbance of UV light by the aromatic amino acids tyrosine and tryptophan, as well as disulfide bonded cysteine [83]. A small peak was detected in fraction 7 to 8, and a larger peak

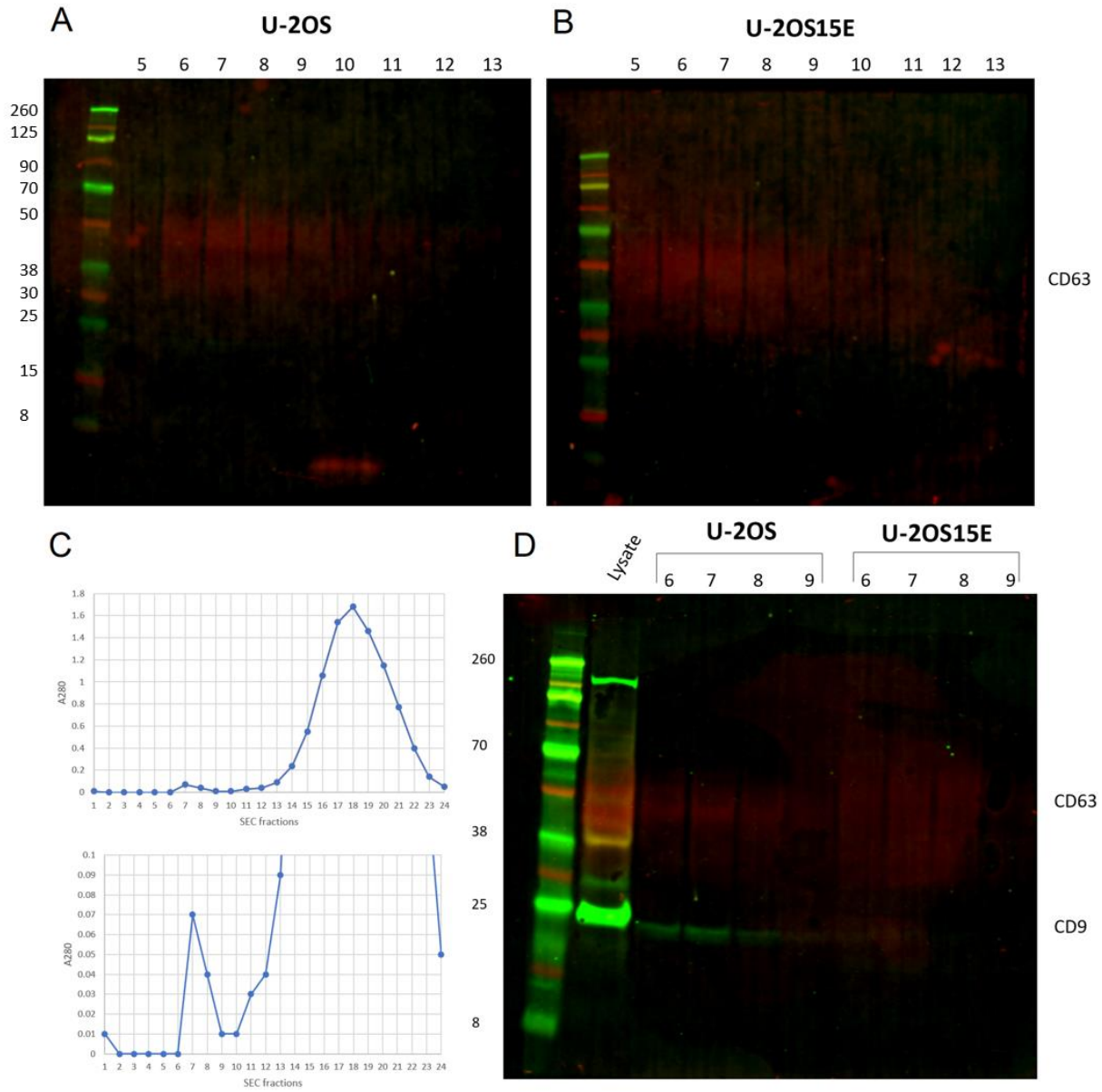

Figure 4.6 *Demonstration of EVs in SEC fractions.* ***(A-B)*** *Western blot analysis of SEC fractions from U-2OS and U-2OS15E, respectively, with antibodies directed against CD63 and CD9.* ***(C)*** *Absorbance at 280 nm was measured of SEC fractions from purification of U-2OS EVs to determine relative protein content in the different fractions.* ***(D)*** *Whole cell lysate from U-2OS and SEC fractions 6-9 from U-2OS and U-2OS15E was loaded on the same gel for western blot analysis. Signal from the green channel (800 nm) was magnified to look for presence of CD9 in SEC fractions.*

starting from fraction 13 and peaking in fraction 18 (**Figure 4.6 C**). This suggested that the majority of EVs were in fractions 7 and 8, while the contaminating proteins, that were of smaller size and therefore needed more time to pass through the column, were mainly found in fractions 13 to 24.

Previously, Herpes simplex virus 1 (HSV-1) infected cells were reported to release EVs containing STING, contributing to an antiviral response in the cells receiving these EVs [43].

We therefore decided to investigate if EVs released from U-2OS15E but not from U-2OS contained STING. This time we used SEC fraction 5 to 10 that were pooled and concentrated with a 10 kDa filter. Since the antibody for STING only could be used on reduced proteins, we this time could not identify EVs by CD63 but had to use other EV markers. Moreover, we also investigated the presence of BKPyV VP1 and agnoprotein. The western blot was performed in a stepwise manner. First, a monoclonal rabbit antibody against annexin A1, a polyclonal rabbit serum against LC3B and a monoclonal mouse anti-VP1 antibody was used (**Figure 4.7 A-C**). While annexin A1, molecular weight of 35-40 kDa, has recently been suggested as a specific

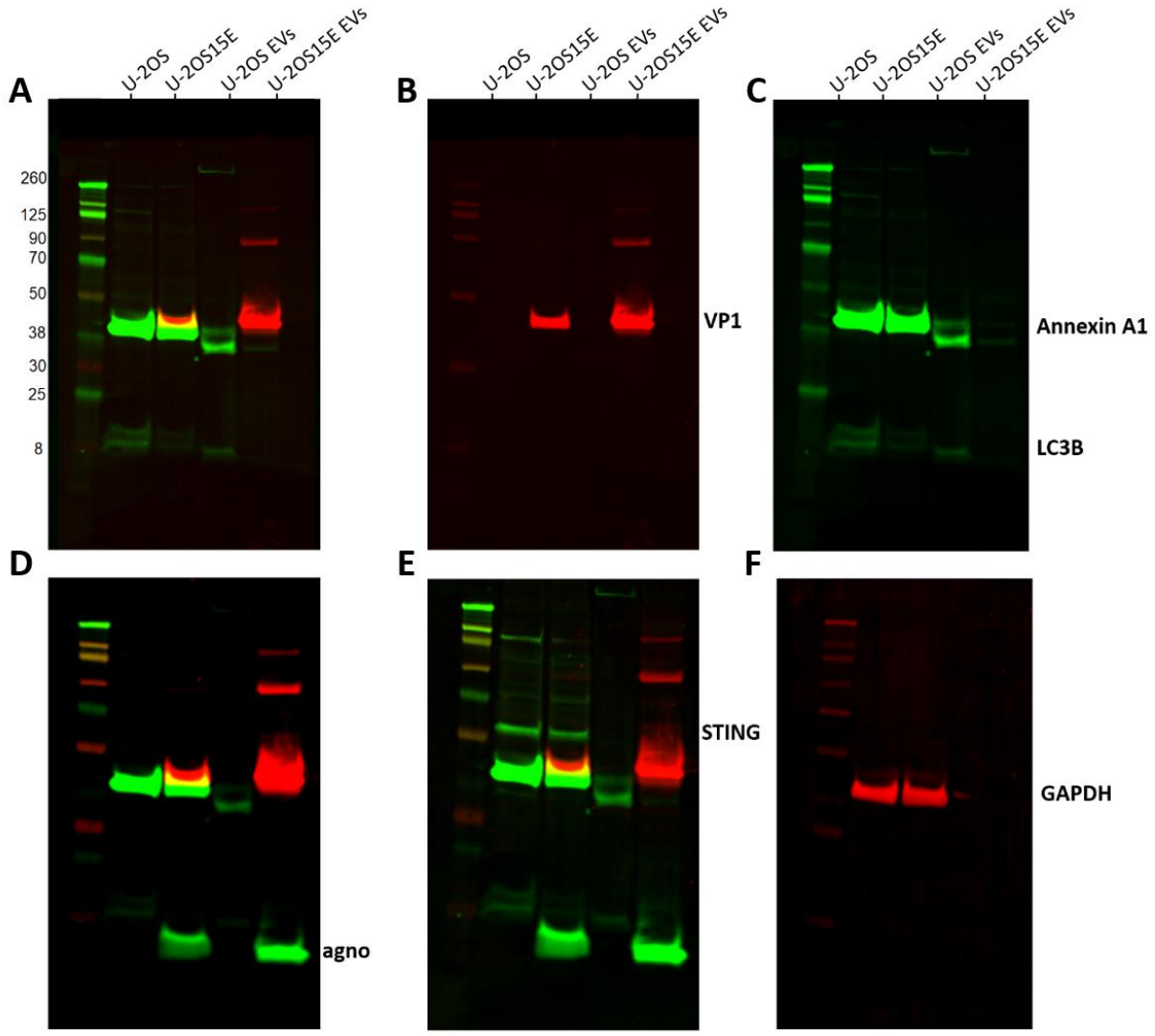

Figure 4.7. *Western blot analysis of EVs and whole cell lysates from U-2OS and U-2OS15E. For cell lysates 15 µg proteins were loaded per lane, and for EVs, 5 µg per lane.* ***(A-C)*** *Antibodies against annexin A1 (rabbit monoclonal), LC3B (rabbit polyclonal) and VP1 (mouse monoclonal) were combined.* ***(D)*** *BKPyV-agno antiserum (rabbit polyclonal),* ***(E)*** *followed up with addition of STING (rabbit polyclonal) antiserum.* ***(F)*** *To avoid misinterpretation with GAPDH (mouse monoclonal) and VP1, blotting with GAPDH was done on a separate memb. As secondary antibodies 800CW anti-rabbit IgG (green) and 680LT anti-mouse (red) were used. The protein ladder was 928-60000 (LI-COR).*

marker for MVs [55], LC3B, molecular weight of 17 kDa, is a common marker for autophagy that has also been detected in EVs [84]. The annexin A1 antibody gave two bands with molecular weight of ~37 and ~33 kDa, respectively, when EVs from U-2OS and U-2OS15E were used (**Figure 4.7 C**). Of note, the bands from U-2OS were much stronger than the bands from U-2OS15E. When cell lysates from U-2OS and U-2OS15E were used, both gave only one band of molecular weight ~37 kDa and they were of similar intensity (**Figure 4.7 C**), suggesting that annexin A1 is expressed at the same level in U-2OS and U-2OS15E cells. When EVs from U-2OS were used, the LC3B antibody gave a band of the expected size, but no band was detected when EVs from U-2OS15E were analyzed (**Figure 4.7 C**). However, cell lysate from both U-2OS and U-2OS15E gave LC3B bands, but they were weaker from U-2OS15E (**Figure 4.7 C**). EVs from U-2OS15E and U-2OS15E lysates both gave a VP1 band of the expected molecular weight (**Figure 4.7 B**). As expected, no positive VP1 band was seen when EVs or lysate from U-2OS were used.

Next, two polyclonal rabbit sera against agnoprotein and STING, respectively, were added in a stepwise manner. Similar to results with VP1 antibody, sera against agnoprotein demonstrated agnoprotein in EVs and lysate from U-2OS15E but not from U-2OS (**Figure 4.7 D**). No STING band was detected when EVs from U-2OS or U-2OS15E were used (**Figure 4.7 E**). However, using whole cell lysates, several bands with a slightly higher molecular weight than the expected 42 kDa was observed (**Figure 4.7 E**). This could be STING but we could not rule out unspecific staining. GAPDH is a cytoplasmic protein that should not be detected in exosomes [55], but sometimes MVs and usually in apoptotic bodies. In order to test the purity of the EVs, a monoclonal mouse antibody directed against GAPDH was used. However, since GAPDH and VP1 have a similar molecular weight (36 kDa and 40 kDa, respectively), blotting was done on a separate membrane (**Figure 4.7 F**). No GAPDH was detected in EVs but in U-2OS and U-2OS15E cell lysates, as expected. The lack of GAPDH in EVs suggests that we did not isolate apoptotic bodies. We also used antibodies against flotillin-1 and ALIX, two exosome markers, but could not detect these proteins in EVs or cell lysates from U-2OS or U-2OS15E (results not shown).

In summary, western blot analysis demonstrated that EVs from U-2OS and U-2OS15E were successfully purified by SEC, as we could detect the EV markers CD63, annexin A1, and LC3B, but not the cytoplasmic marker GAPDH. We were unable to detect the EV markers flotillin-1 and ALIX. Interestingly, we could only detect CD9 in EVs from U-2OS and not U-2OS15E, and EVs from U-2OS apparently contained more annexin A1 and LC3B compared to EVs from

U-2OS15E. This in spite of the fact that at least for annexin A1, similar amounts were found in the cell lysates from U-2OS and U-2OS15E. Finally, we detected the BKPyV viral proteins VP1 and agnoprotein in EVs secreted by U-2OS15E.

In order to assess the morphology of EVs from combined SEC fractions from U-2OS and U-2OS15E, respectively, negative staining followed by TEM was performed. While exosomes are described to be small (30-150 nm) and with a round shape, MVs vary largely in both size (100 nm - 1 µm) and shape. TEM imaging shows a mixed population of EVs thar varied in size and shape for both U-2OS (**Figure 4.8**) and U-2OS15E (**Figure 4.9**). The largest identified vesicle from U-2OS was round and approximately 300 nm (**Figure 4.8**). Although the presence of EVs larger than 100 nm were abundant, most of the EVs from U-2OS were <100 nm and circular, which indicates that the majority of isolated vesicles are exosomes. Similar results were obtained with U-2OS15E (**Figure 4.9**). We could not clearly observe free BKPyV virions or BKPyV inside EVs.

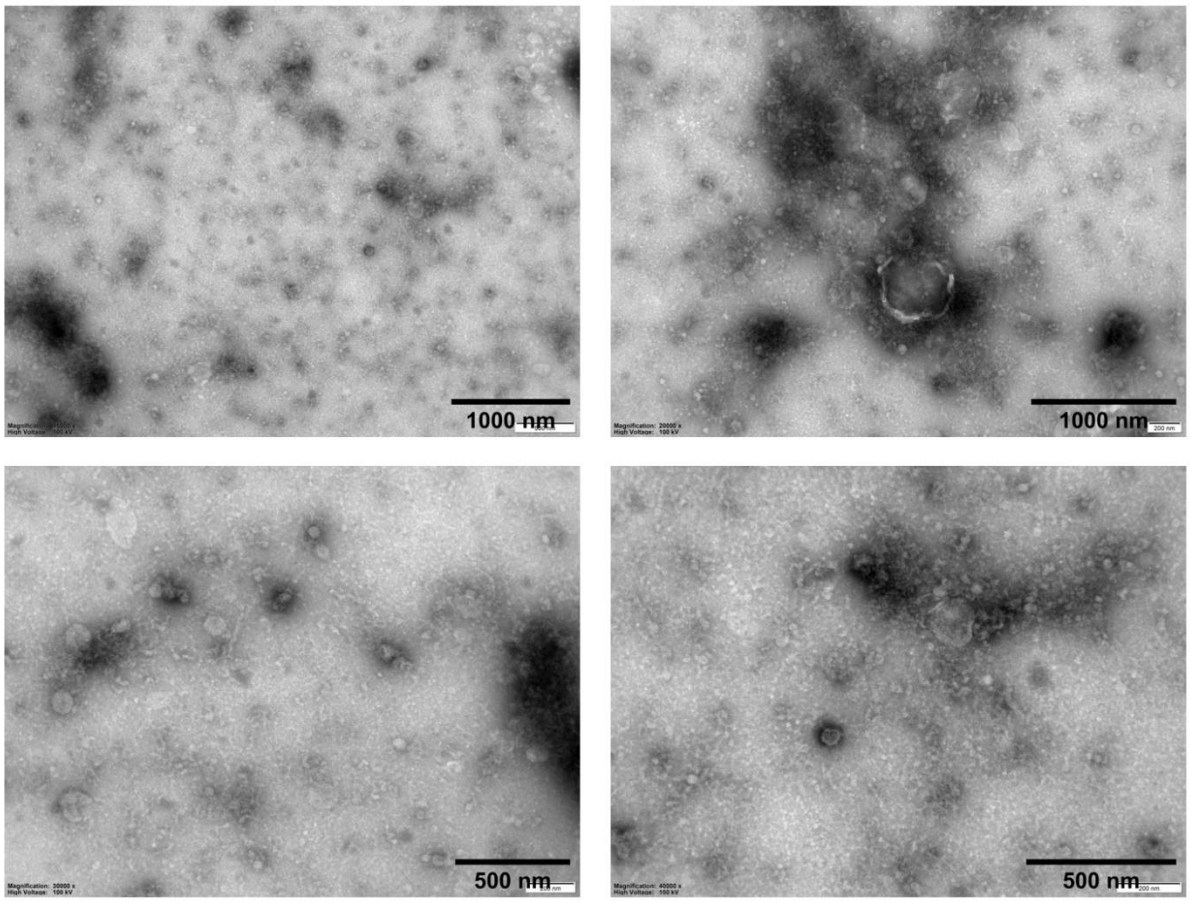

Figure 4.8 *Transmission electron microscopy of SEC-purified U-2OS EVs. SEC fractions 5-10 were pooled together and concentrated before negative staining with 1% uranyl acetate.*

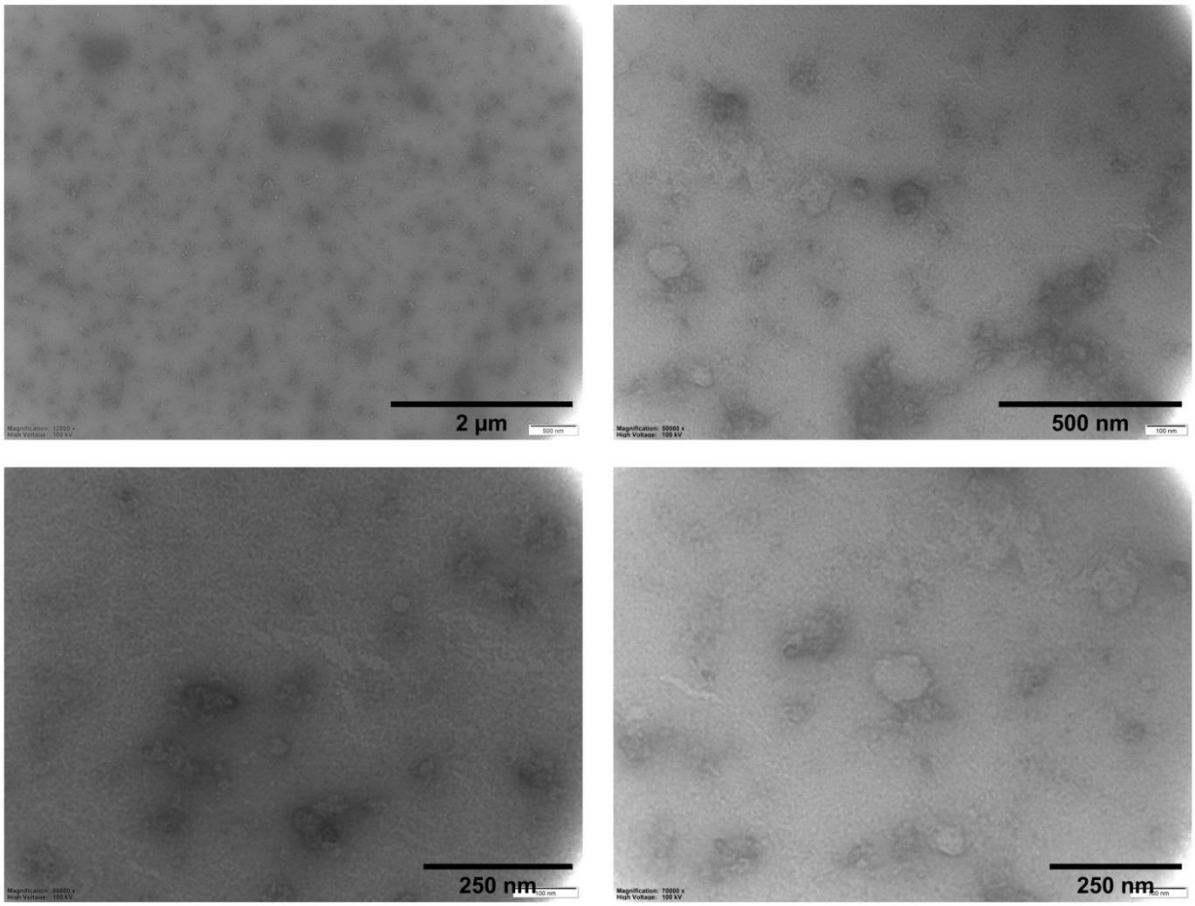

Figure 4.9 *Transmission electron microscopy of SEC-purified U-2OS15E EVs. SEC fractions 5-10 were pooled together and concentrated before negative staining.*

Our final goal was to compare EVs from U-2OS and U-2OS15E by LC-MS/MS. Although TEM did not clearly show viral particles, the research group has previously observed BKPyV, which has a size similar to exosomes, in SEC EV-fractions (Henriksen and Rinaldo, personal communication). Our finding of VP1 in EVs from U-2OS15E could therefore result from contamination by viral particles or be VP1 molecules on the inside or outside of the EVs. To make sure that we could separate viral particles from EVs with OptiPrep, we decided to do a controlled experiment. In this experiment purified BKPyV ($5x10^7$ Geq) was added to EVs from U-2OS before this was mixed with OptiPrep to a final concentration of 40%. OptiPrep solutions of concentration 50%, 30% and 10% were also made and were together with the sample, loaded into a centrifuge tube in the order of decreasing OptiPrep concentration (**Figure 4.10 D**). After centrifugation, 10 fractions of 500 µl were collected from the top of the tube. The buoyant density of all 10 fractions was measured with NanoDrop One™. A buoyant density from 1.05 g/ml to 1.32 g/ml was measured. Based on previously published studies (**Table 1**), EVs from

conditioned media would be expected at a density around 1.06-1.17 g/ml which correlated to fraction 3 and 4 (**Figure 4.10 B**).

Next, 45 µl of each fraction, except fraction 1 and 2 that were combined, were loaded on a non-reducing gel and on a reducing gel. After blotting, the membrane from the non-reducing gel was subjected to antibodies directed against CD9 and CD63 (**Figure 4.10 A**), and the membrane from the reducing gel was subjected to antibodies directed against VP1 and annexin A1 (**Figure 4.10 C**). A strong smeared signal for CD63, within the expected molecular weight, was found from fraction 3 (1.111 g/ml) (**Figure 4.10 A-B**), and a somewhat weaker signal from fraction 4 (1.158 g/ml). However, no signal was observed for CD9. In the reducing western blot analysis, annexin A1 was found in fraction 4 to 9. VP1 which has a molecular weight of 41 kDa was observed in fraction 3 and 4 and weak signal was seen in fraction 5, suggesting that the viral particles were not separated from EVs.

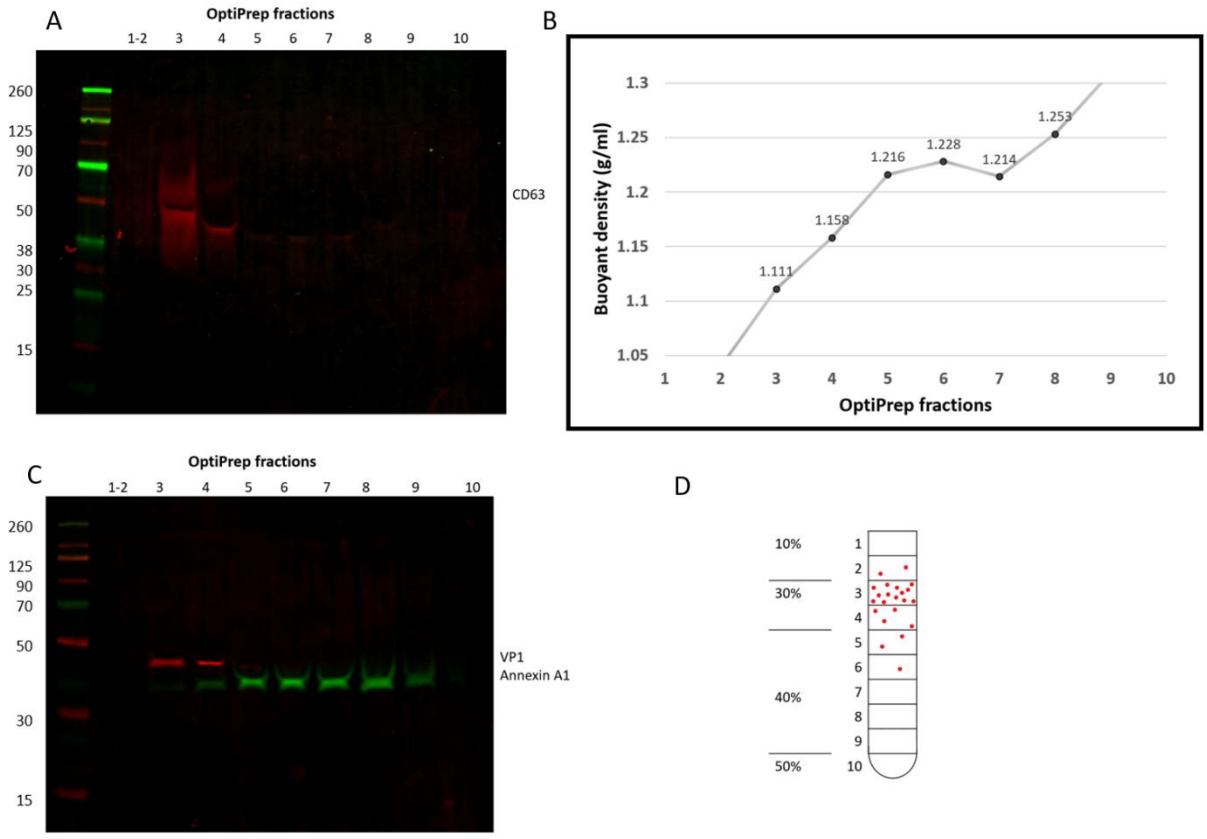

Figure 4.10. (A) *Western blot analysis of OptiPrep fractions under non-reducing conditions with primary antibodies against CD63 (mouse monoclonal) and CD9 (rabbit monoclonal).* ***(B)*** *Buoyant densities of Optiprep fractions measured with NanoDrop One™.* ***(C)*** *Western blot analysis of OptiPrep fraction under reducing conditions with antibodies against annexin A1 (rabbit monoclonal) and VP1 (mouse monoclonal).* ***(D)*** *Representation of the distribution of EVs after density gradient centrifugation.*

In order to study the EV distribution and morphology in each OptiPrep fraction, negative staining followed by TEM was performed. Prior to the negative staining, the fractions were washed 10 times in PBS and centrifuged in a 10 kDa filter in order to remove the OptiPrep. In fraction 1 (OptiPrep 10%), there was no EV-like structure with the desired size range (30-1000 nm), however, a large membrane-enclosed structure was observed (**Figure 4.11**). The size of about 1,5 µm and the shape might indicate that this was an apoptotic body. Apoptotic bodies have a size range of 400 nm to 5 µm and a heterogenous shape and density. In fraction 2, few round structures of approximately 200 nm were observed at low magnification (7000x), however, by increasing the magnification, the structures got blurred out. The most abundantly enriched fraction with EVs was fraction 3 (**Figure 4.11** and **4.12**). Here, a wide variety of EVs were observed with a size range of 50-200 nm. Most EVs observed in fraction 3 had a round uniform shape. In fraction 4, some EVs were observed with a similar morphology to those of

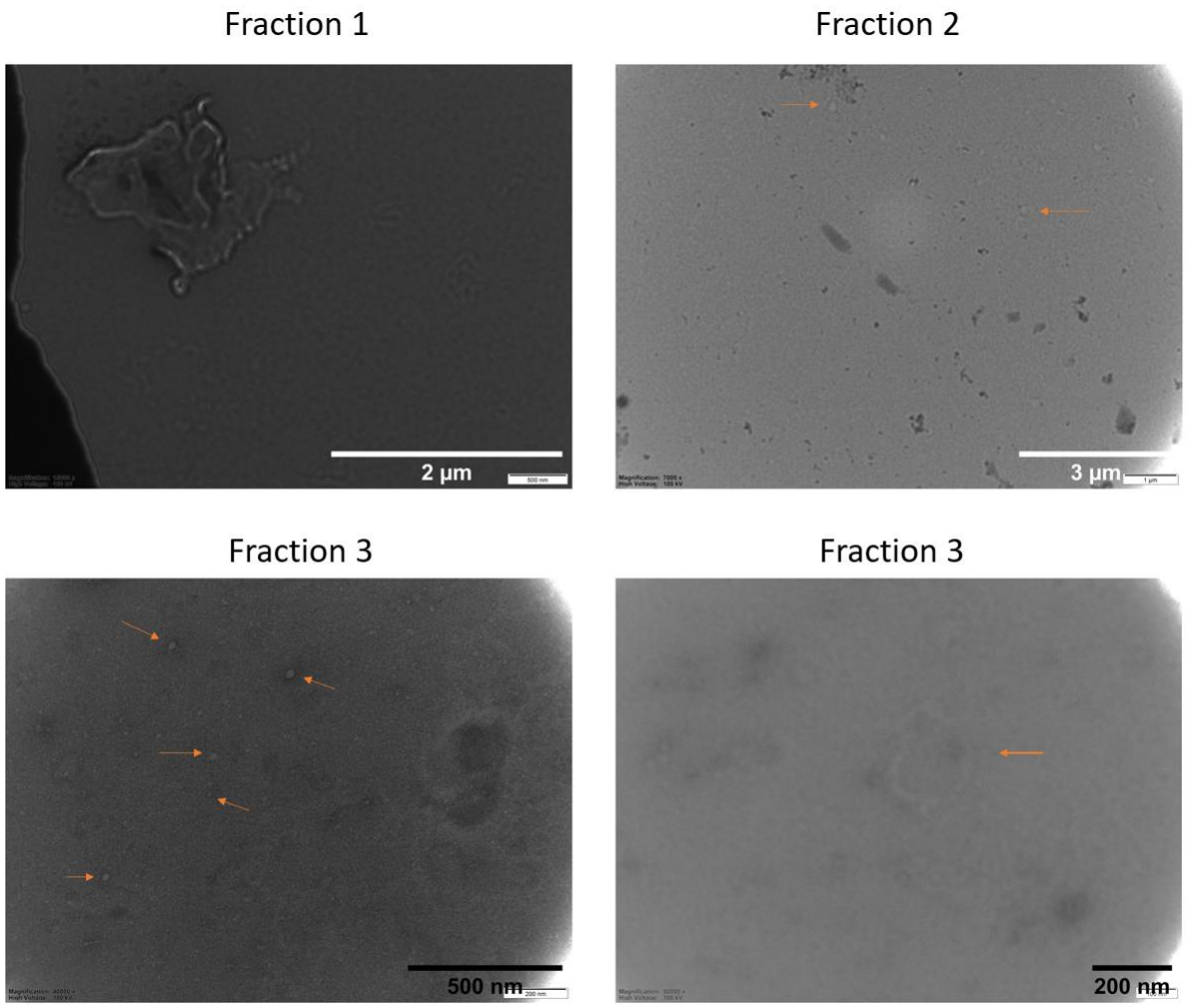

Figure 4.11. *Transmission electron microscopy of OptiPrep fractions 1-3 containing U-2OS EVs after negative staining. Orange arrows indicate EVs.*

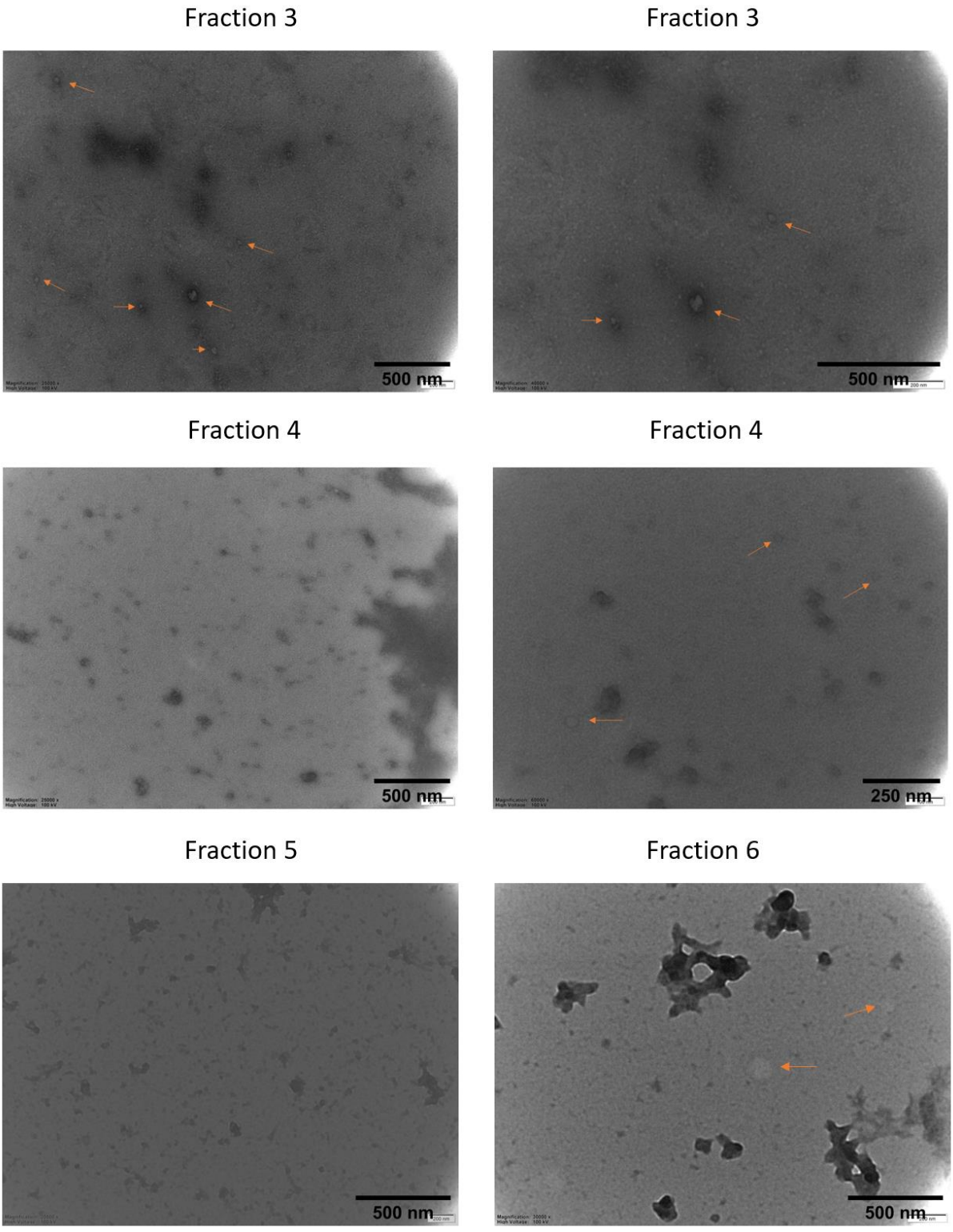

Figure 4.12. *Transmission electron microscopy of OptiPrep fractions 3-6 containing U-2OS EVs after negative staining. Orange arrows indicate EVs.*

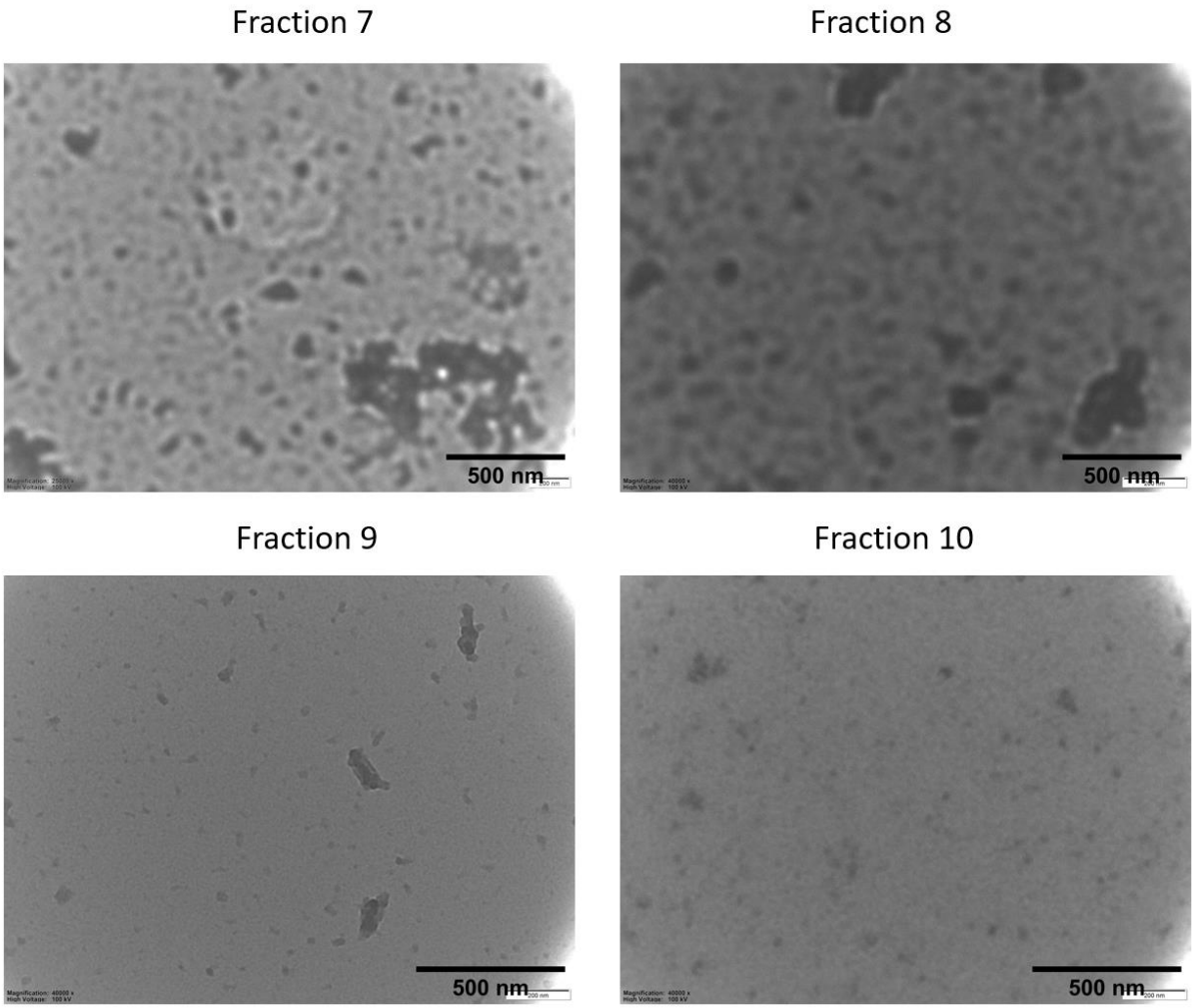

Figure 4.13. *Transmission electron microscopy of OptiPrep fractions 7-10 containing U-2OS EVs.*

fraction 3, however, from fraction 4 and with increasing OptiPrep density it was harder to get structures in focus. Unfortunately, we had not been able to remove all OptiPrep even after 10 cycles of washing which resulted in lots of artefacts for fractions above 4. No EVs were possible to detect in fraction 5, however, some EVs with the size of approximately 100 nm were observed in fraction 6 (**Figure 4.12**). Using fractions 7-10 it was impossible to focus due to the high concentration of OptiPrep (**Figure 4.13**).

As shown in **Figure 4.10 D**, our western blot analysis and buoyant density measurements, EVs are mainly contained in fraction 3 and 4. TEM seemed to correlate with this, as most EVs were detected in fraction 3 and 4. Some particles with round in shape and a diameter of ~100 nm that resembles membrane enclosed vesicles were detected in fraction 6.

To summarize this part of the EV isolation, the TEM imaging revealed a mixed population of exosomes and MVs and correlated with western blot results. However, solely based on morphology, it was challenging to characterize EVs. The tested OptiPrep gradient was not able to separate exosomes from BKPyV but could at least partly separate the endosome-derived exosomes from the plasma-membrane-derived microvesicles, except in fraction 4 where both CD63 and annexin A1 was present (**Figure 4.10 A** and **C)**. Since we wanted to compare all sized EVs from U-2OS and U-2OS15E by liquid chromatography-tandem mass spectrometry (LC-MS/MS), we decided to continue with SEC-purified EVs.

Proteomic profiling of EVs from U-2OS and U-2OS15E

To assess the protein composition of SEC-purified EVs, the EV membranes were lysed and proteins precipitated and digested. Protein profiling of U-2OS and U-2OS15E was performed by LC-MS/MS. LC-MS/MS identified a total of 3227 proteins in which 2805 proteins were identified in EVs from both U-2OS and U-2OS15E (**Figure 4.14 A**). Among the uniquely identified proteins in U-2OS15E, five different BKPyV proteins were detected (**Table 4**), thereby functioning as a quality control.

The identified proteins were grouped according to their cellular location, biological processes, and molecular function in FunRich software by searching protein accessions against the Gene Ontology (GO) database. Briefly, proteins or genes are annotated by different GO-terms according to their cellular component, biological process, and molecular function. One protein can be annotated to several GO-terms, making it possible to group large samples of proteins or genes into different categories

Table 4. *BKPyV viral proteins detected in U-2OS15E EVs by LC-MS/MS*

Identifier	Protein description
118752	Agnoprotein
112419644	Small T antigen
752784399	Large T antigen
16930348	VP1
115343476	VP2

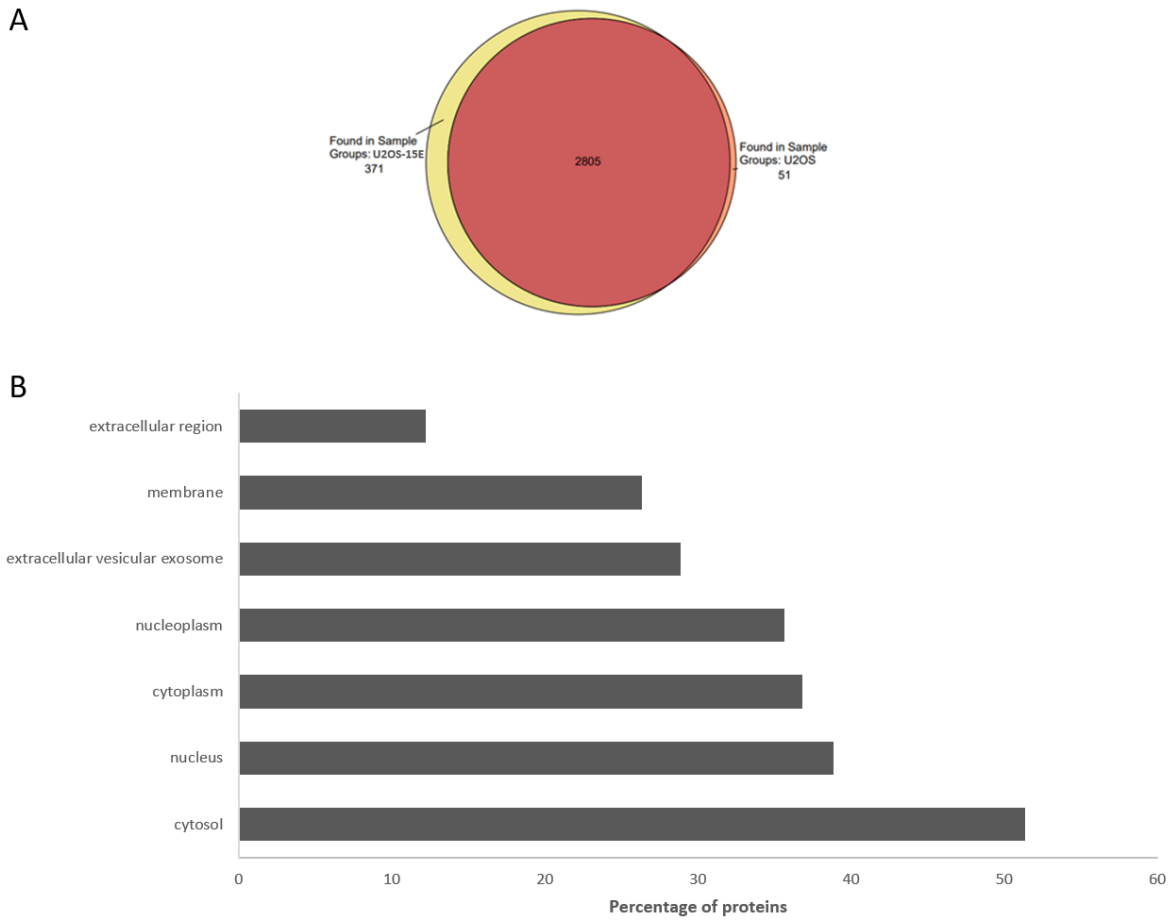

Figure 4.14. *Proteomic profiling of EVs from U-2OS and U-2OS15E.* ***(A)*** *Venn diagram shows the total of 3227 proteins identified. 371 unique proteins were identified in U-2OS15E EVs and 51 unique proteins were identified in U-2OS EVs.* ***(B)*** *The bar chart shows proteins grouped according to their cellular component. The X-axis shows percentage of proteins identified in each group. Some proteins can be present in several groups.*

Looking at all proteins identified in EVs from U-2OS and U-2OS15E, cellular component-based characterization revealed that more than 50% originated from the cytosol and approximately 30% had been previously described in EVs (**Figure 4.14 B**). Further characterization of proteins according to biological process and molecular function was done in FunRich. First looking at the biological process, the largest proportion of proteins from both cell lines, in total 220 proteins, were proteins that normally are involved in viral reproduction (**Figure 4.15 A**). The six most abundantly expressed proteins involved in this GO term included the phospholipid binding annexin A2, the heat shock proteins HSP90AA1 and HSPA8, the E3 ligase UBR4, vimentin and exportin-1. These proteins are also associated with the biological processes: cell organization, cell proliferation, protein metabolism, transport, cell-to-cell signaling and stress response. The second largest proportion, in total 214 proteins, are proteins normally involved in neutrophil degranulation. Neutrophil cells are an important part of the innate immune system. In order to kill invading microorganisms, they can release vesicles also called granules that contain antimicrobial proteins, and this is called degranulation [85]. This process is resulting in the exocytosis or exposure of membrane proteins, processes that also occur in other cells. Neutrophil degranulation has two ancestral go terms that are "cellular localization" and "immune system response". This is followed by proteins involved in nuclear mRNA splicing, post translational protein modification and proteins involved in cell division.

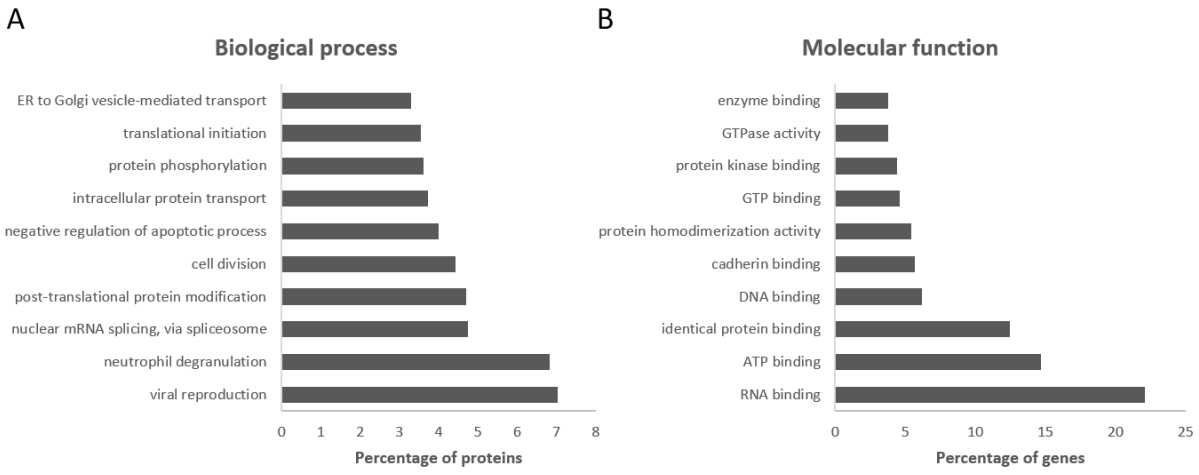

Figure 4.15. *GO-term based characterization of proteins found in EVs from U-2OS and U-2OS15E. Proteins are grouped according to their **(A)** biological process and **(B)** molecular function. The 10 most numerous groups are chosen.*

Next, looking at the molecular functions of the protein cargo of EVs, a large number of proteins, in total 697, were involved in RNA binding (**Figure 4.15 B**). A GO term of particular interest is cadherin binding, which is a part of the ancestry GO term "adhesion molecule binding", and hence can be involved in vesicular transport. The 179 proteins involved in "cadherin binding" were grouped according to their cellular component, and 53 % of those proteins are annotated with the GO term "extracellular exosome" (**Figure 4.16**).

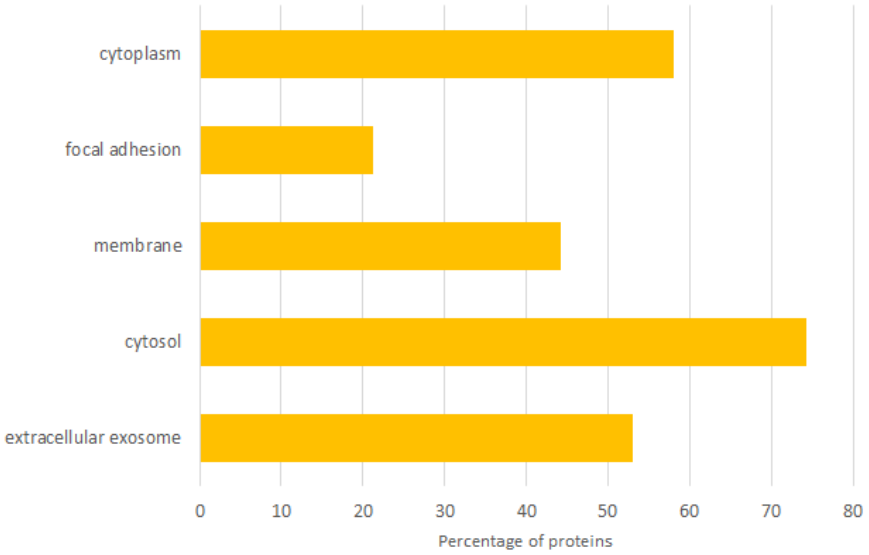

Figure 4.16. *GO term-based characterization of proteins involved in the molecular function "cadherin binding" according to their cellular component.*

To determine the differences in the protein cargo of EVs from U-2OS and U-2OS15E, enrichment analysis was performed in Proteome Discoverer™ v.2.5. Proteins were searched in GO database and grouped into GO terms based on the biological processes in which the proteins are involved. In total, 410 proteins are enriched in EVs from U-2OS15E, and 183 proteins are deprived compared to proteins found in EVs from U-2OS (**Figure 4.17**).

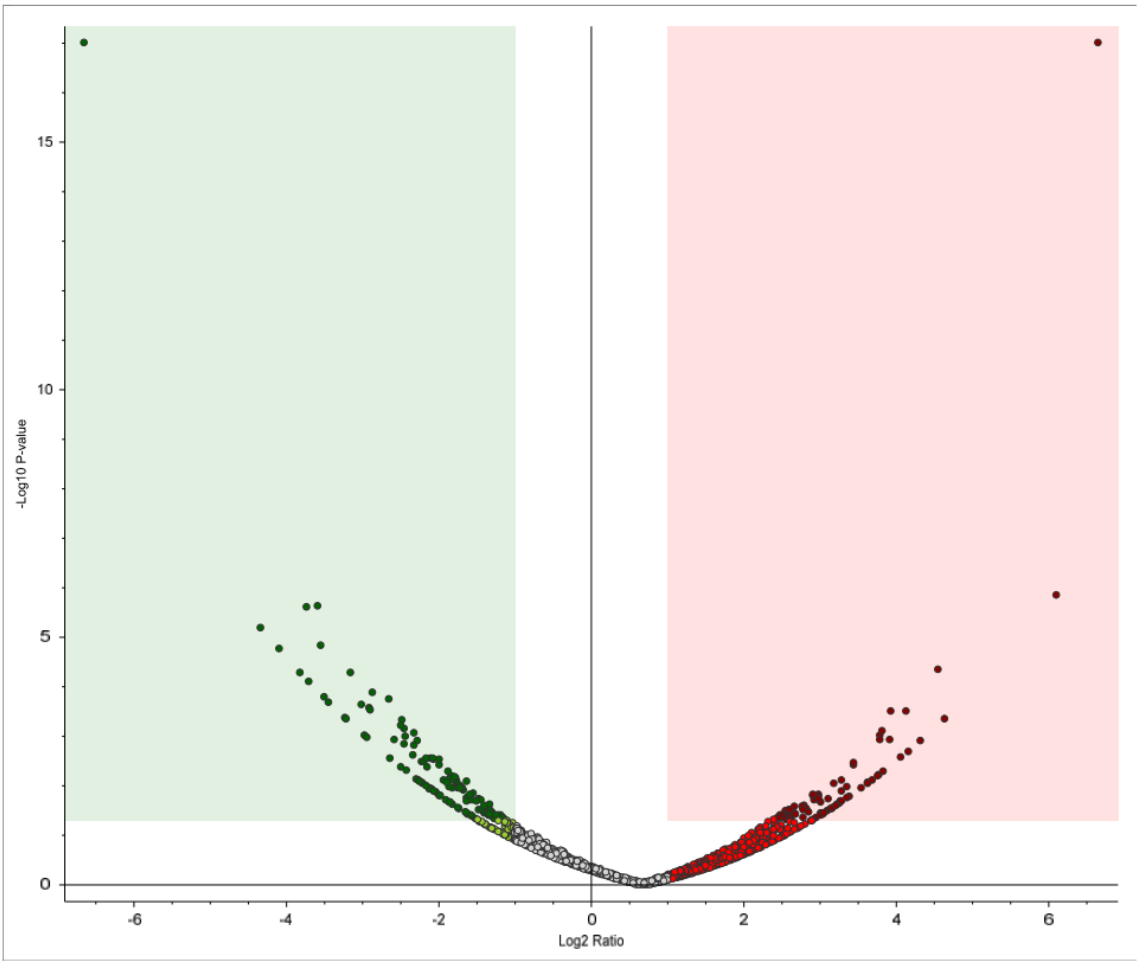

Figure 4.17. *Volcano plot of U-2OS15E vs. U-2OS. Proteins in the red area are enriched in EVs from U-2OS15E, and proteins in green area are deprived in EVs from U-2OS15E.*

Enrichment analysis revealed that the EVs from U-2OS15E were enriched in proteins involved in regulation of DNA recombination, DNA integrity checkpoint, mRNA catabolic process, Golgi organization, cell cycle checkpoint, viral transcription, protein targeting and localization to ER, and protein targeting to membrane (**Figure 4.18 A**).

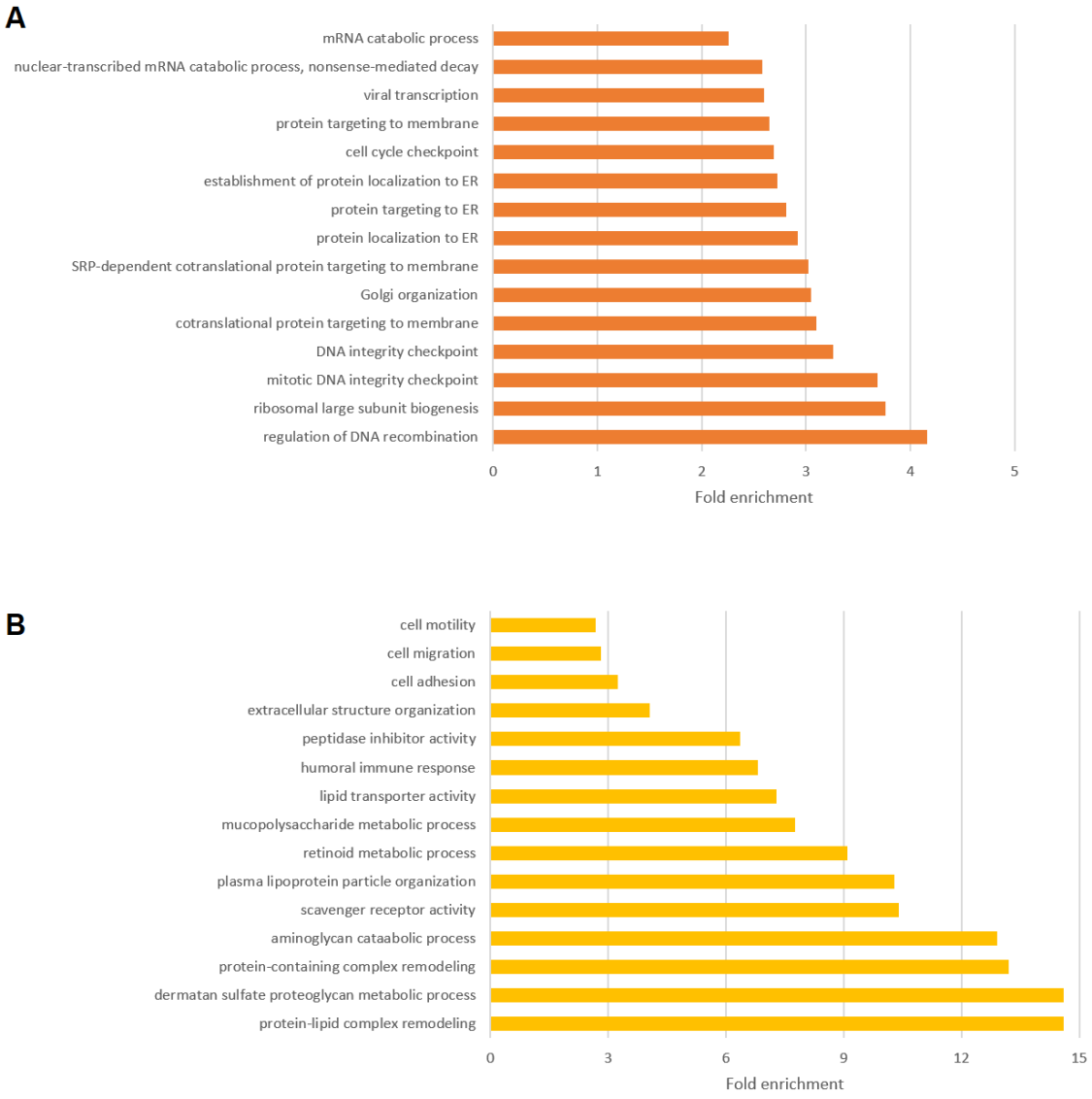

Figure 4.18. *Enrichment analysis of U-2OS15E EVs vs. U-2OS EVs. The 15 most abundantly enriched groups are included.* ***(A)*** *The bar chart shows enriched proteins in U-2OS15E grouped according to their biological processes.* ***(B)*** *The bar chart shows enriched proteins in U-2OS, i.e. deprived in U-2OS15E*

Table 5. *Table shows 20 abundantly enriched and 20 deprived proteins. Proteins written in bold are of particular interest, either due to their involvement in the cGAS-STING pathway, their involvement in cell cycle progression, or because they have been discussed earlier.*

Gene name	UniProt accession	Abundance ratio U-2OS15E/ U-2OS	Protein description
CDK5	Q00535	>100	Cyclin dependent-like kinase 5
GSDMD	P57764	>100	**Gasdermin-D**
CHUK	O15111	>100	**Inhibitor of NFκB kinase subunit alpha**
MAD2L2	Q9UI95	>100	**Mitotic spindle assembly checkpoint protein**
SYNJ2BP	P57105	>100	Synaptojanin-2-binding protein
LARP4	Q71RC2	>100	La-related protein 4
KIF22	Q14807	>100	**Kinesin-like-protein KIF22**
FAM111B	Q6SJ93	>100	Serine protease FAM111B
THOC1	Q96FV9	>100	THO complex subunit 1
ATP2B1	P20020	>100	Plasma membrane calcium transporting ATPase 1
SUCLG1	P53597	>100	Succinate-CoA ligase subunit alpha
RSP6KA3	P51812	>100	Ribosomal protein S6 kinase alpha-3
DIABLO	Q9NR28	>100	Diablo homolog
DNMBP	Q6XZF7	>100	Dynamin-binding protein
GTSE1	Q9NYZ3	>100	**G2 and S phase-expressed protein 1**
UBE3A	Q05086	>100	**Ubiquitin protein ligase E3A**
SEC22A	Q96IW7	>100	Vesicle trafficking protein SEC22a
CHD8	Q9HCK8	>100	Chromodomain-helicase-DNA-binding protein 8
GCC2	Q8IWJ2	>100	GRIP and coiled-coil domain containing protein 2
TAF6	P49848	>100	Transcription initiation factor TFIID subunit 6
EML6	Q6ZMW3	0.294	Echinoderm microtubule-associated protein-like 6
INHBA	P08476	0.361	Inhibin beta A chain
HBA1, HBA2	P69905	0.351	Hemoglobin subunit alpha
ITIH2	P19823	0.283	Inter-alpha-trypsin inhibitor heavy chain H2
FAM168A	Q92567	<0.01	FAM168A
VPS53	Q5VIR6	0.361	Vacuolar protein sorting-associated protein 53 homolog
EDIL3	O43854	0.05	EGF-like repeat and discoidin I-like protein 3
KPNA4	O00629	0.179	Importin subunit alpha-3
TINAGL1	Q9GZM7	0.217	Tubulointerstitial nephritis antigen-like protein
PGM2L1	Q6PCE3	0.263	Glucose-1,6-bisphosphate synthetase
GNB4	Q9HAV0	<0.01	Guanine nucleotide-binding protein subunit beta-4
C6	P13679	<0.01	Complement component C6
PRG4	Q92954	0.296	Proteoglycan 4
DOCK5	Q9H7D0	<0.01	Dedicator of cytokines protein 5
SPRYD7	Q5W111	<0.01	SPRY domain containing protein 7
SURF4	O15260	0.322	Surfeit locus protein 4
GPC4	O75487	0.302	Glypican-4
RASSF10	A6NK89	0.398	Ras association domain-containing protein 7
AHSG	P02765	0.234	Alpha-2-HS-glycoprotein
AMY1A	PODUB6	<0.01	Alpha-amylase 1A
CD9	P21926	0.283	**CD9 antigen**

We searched for ancestral charts in the GO database (QuickGO) for the biological processes shown in **Figure 4.18 A**. U-2OS15E EV cargo was found to be enriched in proteins involved in cell cycle phase transition, intracellular protein transport and RNA metabolism. Three of the most abundantly enriched proteins in U-2OS15E EVs were MAD2L2, KIF22 and GTSE1 (**Table 5**). These proteins are both involved in cell proliferation. For further enriched proteins, see **Table 5** and **Appendix B**.

Looking further into proteins enriched in U-2OS15E EV cargo involved in "viral transcription", 20 proteins were identified in which 17 proteins were 60S ribosomal proteins, two 40S ribosomal proteins and nuclear pore complex protein Nup50. The 17 ribosomal large subunit proteins were also represented in the GO term "ribosomal large subunit biogenesis".

On the other hand, proteins that were more frequently found in EVs from U-2OS than from U-2OS15E EVs were involved in extracellular matrix (ECM) remodeling, glycoprotein metabolism, plasma lipoproteins remodeling, humoral immunity, cell migration, cell adhesion, and cell motility (**Figure 4.18 B**). Proteins involved in the GO-term "humoral immune response" that were deprived in U-2OS15E included trypsin-3, CXCL14, C8B, glucose-6-phosphate isomerase, complement component C9, kininogen-1, IgL-L5, lactotransferin, immunoglobulin J chain. For further deprived proteins see **Table 5** and **Appendix B**.

We concluded that EVs secreted by U-2OS15E have a different protein content than EVs secreted by U-2OS. U-2OS15E EVs are enriched in proteins involved in cell cycle progression, RNA metabolism and also proteins found in the STING pathway. Moreover, EVs from U-2OS15E are deprived in proteins involved in ECM composition, some metabolic processes, and cell motility, adhesion and migration.

Discussion

BKPyV infects the majority of people worldwide and establishes a lifelong persistent infection in the epithelial cells of the renourinary tract. How the virus manages to escape immune detection and persist, is still poorly understood. Over the past decades, it has become clear that EVs are vital for intercellular transport and communication and evaluating their content may be important for understanding pathophysiological processes. In the present study, EVs were purified from the supernatant of U-2OS15E, a BKPyV-persistently infected osteosarcoma cell line, and from the ancestral non-metastatic cell line U-2OS, and the protein content was analyzed by label-free LC-MS/MS-based comparative quantitative proteomic analysis. This is the first proteomic study of EVs from U-2OS and U-2OS15E cells. Our major findings was that 410 proteins were enriched in EVs from U-2OS15E and this included 371 unique proteins. Many of these proteins were involved in **cell proliferation and cell cycle regulation** and some in **innate immunity**. The latter is of particular interest as this may give important clues to understand BKPyV-persistent infection.

LC-MC/MS total analysis

LC-MS/MS analysis of SEC-purified EVs from U-2OS and U-2OS15E detected in total 3227 proteins. The majority of proteins i.e. 2805 (87%) were found in EVs from both cell lines, 371 proteins (11.5%) were found only in EVs from U-2OS15E while 51 proteins (1.5%) were found only in EVs from U-2OS. In addition, 39 of the shared proteins were enriched in U-2OS15E EVs while 183 proteins were deprived. As BKPyV is known to express only seven viral proteins, the vast majority of these proteins are cellular. The result strongly suggests that BKPyV infection has a dramatic effect on the host cells.

The 3227 proteins identified in EVs from U-2OS and U-2OS15E (**Figure 4.14**), are grouped in different groups known to be involved in biological processes and molecular functions (**Figure 4.15**). Interestingly, the largest two groups of proteins are involved in viral reproduction (7%), and in RNA binding (22%). Proteins in this first group can be involved in all steps in the viral replication cycle, like viral entry, uncoating, genome replication, assembly and release. RNA binding proteins can interact with RNA through defined RNA-binding domains to regulate RNA metabolism and function and inversely, the RNA can bind to the RNA binding protein to affect its fate and function [86]. Since the 3227 proteins detected come from all EVs isolated

from uninfected U-2OS cells, uninfected U-2OS15E cells and BKPyV-infected U-2OS15E cells, it is probably of little value to discuss these proteins in detail. However, we noted that almost 30% of proteins have been previously described in EVs, which shows that our purification of EVs has been at least partly successful (**Figure 4.14 B**). Moreover, we noted that about 4% of proteins were negative regulators of the apoptotic process. When healthy cells are damaged by for instance UV radiation, apoptosis is normally triggered to prevent that damaged cells to develop into cancer cells. Cancer cells on the other hand are usually able to evade apoptosis and continue proliferating despite abnormalities. About 50% of human cancer cells have mutations inactivating the tumour suppressor p53. U-2OS are cancer cells but they seem to have wildtype p53 gene [87]. Our results suggest that U-2OS and/or U-2OS15E cells shed EVs with negative regulators of apoptosis, which may set neighbouring cells in an antiapoptotic state. This has previously been described for adipose-stem cells [88].

LC-MS/MS enrichment analysis

Enrichment analysis showed that 410 proteins are enriched in U-2OS15E EVs and 183 proteins are enriched in U-2OS EVs and thereby indirectly deprived in U-2OS15E EVs (**Figure 4.17**). The GO terms in which U-2OS15E EV cargo is most abundantly enriched, containing more than 4% of the proteins, was regulation of DNA recombination (**Figure 4.18 A**). DNA recombination involves the exchange of genetic material either between multiple chromosomes or between different regions of the same chromosome. The non-coding control region (NCCR) of BKPyV may be rearranged by DNA recombination during DNA replication. Rearranged BKPyV variant typically show increased viral replication and cytopathology [16]. The BKPyV strain used to generate U-2OS15E was BKPyV TU, a rearranged BKPyV variant. Unfortunately, we did not have time to DNA sequence the viral genome to check if further rearrangements have occurred. Recombination is also essential for repair of double strand DNA breaks. Defects in regulation of DNA recombination can lead to genomic instability and cancer predisposition [89]. If DNA damage in healthy cells is detected, this can lead to cell cycle arrest or apoptosis.

Cell proliferation and cell cycle control. Three proteins that were >100 fold enriched in EVs from U-2OS15E compared to U-2OS were MAD2L2, KIF22 and GTSE1, which all are involved in cell proliferation and cell cycle control (**Table 4**). Enrichment of proteins involved in cell proliferation and cell cycle control corresponds with previous findings from transcriptomic and proteomic analysis of BKPyV-infected cells [90–92]. The BKPyV encoded LTag induces cell cycle entry, in which several genes associated with cell proliferation are

upregulated [90]. LTag does this by binding to pRb, thereby preventing pRbs ability to bind and inhibit the E2F family of transcription factors [90]. It has been previously shown that inhibition of pRb binding to E2F leads to overexpression of the MAD2L2 gene, which influences chromosome instability and reduces cell proliferation [93]. As far as we know, this is the first time MAD2L2 expression is found to be increased in BKPyV-infected cells and this needs to be further investigated. The reason that BKPyV force cells into S-phase, is probably to gain access to the maximal amount of deoxyribonucleotides and other factors needed for viral DNA replication [94]. In a study of single cell transcriptomics in BKPyV-infected RPTECs, the authors found that almost all cells expressing medium or high levels of BKPyV mRNA, had entered the S or G_2/M phase of the cell cycle. On the other hand, only 25% of mock infected cells had entered the cell cycle [90]. KIF22 overexpression has been linked to increased cell proliferation and cancer progression [95,96]. GTSE1 is a protein that is thought to be involved in different stages of cell cycle progression. It can also cause cell cycle arrest by translocating p53 from the nucleus and to the cytoplasm, and hence prevent apoptosis [97]. BKPyV LTag also prevents apoptosis by binding to p53, blocking its ability to induce transcription of apoptotic genes [98]. Proteomic profiling of the nuclear compartment during lytic BKPyV infection has revealed that many of the cellular pathways that are upregulated are involved in DNA damage repair and cell cycle arrest [92]. BKPyV seems to activate the DNA damage response in order to keep the infected cells in S phase [99]. As discussed above, we found abundant proteins involved in negative regulation of apoptosis (**Figure 4.15**) but since they were not particularly enriched in U-2OS15E EVs (**Figure 4.18**), we think this has more to do with U-2OS being a cancer cell and less with the viral infection.

In our enrichment analysis, “ribosomal large subunit biogenesis” and “viral transcription” were two of the abundantly represented biological processes (**Figure 4.18**). Almost all proteins in these two categories were ribosomal proteins. This finding is consistent with previous reports claiming that SV40 LTag upregulates ribosomal proteins [100,101] and that BKPyV-infected RPTECs have a higher abundancy of mRNA encoding ribosomal proteins than uninfected cells [90]. However, analyzing single RPTECs, cells expressing high levels of BKPyV transcripts, had less transcripts for ribosomal proteins [90], suggesting that this may change during the viral replication cycle. Ribosomes are composed of approximately 40% ribosomal proteins and 60% ribosomal RNA (rRNA). Apparently the tumor suppressor proteins p53 and pRb are able to inhibit rRNA synthesis by repressing RNA polymerase I and III [102]. Since BKPyV LTag can bind to and inhibit pRb and p53, this may prevent the inhibition of rRNA synthesis and lead to

an increase in rRNA. Together with the increase in ribosomal proteins, this may lead to an increase in ribosomes that are essential for protein translation. By secreting ribosomal proteins and possibly rRNA via EVs, BKPyV might facilitate replication in adjacent cells. Further analysis are required to determine this. Another possible explanation for the increase in ribosomal proteins detected could be that more U-2OS15E cells were in the S phase compared to U-2OS.

Innate immunity

The first line host defense against viruses and other infectious agents is activation of the innate immune system. The cytosol is normally a DNA free zone and DNA is therefore signaling an invading microbe or leaked self-DNA from the nucleus [40] or the mitochondria [103]. This is activating cGAS, which generates CDNs. CDNs binding to STING results in NF-κB- and IRF3-dependent cytokine production, including type I IFNs, which move cells into an antiviral state, inhibiting viral replication. Many DNA viruses have been shown to antagonize the cGAS-STING DNA sensing pathway [40]. A recent study of BKPyV-infected vascular endothelial cell culture and RPTECs reported upregulation of type I IFNs but only in BKPyV-infected endothelial cells [91], suggesting that IFN pathway activation may be cell type specific. Another study reported that individual cells within a population reacted heterogeneously to BKPyV infection, hinting that cellular responses varied among individual cells as well as among cell lines [90].

We found enrichment of two proteins involved in the cGAS-STING pathway. Gasdermin D (GSDMD) was >100 times enriched in EVs from U-2OS15E (**Table 5**), suggesting upregulated expression of GSDMD in U-2OS15E cells or increased accumulation in EVs. GSDMD is commonly expressed in epithelial cells and immune cells. This protein can execute pyroptosis, a form of lytic programmed cell death in which gasdermins ruptures the cell membrane upon detection of pathogens, downstream of the inflammasome activation [104]. GSDMD deficiency was recently reported to enhance cGAS-STING mediated IFN production in macrophages [105]. GSDMD targets cGAS activation to inhibit IFN-β response to cytosolic DNA, thereby preventing tissue damage. Interestingly, Zika virus and Enterovirus 17 proteases have been found to cleave GSDMD independent of its upstream mediator caspase, causing the cell to undergo pyroptosis [106,107]. However, evidence relating GSDMD and polyomaviruses, that do not encode any protease, is lacking. Possibly upregulation of GSDMD helps BKPyV to evade cytosolic DNA sensing. If EVs with GSDMD are taken up by neighboring cells, this may help BKPyV to infect these cells.

The other protein from the cGAS-STING pathway that we found to be >100 fold enriched in EVs from U-2OS15E was conserved helix-loop-helix ubiquitous kinase (CHUK), also known as inhibitor of nuclear factor kappa-B kinase subunit alpha (IKKα) (**Table 5**). IKKα is part of IκB kinase (IKK) complex that plays an important role in regulating the NF-κB transcription factor. The IKK family which involves IKKα, IKKβ, IKKγ, and TBK-1 is thought to be a regulator of the cGAS-STING pathway. The IKK proteins form a complex which recruits inhibitor of NF-κBα (IκBα) as well as distinct NF-κB subunits, leading to IKKα and IKKβ phosphorylation and subsequent phosphorylation and degradation of IκBα. Inhibition of IκBα allows the NF-κB subunits to translocate to the nucleus to rapidly promote transcription of NF-κB targeted genes including genes responsible for both the innate and adaptive immune response [108]. Even if IKKα phosphorylation is observed in cGAS-STING mediated NF-κB activation, recent reports suggest that this mechanism is independent of IKKα, and strongly dependent on IKKβ [109]. On the other hand, IKKα is strongly involved in IFNα production induced by TLR 7 and 9, which confers with suggestions that BKPyV can downregulate TLR 9 signaling [37,110]. IKKβ was detected in EVs from both U-2OS15E and U-2OS cells but was apparently not enriched in EVs from BKPyV infected cells.

The E3 ligases TRIM32, TRIM56 and TRAF6 are regulators of the cGAS-STING pathway, as they have the ability to polyubiquitinate components in this pathway [38]. The immediate early protein of HSV-1, ICP0, has been reported to regulate the cGAS-STING complexes with its E3 ligase activity to facilitate infection. The E3 ligase superfamily consists of more than 600 human E3 ligases with a variety of substrates [111]. In our results one E3 ligase, UBE3A, was found to be enriched (**Table 5**). Evidence of UBE3A involvement in cGAS-STING pathway is lacking, however, there have been reports suggesting that UBE3A can upregulate the transcription activity of IRF3 through its E3 ligase activity [112]. Since IRF3 mediated transcription of type-1 IFNs is a downstream effect of the cGAS-STING pathway, there is a theoretic possibility of UBE3A involvement.

A recent study claimed that cytosolic DNA sensing by cGAS-STING was dependent on the FBS concentration in the cell culture medium [109]. They tested the cytosolic DNA sensing abilities relative to FBS concentrations in the media, and reported that by lowering FBS concentrations, the production of type I IFNs and IL-6 increased. Also, the authors reported that the cGAS-STING pathway is either absent or nonfunctional in most, if not all transformed cell lines, whereas primary cells are highly responsive. U-2OS was not included in that study, however, Deschamps *et al.* reported that the cGAS-STING pathway is impaired in U-2OS [41].

A number of cell lines have been tested for DNA sensing, and under regular conditions, none of the cells were responsive to cytosolic DNA. However, results demonstrated that previously unresponsive cells started becoming sensitive to cytosolic DNA upon decrease of FBS concentrations down to 1%. We cultured our cells in 10% FBS, however, two days prior to harvesting EVs, we conditioned our cells in 2% exosome depleted FBS. This was done to avoid the presence of bovine proteins in our proteomic results. Reduction of the FBS concentration, may have had an impact in DNA sensing in our cells. However, since U-2OS and U-2OS15E were treated the same way, our enrichment analysis shows that some cGAS-STING related proteins are upregulated only in U-2OS15E.

One of the major diseases caused by BKPyV is PyVAN. By studying gene expression of kidney biopsies in PyVAN patients, Sigdel *et al.* reported four specific markers for PyVAN. These were LTF, CFD, RPS15, and NOSIP [113]. We looked for those proteins in our enrichment analysis and identified that NOSIP was abundantly enriched in EVs from U-2OS15E (abundance ratio >100, $p = 5.5x10^{-17}$; **Appendix B**). NOSIP negatively regulates nitric oxide production by inducing translocation of NOS1 and NOS3 to actin cytoskeleton and inhibiting their enzymatic activities [113]. In a more recent transcriptomic study with the aim to evaluate the specificity of these four PyVAN specific genes, Pan *et al.* found that these genes overlapped with other non-viral allograft injuries [114]. The results suggested that NOSIP was not a specific marker for PyVAN as previously thought.

Viral proteins

Not unexpectedly, we found BKPyV proteins in EVs from U-2OS15E by western blot (**Figure 4.7**) and by LC-MS/MS (**Table 4**). It has been reported that BKPyV highjack EVs for release and transmission [115], however, in our view the evidence remains insufficient. We were not able to observe BKPyV inside EVs by TEM (**Figure 4.9**). VP1, the major capsid protein, was abundantly present in U-2OS15E EV samples. However, because of the size overlap between exosomes and BKPyV (45 nm), SEC does probably not separate viral particles from vesicles. Alternatively, viral particles could be attached on the outside of the vesicles and/or the vesicles could contain VP1 protein. We tried to remove free viral particles by density gradient centrifugation with OptiPrep but were not successful (**Figure 4.10 C**). Interestingly, we found LTag, which is the most important viral regularly protein. Since LTag is a nuclear protein, its presence in EVs could be of significance. Potentially, transfer of LTag to neighboring cells could make them more permissive for BKPyV infection. Finally, we also found agnoprotein. This is a cytoplasmic protein that recently was found to disrupt the mitochondrial membranes

in order to evade innate immune sensing [14]. Potentially, transfer of agnoprotein to neighboring cells could prepare the cell for BKPyV replication.

Comparison between western blot and LC-MS/MS results

As a quality control of EVs before LC-MS/MS, we performed western blot analysis with antibodies directed against known EV markers. How did our western blot results compare to the LC-MS/MS results? CD9 is a cell surface glycoprotein which is a member of the tetraspanins superfamily. By western blot analysis, we found less CD9 in EVs from U-2OS15E relative to U-2OS (**Figure 4.6**). The proteomic analysis supported these results as about 4 fold more CD9 was detected in EVs from U-2OS compared to U-2OS15E (**Table 5**). In our enrichment analysis, glycoprotein metabolism and ECM remodeling were two of the downregulated biological processes, in which CD9 can be identified in both groups (**Figure 4.18**). As we have only investigated CD9 in cell lysates from U-2OS and not from U-2OS15E, we also need to investigate cell lysates from U-2OS15E to check if CD9 expression is downregulated in U-2OS15E cells. The reason for why BKPyV infection either downregulates CD9 expression or leads to shedding of EVs with less CD9 is unclear.

Western blotting with antibodies directed against the EV markers ALIX (PDCD6IP) and flotillin-1 returned negative results (results not shown), however, proteomic analysis identified both proteins. The failure of flotillin-1 and ALIX detection by western blot could possibly be explained by the antibodies used or by a low amount of proteins. ALIX is part of the ESCRT pathway, and is thought to participate in MVB formation [116].

According to our western blot results, there was less annexin A1 and LC3B in EVs from U-2OS15E than U-2OS (**Figure 4.7**), however, our proteomic profiling did not find that these proteins were downregulated. Of note, while western blot of cell lysates demonstrated one annexin A1 band of the expected molecular weight of 37 kDA, the EV lane from U-2OS15E demonstrated one additional band of slightly lower molecular weight. A cleaved form of annexin A1 of about 33 kDa has been previously reported in cellular membranes and in extracellular space, while the 37 kDa un-cleaved protein has been found inside cells [117] and is probably explaining our finding. We found similar annexin A1 levels in both cell lysates, but higher levels LC3B in cell lysates from U-2OS compared to U-2OS15E.

Methodological aspects and challenges

The ratio of infected to uninfected cells. The U-2OS15E cell line was established in Tromsø in the beginning of 2000. At that time about 10 -20 % of the cells were found to contain BKPyV DNA and express BKPyV proteins [79]. Interestingly, the ratio of infected cells could not be increased by BKPyV superinfection, suggesting that the uninfected cells were resistant to BKPyV infection. Before we started to purify EVs from U-2OS15E, we decided to examine the ratio of infected to uninfected cells in the culture that now had been passaged between 25 and 50 times. We found that at least 29% of the cells were infected. The somewhat higher ratio could possibly be explained by a higher passage number or by a more sensitive immunofluorescence method using a fluorescently labelled instead of a peroxidase labelled secondary antibody. However, performing flow cytometry on LTag stained cells gave a completely different result suggesting that at least 77.5% of the cells were infected. Due to sick leave and lack of personal at AMCF, technical trouble preparing the U-2OS15E cells and limited time, the flow cytometry experiment was only performed once. If this experiment could be repeated, we would include an extra control in which U-2OS were labeled with primary (PAb416) and secondary antibody, and also, we would titrate the primary antibody to find the optimal concentration of PAb416 for our cells. Anyway, from these experiments we could conclude that not all cells expressed BKPyV proteins and were infected and that some of the EVs isolated therefore probably would originate from uninfected cells in the culture.

Methods to isolate EVs. There is not gold standard method for isolating EVs. As described in the introduction, using methods giving high recovery of EVs, typically give poor specificity and vice versa [47]. We tried two methods to purify EVs, SEC (**Figure 4.6**) and density gradient centrifugation with OptiPrep (**Figure 4.7**). Both methods are described to give high specificity. However, prior to purification we had to concentrate the supernatants and chose to do so by ultrafiltration. About 100 ml culture supernatant was concentrated to ~2 ml using a 10 kDa cellulose filter. This filter has a pore size of 220 nm, which means that many particles with a diameter under 220 nm probably were removed from our preparation. These filters are commonly used to concentrate EVs [51], although both exosomes and MVs can be below this size. However, TEM imaging post-purification with either OptiPrep or SEC, revealed EVs with sizes down to 30 nm (**Figure 4.9** and **4.12**), which suggests that not all EVs with a diameter less than 220 nm were removed. In the end, we decided to purify EVs for the proteomic study by SEC. We are aware that our choice of method may have influenced the results and that we ideally should have analyzed EVs purified by different methods.

Methods used to quantitate EVs. In order to compare the protein content in EVs from U-2OS and USOS-15E cells by western blot and LC-MS/MS, we used the same amount of protein from both cells. A stronger western blot signal for CD9, annexin A1 or LC3 using EVs from U-2OS than using EVs from U-2OS15E (**Figure 4.7**), could result either from an increased number of EVs or from EVs with a changed composition. In order to answer this, we would have had to quantitate the EVs. Negative staining followed by TEM is a good method to assess the morphology of EVs, however, it is not suitable for quantification (**Figure 4.8, 4.9** and **4.11-13**). When this study started, we hoped to be able to perform NTA [47]. NTA is a powerful characterization technique that detects and quantitates particles in liquids, however, large EVs (>400 nm) and very small EVs (<50 nm) are not well quantified. Unfortunately, the purchase of such instrument took a lot of time, and it will not be available at the core facility of UiT before summer 2021. As earlier mentioned, all EV markers were weaker in EVs from U-2OS15E than from U-2OS. An alternative explanation for this could be that a large proportion of proteins in EVs from U-2OS15E were BKPyV proteins. By western blot we have shown the presence of VP1 and agnoprotein (**Figure 4.7**) and LC-MS/MS detected VP1, VP2, agnoprotein, LTag and stag (**Table 4**), all uniquely identified in EVs of U-2OS15E. Possibly the large amount of viral proteins led to inclusion of less EVs from U-2OS15E. On the other hand, the proteomic profiling revealed enrichment of more proteins in EVs from U-2OS15E than U-2OS, suggesting that we had enough material for the analysis.

Stability of EVs. The storage temperature and stability of EVs have been discussed in many papers [118]. Possibly the stability depends on the sample source. Unfortunately, it was not always possible to harvest, purify and test EVs in one day and therefore sometimes EVs were stored in the fridge. We experienced that storage over several weeks at 4 °C lead to failed western blots (results not shown). The recommendation from ISEV is that EVs from conditioned media should be stored in PBS at -80 °C in siliconized tubes in order to avoid adherence to the tubes [47]. We were worried that storage at -80 °C would affect EV morphology, but fortunately this was not the case (**Figure 4.8** and **4.9**). EVs were therefore aliquoted and frozen down at -80 °C as soon as possible.

GO annotation. The GO project is one of the more successful initiatives when it comes to systematic descriptions of genes and gene products according to the genes/proteins biological attributes [119]. The accumulation of data produced by larger scale analysis produces large datasets in which manual analysis is both time consuming and inaccurate. With the GO annotations, grouping large samples of proteins or genes is simplified, allowing rapid

classification of proteins. One challenge with annotating genes or proteins with GO terms is that the GO database is continuously updated, where GO terms might be deleted or changed according to newly acquired knowledge [119]. To increase the reproducibility of the experiments, the version of the GO database used, and the date acquired should be included. Another challenge with GO is that only known biological attributes for the known genes or proteins are available. Undescribed genes, or genes with undescribed functions can create noise in the datasets and return false results.

Future experiments

The LC-MS/MS analysis of EVs from U-2OS15E and U-2OS, detected 410 enriched proteins in EVs from U-2OS15E, including five of the seven known BKPyV encoded proteins. We have discussed some of the proteins of particular interest. We are particularly interested in proteins associated with the innate immunity like GSDMD, CHUK, UBE3A and NOSIP. We would like to confirm the increase in these proteins by western blot, and at the same time compare the expression of these proteins in U-2OS and U-2OS15E by analyzing cell lysates. Moreover, we hope to do immunofluorescence staining of U-2OS15E cells using these antibodies in combination with BKPyV antibodies to directly investigate the expression in BKPyV-infected and uninfected cells.

The U-2OS15E cells were established in the beginning of 2000. Although, they have been mainly stored in the nitrogen tank, they have been passaged for about 20 passages and not always in parallel with the U-2OS cells. Notwithstanding that U-2OS are the ancestral cells for U-2OS15E, these cell lines may have diverged independently of the viral infection. To investigate this and at the same time analyze EVs from an acute BKPyV infection, U-2OS cells should be infected with BKPyV TU and EVs from U-2OS and BKPyV-infected U-2OS cells compared by LC-MS/MS.

We have already noted that U-2OS15E cells need more time to establish a confluent monolayer than U-2OS (**Figure 4.1**). This could either be caused by slower cell cycling or by a higher degree of cell death in U-2OS15E than U-2OS or a combination of this. In order to investigate this, we like to perform flow cytometry using a DNA cell stain like propidium iodide and amine dyes binding to proteins [120].

Our working hypothesis is that EVs from U-2OS15E are able to increase and not decrease infection in neighboring cells. In order to investigate this, we like to treat U-2OS cells or highly permissive RPTECs with EVs isolated from U-2OS15E before infecting them with purified BKPyV. This is a complex experiment where proper controls are needed to control for infection from the EVs.

Finally, for a complete analysis of EVs, we would like to characterize nucleic acid (mRNA, rRNA, miRNA) and lipid content analysis of EVs from U-2OS and EVs from U-2OS15E.

Concluding remarks

Based on our results, what is the purpose of EV secretion from the BKPyV-infected cells? Is it to warn neighboring cells about the viral infection or is it to prepare adjacent cells for BKPyV replication, or can it be a mixture of both? While the majority of proteins are secreted in EVs from both U-2OS and U-2OS15E, 371 protein (11.5%) were only found in EVs from U-2OS15E and 39 common proteins were found in significantly higher quantities in EVs from U-2OS15E. In addition, 51 proteins (1.5%) were found only in EVs from U-2OS. These 410 plus 51 proteins are probably the most interesting proteins to study. Unfortunately, there was no time to study them.

By secreting cell proliferative proteins, such as KIF22, GTSE1, or LTag through EVs, BKPyV might engage cells into cell cycle entry before BKPyV progeny enters, giving the infection a kick start. After cell entry, BKPyV is brought to the rough ER where a partly or fully uncoating is taking place [21,121], before the viral DNA enters the nucleus. In our analysis, we found enrichment of proteins involved in ER localization and targeting in U-2OS15E EVs (**Figure 4.18 A**). We also found enrichment of proteins involved in Golgi organization. It has been suggested that BKPyV passes rapidly by the Golgi complex to avoid detection [21]. By putting this knowledge together with our findings, we hypothesize that BKPyV can prepare adjacent cells for infection by downregulating glycoproteins, and upregulating proteins targeting ER and Golgi organization, making viral entry and localization to nucleus more rapid. Additionally, the large presence of ribosomal proteins in EVs of U-2OS15E (**Figure 4.18 A**), may contribute to translation of viral proteins and thereby to effective replication of virus. Furthermore, we detected enriched proteins involved in the innate immune respond like IKKα which is activating gene expression by NF-κB, including pro-inflammatory genes comprising cytokines and chemokines, and also participates in inflammasome regulation. Moreover, we detected GSDMD which may help BKPyV evade immune sensing. Further studies are needed to clarify the role of these proteins.

In conclusion, we found that U-2OS15E release EVs with many unique and enriched proteins. Some of the proteins are involved in increasing cell proliferation and cell cycle arrest, while others EVs are involved in innate immunity and immune evasion. Delivery of these proteins via EVs to adjacent cell, may be an important mechanism to maintain a persistent BKPyV infection within the host.

References

1. Reploeg MD, Storch GA, Clifford DB. BK Virus: A Clinical Review. Clin Infect Dis. 2001 Jul 15;33(2):191–202.

2. Kean JM, Rao S, Wang M, Garcea RL. Seroepidemiology of Human Polyomaviruses. Atwood WJ, editor. PLoS Pathog. 2009 Mar 27;5(3):e1000363.

3. Moens U, Calvignac-Spencer S, Lauber C, Ramqvist T, Feltkamp MCW, Daugherty MD, et al. ICTV virus taxonomy profile: Polyomaviridae. J Gen Virol. 2017 Jun 1;98(6):1159–60.

4. Gross L. A Filterable Agent, Recovered from Ak Leukemic Extracts, Causing Salivary Gland Carcinomas in C3H Mice. Exp Biol Med. 1953 Jun 1;83(2):414–21.

5. Pinto M, Dobson S. BK and JC virus: A review. J Infect. 2014 Jan 1;68(SUPPL1).

6. Wu Z, Graf FE, Hirsch HH. Antivirals against human polyomaviruses: Leaving no stone unturned. Rev Med Virol. 2021;

7. Padgett BL, Zurhein GM, Walker DL, Eckroade RJ, Dessel BH. CULTIVATION OF PAPOVA-LIKE VIRUS FROM HUMAN BRAIN WITH PROGRESSIVE MULTIFOCAL LEUCOENCEPHALOPATHY. Lancet. 1971 Jun 19;297(7712):1257–60.

8. Fanning E, Zhao K. SV40 DNA replication: From the A gene to a nanomachine. Virology. 2009 Feb 20;384(2):352–9.

9. Feng H, Shuda M, Chang Y, Moore PS. Clonal integration of a polyomavirus in human Merkel cell carcinoma. Science (80-). 2008 Feb 22;319(5866):1096–100.

10. Moens U, Krumbholz A, Ehlers B, Zell R, Johne R, Calvignac-Spencer S, et al. Biology, evolution, and medical importance of polyomaviruses: An update. Infect Genet Evol. 2017;54:18–38.

11. An P, Robles MTS, Pipas JM. Large T antigens of polyomaviruses: Amazing molecular machines. Annu Rev Microbiol. 2012 Oct;66:213–36.

12. Rinaldo CH, Traavik T, Hey A. The Agnogene of the Human Polyomavirus BK Is Expressed. J Virol. 1998 Jul 1;72(7):6233–6.

13. Gerits N, Moens U. Agnoprotein of mammalian polyomaviruses. Virology. 2012 Oct 25;432(2):316–26.

14. Manzetti J, Weissbach FH, Graf FE, Unterstab G, Wernli M, Hopfer H, et al. BK Polyomavirus Evades Innate Immune Sensing by Disrupting the Mitochondrial Network and Promotes Mitophagy. iScience. 2020 Jul 24;23(7):101257.

15. Ajuh ET, Wu Z, Kraus E, Weissbach FH, Bethge T, Gosert R, et al. Novel Human Polyomavirus Noncoding Control Regions Differ in Bidirectional Gene Expression according to Host Cell, Large T-Antigen Expression, and Clinically Occurring

Rearrangements. J Virol. 2018 Jan 17;92(7):2231–48.

16. Gosert R, Rinaldo CH, Funk GA, Egli A, Ramos E, Drachenberg CB, et al. Polyomavirus BK with rearranged noncoding control region emerge in vivo in renal transplant patients and increase viral replication and cytopathology. J Exp Med. 2008 Apr 14;205(4):841–52.

17. Olsen GH, Andresen PA, Hilmarsen HT, Bjørang O, Scott H, Midtvedt K, et al. Genetic variability in BK virus regulatory regions in urine and kidney biopsies from renal-transplant patients. J Med Virol. 2006 Mar 1;78(3):384–93.

18. Seo GJ, Fink LHL, O'Hara B, Atwood WJ, Sullivan CS. Evolutionarily Conserved Function of a Viral MicroRNA. J Virol. 2008 Oct 15;82(20):9823–8.

19. Broekema NM, Imperiale MJ. MiRNA regulation of BK polyomavirus replication during early infection. Proc Natl Acad Sci U S A. 2013 May 14;110(20):8200–5.

20. Dugan AS, Eash S, Atwood WJ. An N-Linked Glycoprotein with α(2,3)-Linked Sialic Acid Is a Receptor for BK Virus. J Virol. 2005 Nov 15;79(22):14442–5.

21. Helle F, Brochot E, Handala L, Martin E, Castelain S, Francois C, et al. Biology of the BKPyV: An update. Viruses. 2017 Nov 1;9(11):327.

22. Low J, Humes HD, Szczypka M, Imperiale M. BKV and SV40 infection of human kidney tubular epithelial cells in vitro. Virology. 2004 Jun 1;323(2):182–8.

23. Evans GL, Caller LG, Foster V, Crump CM. Anion homeostasis is important for non-lytic release of BK polyomavirus from infected cells. Open Biol. 2015 Aug 5;5(8).

24. Imlay H, Xie H, Leisenring WM, Duke ER, Kimball LE, Huang ML, et al. Presentation of BK polyomavirus-associated hemorrhagic cystitis after allogeneic hematopoietic cell transplantation. Blood Adv. 2020 Feb 25;4(4):617–28.

25. Cesaro S, Dalianis T, Rinaldo CH, Koskenvuo M, Pegoraro A, Einsele H, et al. ECIL guidelines for the prevention, diagnosis and treatment of BK polyomavirus-associated haemorrhagic cystitis in haematopoietic stem cell transplant recipients. J Antimicrob Chemother. 2018 Jan 1;73(1):12–21.

26. Papadimitriou JC, Randhawa P, Rinaldo CH, Drachenberg CB, Alexiev B, Hirsch HH. BK Polyomavirus Infection and Renourinary Tumorigenesis. Am J Transplant. 2016 Feb 1;16(2):398–406.

27. Müller DC, Rämö M, Naegele K, Ribi S, Wetterauer C, Perrina V, et al. Donor-derived, metastatic urothelial cancer after kidney transplantation associated with a potentially oncogenic BK polyomavirus. J Pathol. 2018 Mar 1;244(3):265–70.

28. Knowles WA. Discovery and Epidemiology of the Human Polyomaviruses BK Virus (BKV) and JC Virus (JCV). In: Ahsan N, editor. Polyomaviruses and Human Diseases. New York, NY: Springer New York; 2006. p. 360. (Advances in Experimental Medicine and Biology; vol. 577).

29. Jiang M, Abend JR, Johnson SF, Imperiale MJ. The role of polyomaviruses in human

disease. Virology. 2008/11/11. 2009;384(2):266–73.

30. Chesters PM, Heritage J, McCance DJ. Persistence of DNA sequences of BK virus and JC virus in normal human tissues and in diseased tissues. J Infect Dis. 1983;147(4):676–84.

31. Vanchiere JA, White ZS, Butel JS. Detection of BK virus and simian virus 40 in the urine of healthy children. J Med Virol. 2005 Mar 1;75(3):447–54.

32. Egli A, Infanti L, Dumoulin A, Buser A, Samaridis J, Stebler C, et al. Prevalence of Polyomavirus BK and JC Infection and Replication in 400 Healthy Blood Donors. J Infect Dis. 2009 Mar 15;199(6):837–46.

33. Gupta N, Lawrence RM, Nguyen C, Modica RF. Review article: BK virus in systemic lupus erythematosus. Pediatr Rheumatol Online J. 2015/08/22. 2015;13:34.

34. Imperiale MJ, Jiang M. Polyomavirus Persistence. Annu Rev Virol. 2016 Sep 29;3(1):517–32.

35. Bauman Y, Nachmani D, Vitenshtein A, Tsukerman P, Drayman N, Stern-Ginossar N, et al. An identical miRNA of the human JC and BK polyoma viruses targets the stress-induced ligand ULBP3 to escape immune elimination. Cell Host Microbe. 2011 Feb 17;9(2):93–102.

36. Lau A, Gray EE, Brunette RL, Stetson DB. DNA tumor virus oncogenes antagonize the cGAS-STING DNA-sensing pathway. Science (80-). 2015 Oct 30;350(6260):568–71.

37. Shahzad N, Shuda M, Gheit T, Kwun HJ, Cornet I, Saidj D, et al. The T Antigen Locus of Merkel Cell Polyomavirus Downregulates Human Toll-Like Receptor 9 Expression. J Virol. 2013 Dec 1;87(23):13009–19.

38. Phelan T, Little MA, Brady G. Targeting of the cGAS-STING system by DNA viruses. Vol. 174, Biochemical Pharmacology. Elsevier Inc.; 2020. p. 113831.

39. Basit A, Cho MG, Kim EY, Kwon D, Kang SJ, Lee JH. The cGAS/STING/TBK1/IRF3 innate immunity pathway maintains chromosomal stability through regulation of p21 levels. Exp Mol Med. 2020 Apr 1;52(4):643–57.

40. Ahn J, Barber GN. STING signaling and host defense against microbial infection. Exp Mol Med. 2019 Dec 1;51(12):1–10.

41. Deschamps T, Kalamvoki M. Impaired STING Pathway in Human Osteosarcoma U2OS Cells Contributes to the Growth of ICP0-Null Mutant Herpes Simplex Virus. J Virol. 2017 May 1;91(9).

42. You H, Zheng S, Huang Z, Lin Y, Shen Q, Zheng C. Herpes simplex virus 1 tegument protein ul46 inhibits tank-binding kinase 1-mediated signaling. MBio. 2019 May 1;10(3).

43. Deschamps T, Kalamvoki M. Extracellular Vesicles Released by Herpes Simplex Virus 1-Infected Cells Block Virus Replication in Recipient Cells in a STING-

Dependent Manner. J Virol. 2018 Jul 5;92(18).

44. Yáñez-Mó M, Siljander PRM, Andreu Z, Zavec AB, Borràs FE, Buzas EI, et al. Biological properties of extracellular vesicles and their physiological functions. Vol. 4, Journal of Extracellular Vesicles. 2015. p. 1–60.

45. Pan BT, Johnstone RM. Fate of the transferrin receptor during maturation of sheep reticulocytes in vitro: Selective externalization of the receptor. Cell. 1983;33(3):967–78.

46. El Andaloussi S, Mäger I, Breakefield XO, Wood MJA. Extracellular vesicles: Biology and emerging therapeutic opportunities. Nat Rev Drug Discov. 2013 May 15;12(5):347–57.

47. Théry C, Witwer KW, Aikawa E, Alcaraz MJ, Anderson JD, Andriantsitohaina R, et al. Minimal information for studies of extracellular vesicles 2018 (MISEV2018): a position statement of the International Society for Extracellular Vesicles and update of the MISEV2014 guidelines. J Extracell Vesicles. 2018 Jan 1;7(1).

48. Nolte-'t Hoen E, Cremer T, Gallo RC, Margolis LB. Extracellular vesicles and viruses: Are they close relatives?

49. Gould SJ, Raposo G. As we wait: Coping with an imperfect nomenclature for extracellular vesicles. J Extracell Vesicles. 2013;2(1).

50. Colombo M, Raposo G, Théry C. Biogenesis, secretion, and intercellular interactions of exosomes and other extracellular vesicles. Annu Rev Cell Dev Biol. 2014 Oct 6;30:255–89.

51. Konoshenko MY, Lekchnov EA, Vlassov A V., Laktionov PP. Isolation of Extracellular Vesicles: General Methodologies and Latest Trends. Biomed Res Int. 2018;2018.

52. Crescitelli R, Lässer C, Szabó TG, Kittel A, Eldh M, Dianzani I, et al. Distinct RNA profiles in subpopulations of extracellular vesicles: Apoptotic bodies, microvesicles and exosomes. J Extracell Vesicles. 2013;2(1).

53. Pessolano, Belvedere, Bizzarro, Franco, Marco, Petrella, et al. Annexin A1 Contained in Extracellular Vesicles Promotes the Activation of Keratinocytes by Mesoglycan Effects: An Autocrine Loop Through FPRs. Cells. 2019 Jul 19;8(7):753.

54. Leoni G, Neumann PA, Kamaly N, Quiros M, Nishio H, Jones HR, et al. Annexin A1'containing extracellular vesicles and polymeric nanoparticles promote epithelial wound repair. J Clin Invest. 2015 Mar 2;125(3):1215–27.

55. Jeppesen DK, Fenix AM, Franklin JL, Higginbotham JN, Zhang Q, Zimmerman LJ, et al. Reassessment of Exosome Composition. Cell. 2019 Apr 4;177(2):428-445.e18.

56. Mittal S, Gupta P, Chaluvally-Raghavan P, Pradeep S. Emerging role of extracellular vesicles in immune regulation and cancer progression. Cancers (Basel). 2020 Dec 1;12(12):1–16.

57. Bello-Morales R, López-Guerrero JA. Extracellular vesicles in herpes viral spread and immune evasion. Front Microbiol. 2018 Oct 25;9(OCT).

58. Cashikar AG, Hanson PI. A cell-based assay for CD63-containing extracellular vesicles. PLoS One. 2019/07/25. 2019;14(7):e0220007.

59. Vader P, Mol EA, Pasterkamp G, Schiffelers RM. Extracellular vesicles for drug delivery. Adv Drug Deliv Rev. 2016 Nov 15;106:148–56.

60. Gardiner C, Vizio D Di, Sahoo S, Théry C, Witwer KW, Wauben M, et al. Techniques used for the isolation and characterization of extracellular vesicles: Results of a worldwide survey. J Extracell Vesicles. 2016;5(1).

61. Ludwig N, Whiteside TL, Reichert TE. Challenges in exosome isolation and analysis in health and disease. Int J Mol Sci. 2019 Oct 1;20(19).

62. Li J, He X, Deng Y, Yang C. An update on isolation methods for proteomic studies of extracellular vesicles in biofluids [Internet]. Vol. 24, Molecules. MDPI AG; 2019.

63. Livshts MA, Khomyakova E, Evtushenko EG, Lazarev VN, Kulemin NA, Semina SE, et al. Isolation of exosomes by differential centrifugation: Theoretical analysis of a commonly used protocol. Sci Rep. 2015 Nov 30;5.

64. Whitham M, Parker BL, Friedrichsen M, Hingst JR, Hjorth M, Hughes WE, et al. Extracellular Vesicles Provide a Means for Tissue Crosstalk during Exercise. Cell Metab. 2018 Jan 9;27(1):237-251.e4.

65. Kim J, Tan Z, Lubman DM. Exosome enrichment of human serum using multiple cycles of centrifugation. Electrophoresis. 2015 Sep 1;36(17):2017–26.

66. Van Deun J, Mestdagh P, Sormunen R, Cocquyt V, Vermaelen K, Vandesompele J, et al. The impact of disparate isolation methods for extracellular vesicles on downstream RNA profiling. J Extracell Vesicles. 2014;3(1).

67. Dettenhofer M, Yu X-F. Highly Purified Human Immunodeficiency Virus Type 1 Reveals a Virtual Absence of Vif in Virions. J Virol. 1999 Feb 1;73(2):1460–7.

68. Karimi N, Cvjetkovic A, Jang SC, Crescitelli R, Hosseinpour Feizi MA, Nieuwland R, et al. Detailed analysis of the plasma extracellular vesicle proteome after separation from lipoproteins. Cell Mol Life Sci. 2018 Aug 1;75(15):2873–86.

69. Feng H, Kwun HJ, Liu X, Gjoerup O, Stolz DB, Chang Y, et al. Cellular and Viral Factors Regulating Merkel Cell Polyomavirus Replication. Qiu J, editor. PLoS One. 2011 Jul 22;6(7):e22468.

70. Iwai K, Minamisawa T, Suga K, Yajima Y, Shiba K. Isolation of human salivary extracellular vesicles by iodixanol density gradient ultracentrifugation and their characterizations. J Extracell Vesicles. 2016 Jan 1;5(1):30829.

71. Ho J, Jedrych JJ, Feng H, Natalie AA, Grandinetti L, Mirvish E, et al. Human polyomavirus 7-associated pruritic rash and viremia in transplant recipients. J Infect Dis. 2015 May 15;211(10):1560–5.

72. Buck CB, Thompson CD. Production of Papillomavirus-Based Gene Transfer Vectors. Curr Protoc Cell Biol. 2007 Dec 1;37(1):26.1.1-26.1.19.

73. Morris-Love J, Gee G V., O'Hara BA, Assetta B, Atkinson AL, Dugan AS, et al. JC polyomavirus uses extracellular vesicles to infect target cells. MBio. 2019 Mar 1;10(2).

74. Kalra H, Adda CG, Liem M, Ang C-S, Mechler A, Simpson RJ, et al. Comparative proteomics evaluation of plasma exosome isolation techniques and assessment of the stability of exosomes in normal human blood plasma. Proteomics. 2013 Nov 1;13(22):3354–64.

75. Tauro BJ, Greening DW, Mathias RA, Ji H, Mathivanan S, Scott AM, et al. Comparison of ultracentrifugation, density gradient separation, and immunoaffinity capture methods for isolating human colon cancer cell line LIM1863-derived exosomes. Methods. 2012 Feb 1;56(2):293–304.

76. Cantin R, Diou J, Bélanger D, Tremblay AM, Gilbert C. Discrimination between exosomes and HIV-1: Purification of both vesicles from cell-free supernatants. J Immunol Methods. 2008 Sep 30;338(1–2):21–30.

77. Böing AN, van der Pol E, Grootemaat AE, Coumans FAW, Sturk A, Nieuwland R. Single-step isolation of extracellular vesicles by size-exclusion chromatography. J Extracell Vesicles. 2014;3(1).

78. American Type Culture Collection. U-2 OS ATCC ® HTB-96™ Homo sapiens bone osteosarcoma [Internet]. [cited 2021 Jan 9]. Available from: https://www.lgcstandards-atcc.org/products/all/HTB-96.aspx?geo_country=no#documentation

79. Rinaldo CH, Myhre MR, Alstad H, Nilssen O, Traavik T, Nilssen Ø, et al. Human polyomavirus BK (BKV) transiently transforms and persistently infects cultured osteosarcoma cells. Virus Res. 2003 Jun 1;93(2):181–7.

80. Dumoulin A, Hirsch HH. Reevaluating and optimizing polyomavirus BK and JC real-time PCR assays to detect rare sequence polymorphisms. J Clin Microbiol. 2011 Apr 1;49(4):1382–8.

81. Kao CL, Wu MC, Chiu YH, Lin JL, Wu YC, Yueh YY, et al. Flow cytometry compared with indirect immunofluorescence for rapid detection of dengue virus type 1 after amplification in tissue culture. J Clin Microbiol. 2001;39(10):3672–7.

82. Raab-Traub N, Dittmer DP. Viral effects on the content and function of extracellular vesicles. Nat Rev Microbiol. 2017 Sep 1;15(9):559–72.

83. Schmid F-X. Biological Macromolecules: UV-visible Spectrophotometry. In: Encyclopedia of Life Sciences. Chichester, UK: John Wiley & Sons, Ltd; 2001.

84. Leidal AM, Debnath J. LC3-dependent extracellular vesicle loading and secretion (LDELS). Autophagy. 2020 Jun 2;16(6):1162–3.

85. Eichelberger KR, Goldman WE. Manipulating neutrophil degranulation as a bacterial virulence strategy. PLoS Pathog. 2020 Dec 10;16(12):e1009054.

86. Hentze MW, Castello A, Schwarzl T, Preiss T. A brave new world of RNA-binding proteins. Nat Rev Mol Cell Biol. 2018 May 1;19(5):327–41.

87. Novello C, Pazzaglia L, Conti A, Quattrini I, Pollino S, Perego P, et al. P53-dependent activation of microRNA-34a in response to etoposide-induced DNA damage in osteosarcoma cell lines not impaired by dominant negative p53 expression. PLoS One. 2014 Dec 9;9(12).

88. Bonafede R, Brandi J, Manfredi M, Scambi I, Schiaffino L, Merigo F, et al. The Anti-Apoptotic Effect of ASC-Exosomes in an In Vitro ALS Model and Their Proteomic Analysis. Cells. 2019 Sep 14;8(9).

89. Heyer WD, Ehmsen KT, Liu J. Regulation of homologous recombination in eukaryotes. Annu Rev Genet. 2010 Dec 1;44:113–39.

90. An P, Cantalupo PG, Zheng W, Sáenz-Robles MT, Duray AM, Weitz D, et al. Single-Cell Transcriptomics Reveals a Heterogeneous Cellular Response to BK Virus Infection. J Virol. 2020 Dec 23;95(6).

91. An P, Sáenz Robles MT, Duray AM, Cantalupo PG, Pipas JM. Human polyomavirus BKV infection of endothelial cells results in interferon pathway induction and persistence. PLoS Pathog. 2019;15(1).

92. Justice JL, Verhalen B, Kumar R, Lefkowitz EJ, Imperiale MJ, Jiang M. Quantitative Proteomic Analysis of Enriched Nuclear Fractions from BK Polyomavirus-Infected Primary Renal Proximal Tubule Epithelial Cells. J Proteome Res. 2015 Oct 2;14(10):4413–24.

93. Schvartzman JM, Duijf PHG, Sotillo R, Coker C, Benezra R. Mad2 is a critical mediator of the chromosome instability observed upon Rb and p53 pathway inhibition. Cancer Cell. 2011 Jun 14;19(6):701–14.

94. Hume S, Dianov GL, Ramadan K. A unified model for the G1/S cell cycle transition. Nucleic Acids Res. 2020 Dec 16;48(22):12483–501.

95. Yu Y, Wang XY, Sun L, Wang YL, Wan YF, Li XQ, et al. Inhibition of KIF22 suppresses cancer cell proliferation by delaying mitotic exit through upregulating CDC25C expression. Carcinogenesis. 2014 Jun 1;35(6):1416–25.

96. Fischer M, Müller GA. Cell cycle transcription control: DREAM/MuvB and RB-E2F complexes. Crit Rev Biochem Mol Biol. 2017 Nov 2;52(6):638–62.

97. Wu X, Wang H, Lian Y, Chen L, Gu L, Wang J, et al. GTSE1 promotes cell migration and invasion by regulating EMT in hepatocellular carcinoma and is associated with poor prognosis. Sci Rep. 2017 Dec 1;7(1):1–12.

98. Lilyestrom W, Klein MG, Zhang R, Joachimiak A, Chen XS. Crystal structure of SV40 large T-antigen bound to p53: Interplay between a viral oncoprotein and a cellular tumor suppressor. Genes Dev. 2006 Sep 1;20(17):2373–82.

99. Justice JL, Needham JM, Thompson SR. BK Polyomavirus Activates the DNA Damage Response To Prolong S Phase. J Virol. 2019 May 1;93(14).

100. Zhai W, Tuan JA, Comai L. SV40 large T antigen binds to the TBP-TAF(I) complex SL1 and coactivates ribosomal RNA transcription. Genes Dev. 1997 Jun 15;11(12):1605–17.

101. Cavender JF, Mummert C, Tevethia MJ. Transactivation of a Ribosomal Gene by Simian Virus 40 Large-T Antigen Requires at Least Three Activities of the Protein. J Virol. 1999 Jan 1;73(1):214–24.

102. Chakraborty A, Uechi T, Kenmochi N. Guarding the "translation apparatus": Defective ribosome biogenesis and the p53 signaling pathway. Wiley Interdiscip Rev RNA. 2011 Jul 1;2(4):507–22.

103. Guo Y, Gu R, Gan D, Hu F, Li G, Xu G. Mitochondrial DNA drives noncanonical inflammation activation via cGAS–STING signaling pathway in retinal microvascular endothelial cells. Cell Commun Signal. 2020 Dec 1;18(1):1–12.

104. Banerjee I, Behl B, Mendonca M, Sarkar SN, Fitzgerald KA, Rathinam Correspondence VAK. Gasdermin D Restrains Type I Interferon Response to Cytosolic DNA by Disrupting Ionic Homeostasis. Immunity. 2018;49:413–26.

105. Chunmei M, Yang D, Wang B, Wu C, Wu Y, Li S, et al. Gasdermin d in macrophages restrains colitis by controlling cgas-mediated inflammation. Sci Adv. 2020 May 1;6(21):eaaz6717.

106. Yamaoka Y, Matsunaga S, Jeremiah SS, Nishi M, Miyakawa K, Morita T, et al. Zika virus protease induces caspase-independent pyroptotic cell death by directly cleaving gasdermin D. Biochem Biophys Res Commun. 2021 Jan 1;534:666–71.

107. Lei X, Zhang Z, Xiao X, Qi J, He B, Wang J. Enterovirus 71 Inhibits Pyroptosis through Cleavage of Gasdermin D. J Virol. 2017 Sep 15;91(18).

108. Davis ME, Gack MU. Ubiquitination in the antiviral immune response. Virology. 2015 May 1;479–480:52–65.

109. Fang R, Wang C, Jiang Q, Lv M, Gao P, Yu X, et al. NEMO–IKKβ Are Essential for IRF3 and NF-κB Activation in the cGAS–STING Pathway. J Immunol. 2017 Nov 1;199(9):3222–33.

110. Hoshino K, Sugiyama T, Matsumoto M, Tanaka T, Saito M, Hemmi H, et al. IκB kinase-α is critical for interferon-α production induced by Toll-like receptors 7 and 9. Nature. 2006 Apr 13;440(7086):949–53.

111. Li W, Bengtson MH, Ulbrich A, Matsuda A, Reddy VA, Orth A, et al. Genome-wide and functional annotation of human E3 ubiquitin ligases identifies MULAN, a mitochondrial E3 that regulates the organelle's dynamics and signaling. PLoS One. 2008 Jan 23;3(1).

112. Furumai R, Tamada K, Liu X, Takumi T. UBE3A regulates the transcription of IRF, an antiviral immunity. Hum Mol Genet. 2019 Jun 15;28(12):1947–58.

113. Sigdel TK, Bestard O, Salomonis N, Hsieh SC, Torras J, Naesens M, et al. Intragraft Antiviral-Specific Gene Expression as a Distinctive Transcriptional Signature for

Studies in Polyomavirus-Associated Nephropathy. Transplantation. 2016 Oct 1;100(10):2062–70.

114. Pan L, Lyu Z, Adam B, Zeng G, Wang Z, Huang Y, et al. Polyomavirus BK nephropathy-associated transcriptomic signatures: A critical reevaluation. Transplant Direct. 2018 Feb 1;4(2).

115. Handala L, Blanchard E, Raynal P-I, Roingeard P, Morel V, Descamps V, et al. BK Polyomavirus Hijacks Extracellular Vesicles for En Bloc Transmission. J Virol. 2020 Jan 2;94(6).

116. Vietri M, Radulovic M, Stenmark H. The many functions of ESCRTs. Nat Rev Mol Cell Biol. 2020 Jan 1;21(1):25–42.

117. Belvedere R, Bizzarro V, Popolo A, Dal Piaz F, Vasaturo M, Picardi P, et al. Role of intracellular and extracellular annexin A1 in migration and invasion of human pancreatic carcinoma cells. BMC Cancer. 2014;14(1).

118. Jeyaram A, Jay SM. Preservation and Storage Stability of Extracellular Vesicles for Therapeutic Applications. AAPS J. 2018 Jan 1;20(1):1.

119. Yon Rhee S, Wood V, Dolinski K, Draghici S. Use and misuse of the gene ontology annotations. Nat Rev Genet. 2008 Jul 13;9(7):509–15.

120. Perfetto SP, Chattopadhyay PK, Lamoreaux L, Nguyen R, Ambrozak D, Koup RA, et al. Amine-reactive dyes for dead cell discrimination in fixed samples. Curr Protoc Cytom. 2010 Jul;CHAPTER(SUPPL. 53):Unit.

121. Jiang M, Abend JR, Tsai B, Imperiale MJ. Early Events during BK Virus Entry and Disassembly. J Virol. 2009 Feb 1;83(3):1350–8.

122. Margolis SR, Wilson SC, Vance RE. Evolutionary Origins of cGAS-STING Signaling. Trends Immunol. 2017 Oct 1;38(10):733–43.

Appendix A: Solutions and Reagents

Radioimmunoprecipitation assay (RIPA) buffer

150	mM	NaCl
1%	(v/v)	Nonidet-P40
0.5%	(w/v)	Na-deoxycholate
0.1%	(w/v)	Sodium dodecyl sulfate (SDS)
50	mM	Tris, pH 8.0

Store at 4 °C

10x Blotting buffer

144 g	Glycine
30.3 g	Trizma base

Fill up with ddH_2O to a final volume of 1000 ml.

Store in room temp

Blotting buffer

50	ml	10x Blotting buffer
100	ml	Methanol
350	ml	ddH_2O

Store in room temp

10x TBS

24.23	g	Trizma HCl
80.06	g	NaCl
800	ml	ddH_2O

Adjust the pH to 7.6 with HCl

Fill up with ddH_2O to a final volume of 1000 ml.

Dilute 1:10 in ddH_2O to get 1x working dilution

Store in room temp

TBST

100	ml	10x TBS
899	ml	ddH_2O
1	ml	Tween® 20

Store in room temp

Appendix B: Supplementary Data

Flow Cytometry

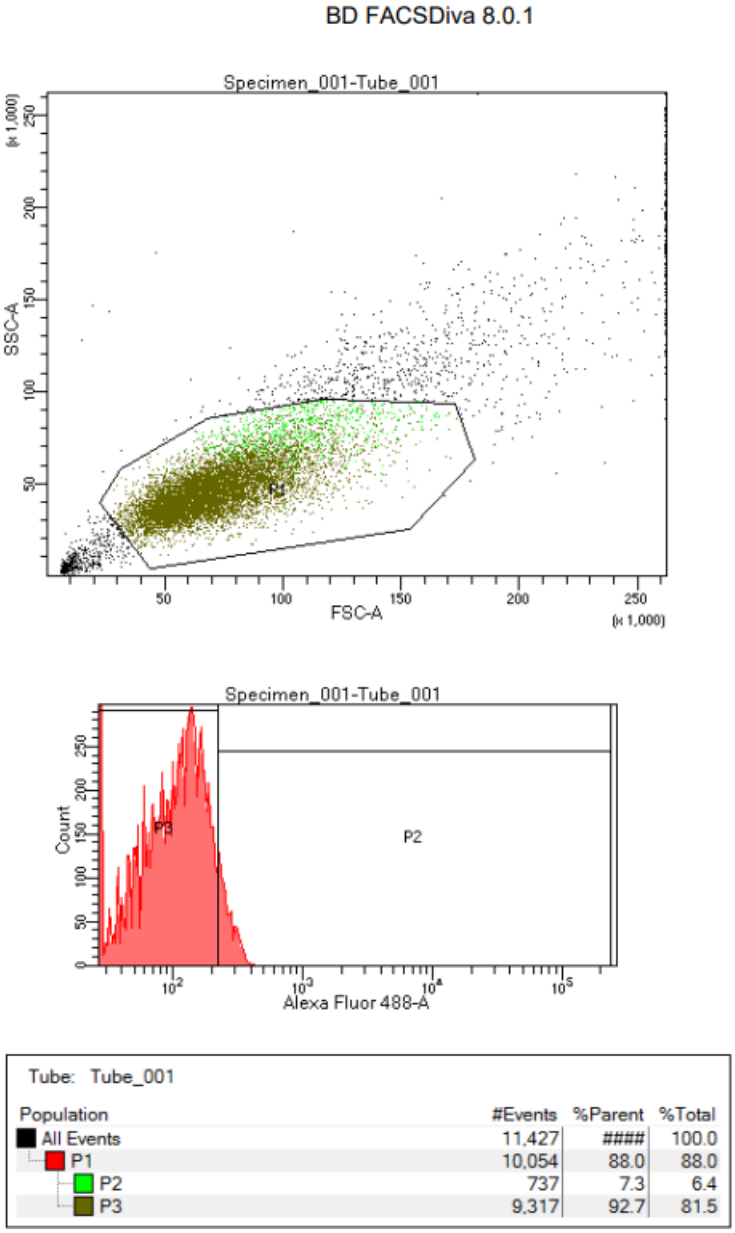

Figure S1. *Control 1: Flow cytometric analysis on U-2OS with no staining. Scatter plot shows 10,000 events occurring within P1 in which forward scatter (FSC) is plotted against side scatter (SSC). P1 represents the population of cells that are analyzed. All the green dots are representing autofluorescing cells. Histogram shows distribution of analyzed cells and their fluorescence.*

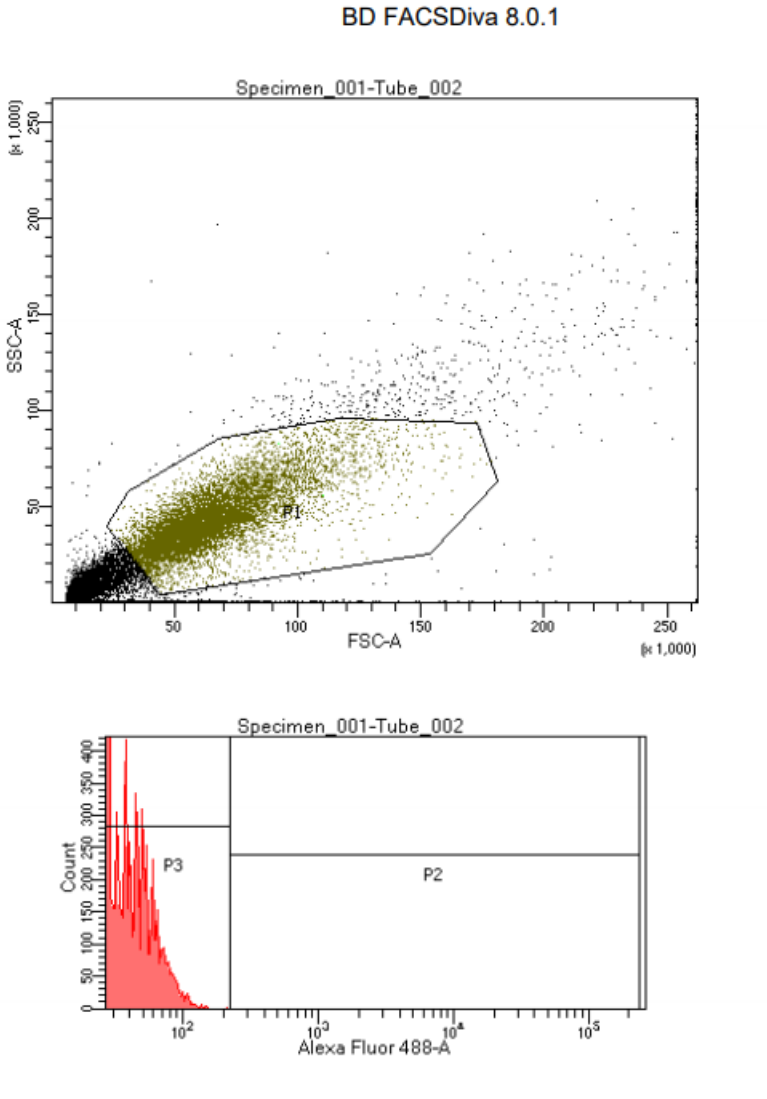

Figure S2. *Control 2: Flow cytometric analysis on U-2OS15E with no staining. Scatter plot shows 10,000 events occurring within P1 in which forward scatter (FSC) is plotted against side scatter (SSC). P1 represents the population of cells that are analyzed. All the green dots within P1 are representing cells that are positive for PAb416-labeled BKPyV and the brown dots are U-2OS15E cells that are LT-ag negative. Histogram shows distribution of analyzed cells and their fluorescence. Statistical analysis shows 4 cells in P2.*

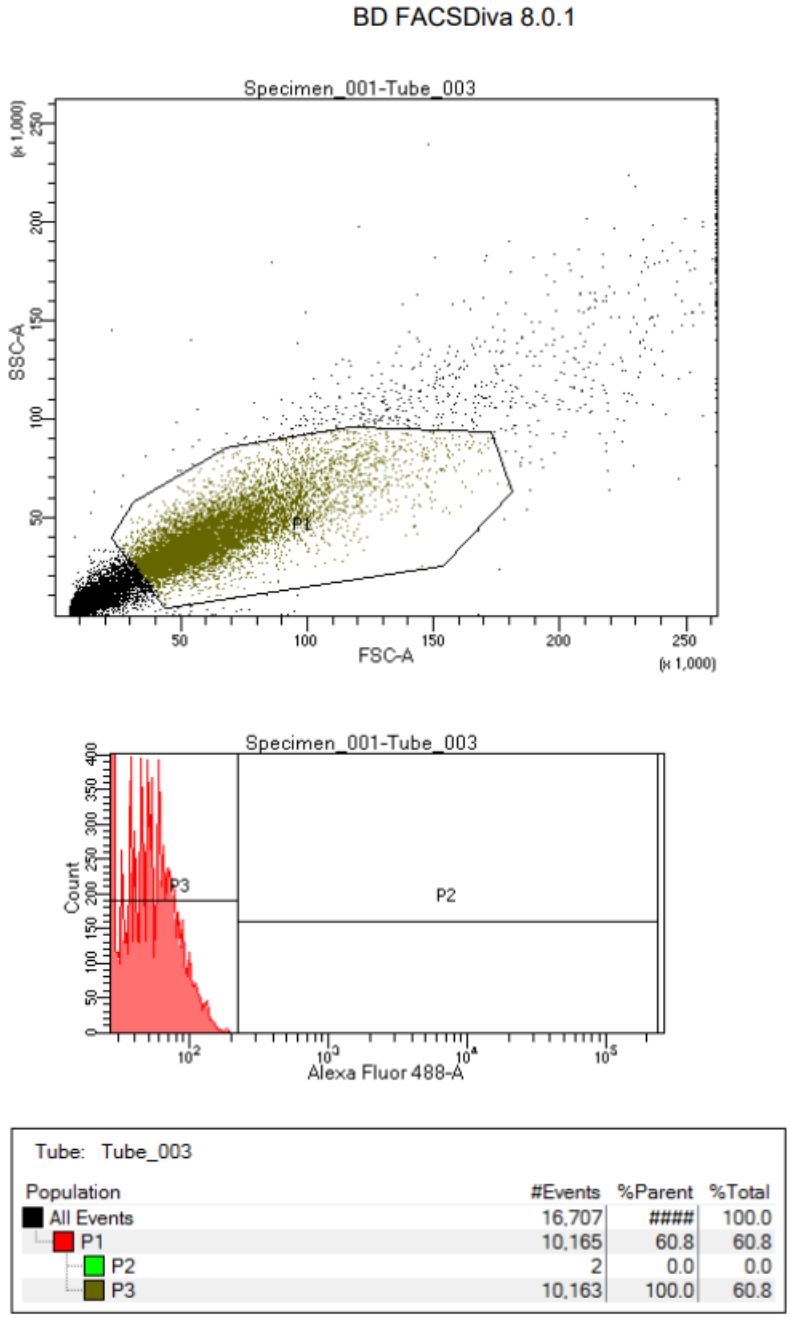

Figure S3. *Control 3: Flow cytometric analysis on U-2OS15E stained with Alexa Fluor™ 488. Scatter plot shows 10,000 events occurring within P1 in which forward scatter (FSC) is plotted against side scatter (SSC). P1 represents the population of cells that are analyzed. All the green dots are representing cells that are stained with secondary antibody and the brown dots are U-2OS15E cells that are negative. Histogram shows distribution of analyzed cells and their fluorescence. Statistical analysis shows 2 events in P2.*

Proteomics

PCA plot:

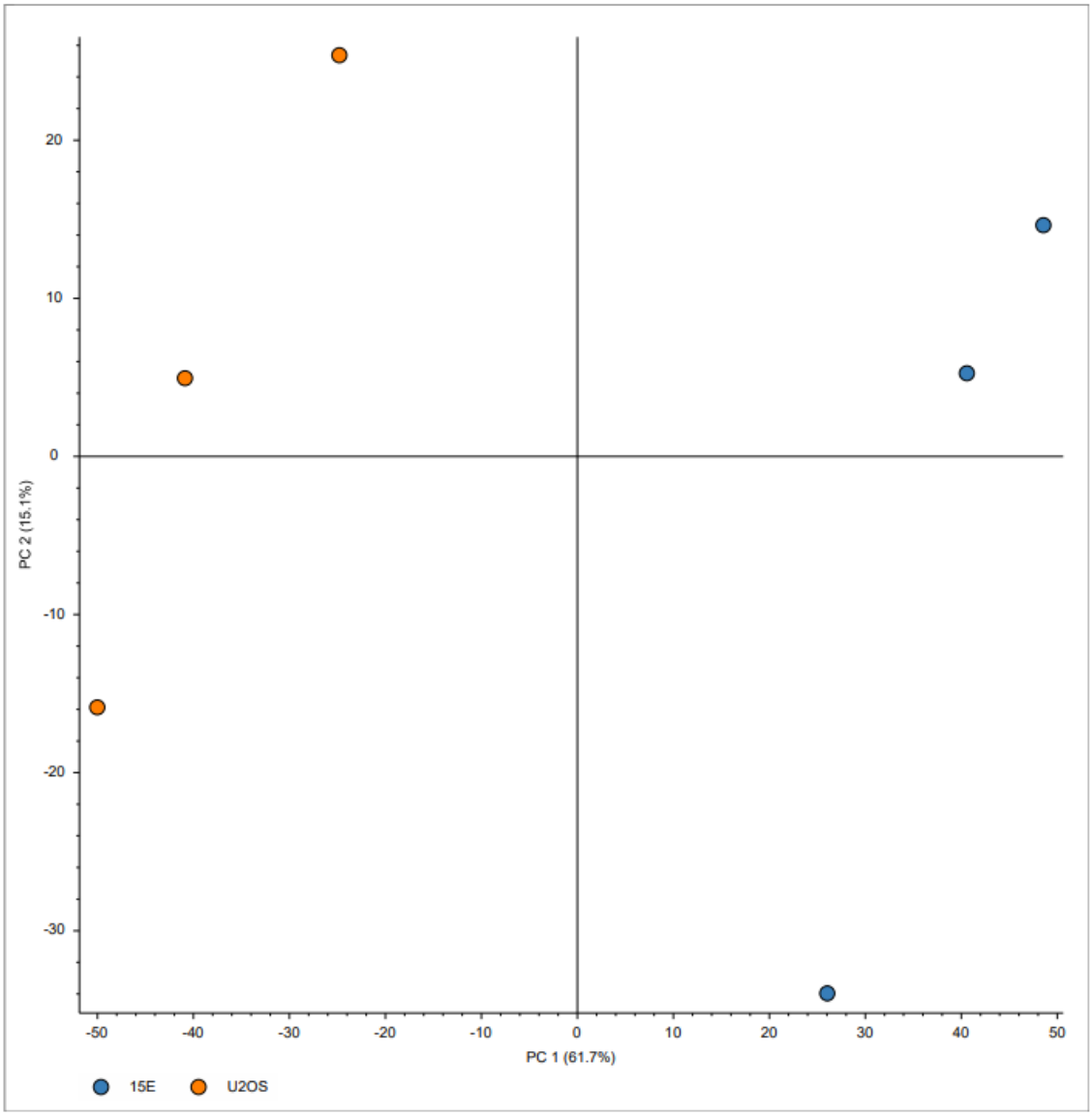

Figure S4. *PCA plot of three replicates U-2OS EVs against U-2OS15E EVs (15E). Plot showing that EV isolates from U-2OS and U-2OS15E are significantly different.*

Table S1. List of all detected proteins enriched in U-2OS15E EVs.

UniProt Accession	Protein Description	Gene Symbol	Abundance Ratio	Adjusted p-value
Q9UI95	Mitotic spindle assembly checkpoint protein	MAD2L2	100	5.57E-17
P57105	Synaptojanin-2-binding protein	SYNJ2BP	100	5.57E-17
Q71RC2	La-related protein 4	LARP4	100	5.57E-17
Q9UH17	DNA dC->dU-editing enzyme APOBEC-3B	APOBEC3B	9.734	0.060245
Q6SJ93	Serine protease FAM111B	FAM111B	100	5.57E-17
Q96FV9	THO complex subunit 1	THOC1	100	5.57E-17
Q9UNN8	Endothelial protein C receptor	PROCR	17.854	0.010574
915122019	VP1, partial		5.417	0.180269
P53597	Succinate--CoA ligase [ADP/GDP-forming] subunit alpha, mitochondrial	SUCLG1	100	5.57E-17
Q9UBS4	DnaJ homolog subfamily B member 11	DNAJB11	10.929	0.01924
Q9NR28	Diablo homolog, mitochondrial	DIABLO	100	5.57E-17
Q6XZF7	Dynamin-binding protein	DNMBP	100	5.57E-17
Q9NYZ3	G2 and S phase-expressed protein 1	GTSE1	100	5.57E-17
P39023	60S ribosomal protein L3	RPL3	13.721	0.03006
Q96IW7	Vesicle-trafficking protein SEC22a	SEC22A	100	5.57E-17
P18583	Protein SON	SON	100	5.57E-17
P33947	ER lumen protein-retaining receptor 2	KDELR2	10.841	0.017728
Q9HCK8	Chromodomain-helicase-DNA-binding protein 8	CHD8	100	5.57E-17
Q8IWJ2	GRIP and coiled-coil domain-containing protein 2	GCC2	100	5.57E-17
P07305	Histone H1.0	H1-0	10.227	0.050468
Q14807	Kinesin-like protein KIF22	KIF22	100	5.57E-17
P20020	Plasma membrane calcium-transporting ATPase 1	ATP2B1	100	5.57E-17
P13010	X-ray repair cross-complementing protein 5	XRCC5	9.592	0.100132
Q9NZM1	Myoferlin	MYOF	100	5.57E-17
P49848	Transcription initiation factor TFIID subunit 6	TAF6	100	5.57E-17
P0DMU7	Cancer/testis antigen family 45 member A6	CT45A6	100	5.57E-17
P06865	Beta-hexosaminidase subunit alpha	HEXA	68.649	7.72E-06
Q12959	Disks large homolog 1	DLG1	100	5.57E-17
Q92845	Kinesin-associated protein 3	KIFAP3	5.857	0.137982
Q9UNS1	Protein timeless homolog	TIMELESS	100	5.57E-17
Q8IWZ3	Ankyrin repeat and KH domain-containing protein 1	ANKHD1	100	5.57E-17
Q8IZH2	5'-3' exoribonuclease 1	XRN1	100	5.57E-17
Q9UID3	Vacuolar protein sorting-associated protein 51 homolog	VPS51	15.303	0.001674
Q9Y2Z4	Tyrosine--tRNA ligase, mitochondrial	YARS2	100	5.57E-17
Q7KZ85	Transcription elongation factor SPT6	SUPT6H	100	5.57E-17
P52435	DNA-directed RNA polymerase II subunit RPB11-a	POLR2J	100	5.57E-17
Q99543	DnaJ homolog subfamily C member 2	DNAJC2	100	5.57E-17
Q96BW5	Phosphotriesterase-related protein	PTER	100	5.57E-17
Q9BZD4	Kinetochore protein Nuf2	NUF2	100	5.57E-17
16930348	VP1 protein, partial		100	5.57E-17
Q9BZE4	Nucleolar GTP-binding protein 1	GTPBP4	100	5.57E-17
Q05086	Ubiquitin-protein ligase E3A	UBE3A	100	5.57E-17
P00390	Glutathione reductase, mitochondrial	GSR	100	5.57E-17
Q9NV31	U3 small nucleolar ribonucleoprotein protein IMP3	IMP3	100	5.57E-17
Q9H0A8	COMM domain-containing protein 4	COMMD4	100	5.57E-17
Q9BYC5	Alpha-(1,6)-fucosyltransferase	FUT8	100	5.57E-17
Q9NYY8	FAST kinase domain-containing protein 2, mitochondrial	FASTKD2	100	5.57E-17
Q96FZ5	CKLF-like MARVEL transmembrane domain-containing protein 7	CMTM7	100	5.57E-17

P08670	Vimentin	VIM	12.434	0.042779
Q03701	CCAAT/enhancer-binding protein zeta	CEBPZ	100	5.57E-17
O95793	Double-stranded RNA-binding protein Staufen homolog 1	STAU1	100	5.57E-17
P50914	60S ribosomal protein L14	RPL14	10.478	0.075969
Q9NW64	Pre-mRNA-splicing factor RBM22	RBM22	100	5.57E-17
Q8WXI9	Transcriptional repressor p66-beta	GATAD2B	100	5.57E-17
Q9H3N1	Thioredoxin-related transmembrane protein 1	TMX1	6.966	0.110447
P43355	Melanoma-associated antigen 1	MAGEA1	9.107	0.043178
O00762	Ubiquitin-conjugating enzyme E2 C	UBE2C	100	5.57E-17
Q02880	DNA topoisomerase 2-beta	TOP2B	100	5.57E-17
O43719	HIV Tat-specific factor 1	HTATSF1	100	5.57E-17
P29083	General transcription factor IIE subunit 1	GTF2E1	100	5.57E-17
O14662	Syntaxin-16	STX16	100	5.57E-17
Q8TEA1	tRNA (cytosine(72)-C(5))-methyltransferase NSUN6	NSUN6	100	5.57E-17
Q9H4M3	F-box only protein 44	FBXO44	100	5.57E-17
Q8WVC0	RNA polymerase-associated protein LEO1	LEO1	100	5.57E-17
Q9Y508	E3 ubiquitin-protein ligase RNF114	RNF114	100	5.57E-17
Q9GZQ3	COMM domain-containing protein 5	COMMD5	100	5.57E-17
O94829	Importin-13	IPO13	100	5.57E-17
Q92879	CUGBP Elav-like family member 1	CELF1	6.362	0.147078
Q96DH6	RNA-binding protein Musashi homolog 2	MSI2	100	5.57E-17
Q13151	Heterogeneous nuclear ribonucleoprotein A0	HNRNPA0	7.903	0.071521
Q7L7X3	Serine/threonine-protein kinase TAO1	TAOK1	100	5.57E-17
Q00535	Cyclin-dependent-like kinase 5	CDK5	100	5.57E-17
O95059	Ribonuclease P protein subunit p14	RPP14	100	5.57E-17
Q2NL82	Pre-rRNA-processing protein TSR1 homolog	TSR1	100	5.57E-17
Q96FL9	Polypeptide N-acetylgalactosaminyltransferase 14	GALNT14	100	5.57E-17
Q14674	Separin	ESPL1	100	5.57E-17
Q13795	ADP-ribosylation factor-related protein 1	ARFRP1	100	5.57E-17
Q96P11	28S rRNA (cytosine-C(5))-methyltransferase	NSUN5	100	5.57E-17
P61513	60S ribosomal protein L37a	RPL37A	100	5.57E-17
Q15363	Transmembrane emp24 domain-containing protein 2	TMED2	100	5.57E-17
O75179	Ankyrin repeat domain-containing protein 17	ANKRD17	100	5.57E-17
Q8IUC4	Rhophilin-2	RHPN2	100	5.57E-17
Q15050	Ribosome biogenesis regulatory protein homolog	RRS1	100	5.57E-17
Q9UHI6	Probable ATP-dependent RNA helicase DDX20	DDX20	100	5.57E-17
O95470	Sphingosine-1-phosphate lyase 1	SGPL1	100	5.57E-17
Q02878	60S ribosomal protein L6	RPL6	8.579	0.139143
Q9HBM6	Transcription initiation factor TFIID subunit 9B	TAF9B	100	5.57E-17
Q9Y4C2	TRPM8 channel-associated factor 1	TCAF1	100	5.57E-17
Q9Y244	Proteasome maturation protein	POMP	100	5.57E-17
P42766	60S ribosomal protein L35	RPL35	8.044	0.146613
Q96K76	Ubiquitin carboxyl-terminal hydrolase 47	USP47	100	5.57E-17
Q9Y448	Small kinetochore-associated protein	KNSTRN	100	5.57E-17
Q9H0V9	VIP36-like protein	LMAN2L	7.583	0.086552
Q8IW35	Centrosomal protein of 97 kDa	CEP97	100	5.57E-17
Q7L0Y3	tRNA methyltransferase 10 homolog C	TRMT10C	100	5.57E-17
Q9H981	Actin-related protein 8	ACTR8	100	5.57E-17
O00233	26S proteasome non-ATPase regulatory subunit 9	PSMD9	100	5.57E-17
P50336	Protoporphyrinogen oxidase	PPOX	100	5.57E-17

P06493	Cyclin-dependent kinase 1	CDK1	11.697	0.052649
Q8TAL6	Fin bud initiation factor homolog	FIBIN	100	5.57E-17
Q9Y3U8	60S ribosomal protein L36	RPL36	6.347	0.116996
P52292	Importin subunit alpha-1	KPNA2	8.848	0.128093
P20337	Ras-related protein Rab-3B	RAB3B	100	5.57E-17
O00422	Histone deacetylase complex subunit SAP18	SAP18	100	5.57E-17
O60499	Syntaxin-10	STX10	100	5.57E-17
118752	Full=Agnoprotein; AltName: Full=Agno		100	5.57E-17
Q86UY6	N-alpha-acetyltransferase 40	NAA40	100	5.57E-17
O75175	CCR4-NOT transcription complex subunit 3	CNOT3	100	5.57E-17
P11309	Serine/threonine-protein kinase pim-1	PIM1	100	5.57E-17
Q8N8N7	Prostaglandin reductase 2	PTGR2	100	5.57E-17
Q92547	DNA topoisomerase 2-binding protein 1	TOPBP1	100	5.57E-17
Q14690	Protein RRP5 homolog	PDCD11	100	5.57E-17
Q9Y6E0	Serine/threonine-protein kinase 24	STK24	100	5.57E-17
Q5T5X7	BEN domain-containing protein 3	BEND3	100	5.57E-17
Q8TDB6	E3 ubiquitin-protein ligase DTX3L	DTX3L	100	5.57E-17
Q9UGN5	Poly [ADP-ribose] polymerase 2	PARP2	100	5.57E-17
Q13416	Origin recognition complex subunit 2	ORC2	100	5.57E-17
P36578	60S ribosomal protein L4	RPL4	13.534	0.03164
Q5BKZ1	DBIRD complex subunit ZNF326	ZNF326	100	5.57E-17
O94921	Cyclin-dependent kinase 14	CDK14	100	5.57E-17
Q8WU76	Sec1 family domain-containing protein 2	SCFD2	100	5.57E-17
Q99418	Cytohesin-2	CYTH2	100	5.57E-17
P49755	Transmembrane emp24 domain-containing protein 10	TMED10	8.658	0.08411
P53582	Methionine aminopeptidase 1	METAP1	5.803	0.159767
Q9Y266	Nuclear migration protein nudC	NUDC	20.043	0.006385
P29279	CCN family member 2	CCN2	100	5.57E-17
P20339	Ras-related protein Rab-5A	RAB5A	100	5.57E-17
P57764	Gasdermin-D	GSDMD	100	5.57E-17
P05423	DNA-directed RNA polymerase III subunit RPC4	POLR3D	100	5.57E-17
587572757	viral protein-1, partial	VP-1	100	5.57E-17
Q969M3	Protein YIPF5	YIPF5	100	5.57E-17
Q9NUQ6	SPATS2-like protein	SPATS2L	100	5.57E-17
O43414	ERI1 exoribonuclease 3	ERI3	100	5.57E-17
P62753	40S ribosomal protein S6	RPS6	8.216	0.14855
Q7RTP6	[F-actin]-monooxygenase MICAL3	MICAL3	100	5.57E-17
Q9UKU9	Angiopoietin-related protein 2	ANGPTL2	100	5.57E-17
Q96EP5	DAZ-associated protein 1	DAZAP1	100	5.57E-17
554504645	capsid, partial	VP1	100	5.57E-17
Q16637	Survival motor neuron protein	SMN1; SMI	100	5.57E-17
P27635	60S ribosomal protein L10	RPL10	8.262	0.146613
Q02447	Transcription factor Sp3	SP3	100	5.57E-17
Q9NXJ5	Pyroglutamyl-peptidase 1	PGPEP1	100	5.57E-17
Q03181	Peroxisome proliferator-activated receptor delta	PPARD	100	5.57E-17
Q9H2G4	Testis-specific Y-encoded-like protein 2	TSPYL2	100	5.57E-17
Q96MG7	Non-structural maintenance of chromosomes element 3 homolog	NSMCE3	100	5.57E-17
P51812	Ribosomal protein S6 kinase alpha-3	RPS6KA3	100	5.57E-17
Q8N6T3	ADP-ribosylation factor GTPase-activating protein 1	ARFGAP1	100	5.57E-17
Q9Y3S1	Serine/threonine-protein kinase WNK2	WNK2	100	5.57E-17

P51571	Translocon-associated protein subunit delta	SSR4	100	5.57E-17
P0DI82	Trafficking protein particle complex subunit 2B	TRAPPC2B	100	5.57E-17
Q9UP83	Conserved oligomeric Golgi complex subunit 5	COG5	100	5.57E-17
Q9BVQ7	Spermatogenesis-associated protein 5-like protein 1	SPATA5L1	100	5.57E-17
O43493	Trans-Golgi network integral membrane protein 2	TGOLN2	100	5.57E-17
P16591	Tyrosine-protein kinase Fer	FER	100	5.57E-17
Q14533	Keratin, type II cuticular Hb1	KRT81	100	5.57E-17
Q86VR2	Reticulophagy regulator 3	RETREG3	100	5.57E-17
O75953	DnaJ homolog subfamily B member 5	DNAJB5	100	5.57E-17
Q96RN5	Mediator of RNA polymerase II transcription subunit 15	MED15	100	5.57E-17
Q8WTT2	Nucleolar complex protein 3 homolog	NOC3L	100	5.57E-17
Q9C0C4	Semaphorin-4C	SEMA4C	100	5.57E-17
O95905	Protein ecdysoneless homolog	ECD	9.791	0.037454
Q9BV68	E3 ubiquitin-protein ligase RNF126	RNF126	100	5.57E-17
O14656	Torsin-1A	TOR1A	13.859	0.004973
P21980	Protein-glutamine gamma-glutamyltransferase 2	TGM2	10.276	0.08107
E9PAV3	Nascent polypeptide-associated complex subunit alpha	NACA	100	5.57E-17
P56182	Ribosomal RNA processing protein 1 homolog A	RRP1	100	5.57E-17
Q9UKX7	Nuclear pore complex protein Nup50	NUP50	100	5.57E-17
P84098	60S ribosomal protein L19	RPL19	100	5.57E-17
P52926	High mobility group protein HMGI-C	HMGA2	100	5.57E-17
P0DJI8	Serum amyloid A-1 protein	SAA1	100	5.57E-17
P57678	Gem-associated protein 4	GEMIN4	12.893	0.037826
O00592	Podocalyxin	PODXL	100	5.57E-17
Q9GZM5	Protein YIPF3	YIPF3	100	5.57E-17
Q5MIZ7	Serine/threonine-protein phosphatase 4 regulatory subunit 3B	PPP4R3B	100	5.57E-17
Q96I51	RCC1-like G exchanging factor-like protein	RCC1L	100	5.57E-17
Q9NXN4	Ganglioside-induced differentiation-associated protein 2	GDAP2	100	5.57E-17
Q5TAX3	Terminal uridylyltransferase 4	TUT4	100	5.57E-17
Q14257	Reticulocalbin-2	RCN2	100	5.57E-17
Q96DM3	Regulator of MON1-CCZ1 complex	RMC1	100	5.57E-17
Q9BZV1	UBX domain-containing protein 6	UBXN6	100	5.57E-17
P40429	60S ribosomal protein L13a	RPL13A	9.358	0.108019
Q9UP95	Solute carrier family 12 member 4	SLC12A4	100	5.57E-17
Q86X51	EZH inhibitory protein	EZHIP	23.376	0.000244
Q9UIG0	Tyrosine-protein kinase BAZ1B	BAZ1B	100	5.57E-17
P21796	Voltage-dependent anion-selective channel protein 1	VDAC1	100	5.57E-17
P31943	Heterogeneous nuclear ribonucleoprotein H	HNRNPH1	100	5.57E-17
Q96SB8	Structural maintenance of chromosomes protein 6	SMC6	100	5.57E-17
Q8IY81	pre-rRNA 2'-O-ribose RNA methyltransferase FTSJ3	FTSJ3	100	5.57E-17
Q00534	Cyclin-dependent kinase 6	CDK6	100	5.57E-17
O60732	Melanoma-associated antigen C1	MAGEC1	9.641	0.090331
Q13671	Ras and Rab interactor 1	RIN1	6.834	0.116324
Q6P996	Pyridoxal-dependent decarboxylase domain-containing protein 1	PDXDC1	100	5.57E-17
Q71U36	Tubulin alpha-1A chain	TUBA1A	7.08	0.129969
Q86XI2	Condensin-2 complex subunit G2	NCAPG2	100	5.57E-17
Q96JI7	Spatacsin	SPG11	100	5.57E-17
Q8NBN3	Transmembrane protein 87A	TMEM87A	100	5.57E-17
P24390	ER lumen protein-retaining receptor 1	KDELR1	100	5.57E-17
P17096	High mobility group protein HMG-I/HMG-Y	HMGA1	24.919	0.002363

Q07020	60S ribosomal protein L18	RPL18	8.204	0.149082
O43670	BUB3-interacting and GLEBS motif-containing protein ZNF207	ZNF207	100	5.57E-17
O75427	Leucine-rich repeat and calponin homology domain-containing protein 4	LRCH4	100	5.57E-17
Q14657	EKC/KEOPS complex subunit LAGE3	LAGE3	100	5.57E-17
Q8IWS0	PHD finger protein 6	PHF6	100	5.57E-17
O15111	Inhibitor of nuclear factor kappa-B kinase subunit alpha	CHUK	100	5.57E-17
P26885	Peptidyl-prolyl cis-trans isomerase FKBP2	FKBP2	100	5.57E-17
Q13546	Receptor-interacting serine/threonine-protein kinase 1	RIPK1	100	5.57E-17
Q32MZ4	Leucine-rich repeat flightless-interacting protein 1	LRRFIP1	100	5.57E-17
Q3MHD2	Protein LSM12 homolog	LSM12	100	5.57E-17
Q96RU2	Ubiquitin carboxyl-terminal hydrolase 28	USP28	100	5.57E-17
P18440	Arylamine N-acetyltransferase 1	NAT1	100	5.57E-17
Q9GZT4	Serine racemase	SRR	100	5.57E-17
Q14168	MAGUK p55 subfamily member 2	MPP2	100	5.57E-17
P62081	40S ribosomal protein S7	RPS7	8.905	0.125816
Q8TC12	Retinol dehydrogenase 11	RDH11	100	5.57E-17
P67936	Tropomyosin alpha-4 chain	TPM4	100	5.57E-17
Q9P000	COMM domain-containing protein 9	COMMD9	100	5.57E-17
Q9NY27	Serine/threonine-protein phosphatase 4 regulatory subunit 2	PPP4R2	100	5.57E-17
Q5SY16	Polynucleotide 5'-hydroxyl-kinase NOL9	NOL9	7.228	0.144733
Q9BQE5	Apolipoprotein L2	APOL2	100	5.57E-17
P35637	RNA-binding protein FUS	FUS	6.035	0.134925
Q96RS0	Trimethylguanosine synthase	TGS1	100	5.57E-17
Q9H8Y8	Golgi reassembly-stacking protein 2	GORASP2	100	5.57E-17
O14880	Microsomal glutathione S-transferase 3	MGST3	100	5.57E-17
Q7L2J0	7SK snRNA methylphosphate capping enzyme	MEPCE	100	5.57E-17
Q9BVK6	Transmembrane emp24 domain-containing protein 9	TMED9	100	5.57E-17
Q12846	Syntaxin-4	STX4	6.872	0.134271
O43663	Protein regulator of cytokinesis 1	PRC1	100	5.57E-17
P00519	Tyrosine-protein kinase ABL1	ABL1	100	5.57E-17
Q9Y3Q3	Transmembrane emp24 domain-containing protein 3	TMED3	100	5.57E-17
Q5PRF9	Protein Smaug homolog 2	SAMD4B	100	5.57E-17
Q9NV88	Integrator complex subunit 9	INTS9	100	5.57E-17
Q96CS3	FAS-associated factor 2	FAF2	100	5.57E-17
Q03426	Mevalonate kinase	MVK	100	5.57E-17
Q6UWP2	Dehydrogenase/reductase SDR family member 11	DHRS11	100	5.57E-17
Q13724	Mannosyl-oligosaccharide glucosidase	MOGS	100	5.57E-17
Q96LD4	E3 ubiquitin-protein ligase TRIM47	TRIM47	100	5.57E-17
Q12933	TNF receptor-associated factor 2	TRAF2	100	5.57E-17
Q9BV38	WD repeat-containing protein 18	WDR18	6.089	0.135869
Q68CQ4	Digestive organ expansion factor homolog	DIEXF	100	5.57E-17
P50452	Serpin B8	SERPINB8	100	5.57E-17
Q9Y6A5	Transforming acidic coiled-coil-containing protein 3	TACC3	100	5.57E-17
929234814			100	5.57E-17
P19784	Casein kinase II subunit alpha'	CSNK2A2	100	5.57E-17
P18621	60S ribosomal protein L17	RPL17	8.602	0.138109
O75326	Semaphorin-7A	SEMA7A	100	5.57E-17
A5PLN9	Trafficking protein particle complex subunit 13	TRAPPC13	100	5.57E-17
Q9NRY4	Rho GTPase-activating protein 35	ARHGAP35	100	5.57E-17
O95218	Zinc finger Ran-binding domain-containing protein 2	ZRANB2	100	5.57E-17

P62910	60S ribosomal protein L32	RPL32	8.995	0.121882
Q9NS00	Glycoprotein-N-acetylgalactosamine 3-beta-galactosyltransferase 1	C1GALT1	100	5.57E-17
Q13162	Peroxiredoxin-4	PRDX4	5.966	0.186587
Q9H079	KATNB1-like protein 1	KATNBL1	100	5.57E-17
P12956	X-ray repair cross-complementing protein 6	XRCC6	12.402	0.043048
Q9UBW7	Zinc finger MYM-type protein 2	ZMYM2	7.906	0.077089
Q86VS8	Protein Hook homolog 3	HOOK3	100	5.57E-17
Q8NI22	Multiple coagulation factor deficiency protein 2	MCFD2	100	5.57E-17
P35625	Metalloproteinase inhibitor 3	TIMP3	100	5.57E-17
O94923	D-glucuronyl C5-epimerase	GLCE	100	5.57E-17
O15240	Neurosecretory protein VGF	VGF	6.053	0.16602
Q8NBJ7	Inactive C-alpha-formylglycine-generating enzyme 2	SUMF2	100	5.57E-17
Q86U90	YrdC domain-containing protein, mitochondrial	YRDC	100	5.57E-17
P04843	Dolichyl-diphosphooligosaccharide--protein glycosyltransferase subunit 1	RPN1	13.793	0.006071
Q9H0V1	Transmembrane protein 168	TMEM168	100	5.57E-17
Q96QR8	Transcriptional activator protein Pur-beta	PURB	5.907	0.183489
P53384	Cytosolic Fe-S cluster assembly factor NUBP1	NUBP1	100	5.57E-17
Q8IXU6	Solute carrier family 35 member F2	SLC35F2	100	5.57E-17
P14635	G2/mitotic-specific cyclin-B1	CCNB1	100	5.57E-17
O00329	Phosphatidylinositol 4,5-bisphosphate 3-kinase catalytic subunit delta isoform	PIK3CD	100	5.57E-17
Q9H7B2	Ribosome production factor 2 homolog	RPF2	6.172	0.172716
P10412	Histone H1.4	H1-4	100	5.57E-17
Q15041	ADP-ribosylation factor-like protein 6-interacting protein 1	ARL6IP1	100	5.57E-17
P16403	Histone H1.2	H1-2	100	5.57E-17
Q9Y6D6	Brefeldin A-inhibited guanine nucleotide-exchange protein 1	ARFGEF1	100	5.57E-17
Q15051	IQ calmodulin-binding motif-containing protein 1	IQCB1	100	5.57E-17
Q6IBW4	Condensin-2 complex subunit H2	NCAPH2	100	5.57E-17
Q9P2D0	Inhibitor of Bruton tyrosine kinase	IBTK	100	5.57E-17
Q9NX24	H/ACA ribonucleoprotein complex subunit 2	NHP2	100	5.57E-17
O95232	Luc7-like protein 3	LUC7L3	100	5.57E-17
Q9C0C2	182 kDa tankyrase-1-binding protein	TNKS1BP1	100	5.57E-17
Q9BQ39	ATP-dependent RNA helicase DDX50	DDX50	100	5.57E-17
Q14181	DNA polymerase alpha subunit B	POLA2	17.574	0.001706
P83731	60S ribosomal protein L24	RPL24	7.722	0.175121
P10515	Dihydrolipoyllysine-residue acetyltransferase component of pyruvate dehydrogenase complex	DLAT	100	5.57E-17
Q9Y478	5'-AMP-activated protein kinase subunit beta-1	PRKAB1	100	5.57E-17
Q9UKZ1	CCR4-NOT transcription complex subunit 11	CNOT11	100	5.57E-17
Q9GZS1	DNA-directed RNA polymerase I subunit RPA49	POLR1E	100	5.57E-17
P17252	Protein kinase C alpha type	PRKCA	100	5.57E-17
Q8N3C0	Activating signal cointegrator 1 complex subunit 3	ASCC3	5.964	0.186535
O43709	Probable 18S rRNA (guanine-N(7))-methyltransferase	BUD23	100	5.57E-17
Q9UJY1	Heat shock protein beta-8	HSPB8	100	5.57E-17
197941286	VP1, partial		100	5.57E-17
P52701	DNA mismatch repair protein Msh6	MSH6	8.046	0.157284
P48729	Casein kinase I isoform alpha	CSNK1A1	5.569	0.159582
P78395	Melanoma antigen preferentially expressed in tumors	PRAME	100	5.57E-17
Q9NSP4	Centromere protein M	CENPM	100	5.57E-17
P53667	LIM domain kinase 1	LIMK1	100	5.57E-17
Q96RQ1	Endoplasmic reticulum-Golgi intermediate compartment protein 2	ERGIC2	100	5.57E-17
P51553	Isocitrate dehydrogenase [NAD] subunit gamma, mitochondrial	IDH3G	100	5.57E-17

Q9H8V3	Protein ECT2	ECT2	100	5.57E-17
Q9H6W3	Ribosomal oxygenase 1	RIOX1	100	5.57E-17
Q9P291	Armadillo repeat-containing X-linked protein 1	ARMCX1	100	5.57E-17
P23458	Tyrosine-protein kinase JAK1	JAK1	100	5.57E-17
Q9BQ13	BTB/POZ domain-containing protein KCTD14	KCTD14	100	5.57E-17
Q08379	Golgin subfamily A member 2	GOLGA2	100	5.57E-17
Q9BTZ2	Dehydrogenase/reductase SDR family member 4	DHRS4	100	5.57E-17
Q8IWW6	Rho GTPase-activating protein 12	ARHGAP12	100	5.57E-17
Q68CQ7	Glycosyltransferase 8 domain-containing protein 1	GLT8D1	100	5.57E-17
Q9ULX3	RNA-binding protein NOB1	NOB1	100	5.57E-17
Q15773	Myeloid leukemia factor 2	MLF2	100	5.57E-17
P01034	Cystatin-C	CST3	100	5.57E-17
Q14160	Protein scribble homolog	SCRIB	5.684	0.16602
Q9BV86	N-terminal Xaa-Pro-Lys N-methyltransferase 1	NTMT1	7.511	0.074566
Q02224	Centromere-associated protein E	CENPE	100	5.57E-17
Q8IZA0	Dyslexia-associated protein KIAA0319-like protein	KIAA0319L	5.488	0.17048
Q96IV0	Peptide-N(4)-(N-acetyl-beta-glucosaminyl)asparagine amidase	NGLY1	100	5.57E-17
Q9BYD1	39S ribosomal protein L13, mitochondrial	MRPL13	100	5.57E-17
P46020	Phosphorylase b kinase regulatory subunit alpha, skeletal muscle isoform	PHKA1	100	5.57E-17
O75494	Serine/arginine-rich splicing factor 10	SRSF10	8.052	0.097467
Q8IYD1	Eukaryotic peptide chain release factor GTP-binding subunit ERF3B	GSPT2	100	5.57E-17
O00461	Golgi integral membrane protein 4	GOLIM4	100	5.57E-17
Q9H0R1	AP-5 complex subunit mu-1	AP5M1	100	5.57E-17
Q8WVB6	Chromosome transmission fidelity protein 18 homolog	CHTF18	100	5.57E-17
Q9Y314	Nitric oxide synthase-interacting protein	NOSIP	100	5.57E-17
Q9H845	Complex I assembly factor ACAD9, mitochondrial	ACAD9	6.395	0.150797
P61313	60S ribosomal protein L15	RPL15	12.43	0.042784
O75448	Mediator of RNA polymerase II transcription subunit 24	MED24	100	5.57E-17
O94889	Kelch-like protein 18	KLHL18	15.071	0.006281
Q9HBF4	Zinc finger FYVE domain-containing protein 1	ZFYVE1	100	5.57E-17
P18124	60S ribosomal protein L7	RPL7	16.743	0.013874
Q96FZ2	Abasic site processing protein HMCES	HMCES	100	5.57E-17
P84022	Mothers against decapentaplegic homolog 3	SMAD3	5.764	0.172774
Q9Y4C8	Probable RNA-binding protein 19	RBM19	100	5.57E-17
Q9BRG1	Vacuolar protein-sorting-associated protein 25	VPS25	5.641	0.156195
O14646	Chromodomain-helicase-DNA-binding protein 1	CHD1	100	5.57E-17
Q7Z4V5	Hepatoma-derived growth factor-related protein 2	HDGFL2	100	5.57E-17
Q01081	Splicing factor U2AF 35 kDa subunit U2AF1	U2AF1	6.132	0.183677
Q9H6X2	Anthrax toxin receptor 1	ANTXR1	7.523	0.070984
P32780	General transcription factor IIH subunit 1	GTF2H1	100	5.57E-17
Q8NC54	Keratinocyte-associated transmembrane protein 2	KCT2	100	5.57E-17
Q9UPN7	Serine/threonine-protein phosphatase 6 regulatory subunit 1	PPP6R1	100	5.57E-17
P62750	60S ribosomal protein L23a	RPL23A	100	5.57E-17
P00387	NADH-cytochrome b5 reductase 3	CYB5R3	9.772	0.09438
Q16850	Lanosterol 14-alpha demethylase	CYP51A1	100	5.57E-17
O60711	Leupaxin	LPXN	100	5.57E-17
Q96KR1	Zinc finger RNA-binding protein	ZFR	100	5.57E-17
P10398	Serine/threonine-protein kinase A-Raf	ARAF	5.531	0.17431
P52294	Importin subunit alpha-5	KPNA1	100	5.57E-17
Q8N1G4	Leucine-rich repeat-containing protein 47	LRRC47	100	5.57E-17

Q8IXB1	DnaJ homolog subfamily C member 10	DNAJC10	100	5.57E-17
112419644	small T		100	5.57E-17
Q13107	Ubiquitin carboxyl-terminal hydrolase 4	USP4	100	5.57E-17
O95864	Acyl-CoA 6-desaturase	FADS2	100	5.57E-17
Q6IQ32	Activity-dependent neuroprotector homeobox protein 2	ADNP2	100	5.57E-17
Q01831	DNA repair protein complementing XP-C cells	XPC	100	5.57E-17
Q2VPB7	AP-5 complex subunit beta-1	AP5B1	100	5.57E-17
P42695	Condensin-2 complex subunit D3	NCAPD3	100	5.57E-17
Q9HCM4	Band 4.1-like protein 5	EPB41L5	100	5.57E-17
752784399	large T-antigen		8.303	0.144733
Q96C19	EF-hand domain-containing protein D2	EFHD2	100	5.57E-17
Q9Y3B3	Transmembrane emp24 domain-containing protein 7	TMED7	14.088	0.004198
Q9UBB6	Neurochondrin	NCDN	100	5.57E-17
Q9UKM9	RNA-binding protein Raly	RALY	7.559	0.184732
Q8N5K1	CDGSH iron-sulfur domain-containing protein 2	CISD2	100	5.57E-17
P37268	Squalene synthase	FDFT1	100	5.57E-17
Q8WWK9	Cytoskeleton-associated protein 2	CKAP2	100	5.57E-17
Q15208	Serine/threonine-protein kinase 38	STK38	100	5.57E-17
Q06787	Synaptic functional regulator FMR1	FMR1	100	5.57E-17
Q8NEC7	Glutathione S-transferase C-terminal domain-containing protein	GSTCD	100	5.57E-17
Q6ZRS2	Helicase SRCAP	SRCAP	100	5.57E-17
Q9BVL4	Protein adenylyltransferase SelO, mitochondrial	SELENOO	100	5.57E-17
O60870	DNA/RNA-binding protein KIN17	KIN	100	5.57E-17
P04424	Argininosuccinate lyase	ASL	100	5.57E-17
O15258	Protein RER1	RER1	100	5.57E-17
Q9H0U9	Testis-specific Y-encoded-like protein 1	TSPYL1	100	5.57E-17
P02786	Transferrin receptor protein 1	TFRC	9.263	0.111492
Q6ZN44	Netrin receptor UNC5A	UNC5A	100	5.57E-17
Q86TB9	Protein PAT1 homolog 1	PATL1	100	5.57E-17
Q9UIU6	Homeobox protein SIX4	SIX4	100	5.57E-17
Q16348	Solute carrier family 15 member 2	SLC15A2	100	5.57E-17
Q13177	Serine/threonine-protein kinase PAK 2	PAK2	100	5.57E-17
Q7L311	Armadillo repeat-containing X-linked protein 2	ARMCX2	100	5.57E-17
Q9H6V9	Lipid droplet-associated hydrolase	LDAH	100	5.57E-17
P53814	Smoothelin	SMTN	100	5.57E-17
O94761	ATP-dependent DNA helicase Q4	RECQL4	100	5.57E-17
P54727	UV excision repair protein RAD23 homolog B	RAD23B	100	5.57E-17
Q86U38	Nucleolar protein 9	NOP9	100	5.57E-17
O15091	Mitochondrial ribonuclease P catalytic subunit	PRORP	100	5.57E-17
52839614	VP1, partial		100	5.57E-17
Q6ZRV2	Protein FAM83H	FAM83H	100	5.57E-17
Q8NCE2	Myotubularin-related protein 14	MTMR14	100	5.57E-17
P15927	Replication protein A 32 kDa subunit RPA2	RPA2	6.852	0.169347
Q9NVH2	Integrator complex subunit 7	INTS7	100	5.57E-17
P52655	Transcription initiation factor IIA subunit 1	GTF2A1	100	5.57E-17
Q8WVM0	Dimethyladenosine transferase 1, mitochondrial	TFB1M	100	5.57E-17
Q15056	Eukaryotic translation initiation factor 4H	EIF4H	100	5.57E-17
Q8NBT2	Kinetochore protein Spc24	SPC24	100	5.57E-17
O43759	Synaptogyrin-1	SYNGR1	100	5.57E-17
Q13277	Syntaxin-3	STX3	100	5.57E-17

Q13428	Treacle protein	TCOF1	100	5.57E-17
Q9BY42	Replication termination factor 2	RTF2	100	5.57E-17
115343476	VP2		14.247	0.026055
Q9NZN8	CCR4-NOT transcription complex subunit 2	CNOT2	100	5.57E-17
Q9Y2L5	Trafficking protein particle complex subunit 8	TRAPPC8	7.897	0.085014
Q12851	Mitogen-activated protein kinase kinase kinase kinase 2	MAP4K2	100	5.57E-17
Q9BZF1	Oxysterol-binding protein-related protein 8	OSBPL8	100	5.57E-17
P23443	Ribosomal protein S6 kinase beta-1	RPS6KB1	100	5.57E-17
Q02818	Nucleobindin-1	NUCB1	100	5.57E-17
P04156	Major prion protein	PRNP	100	5.57E-17
Q6Y7W6	GRB10-interacting GYF protein 2	GIGYF2	100	5.57E-17

Table S2. List of all detected deprived in U-2OS15E EVs.

Accession	Description	Gene Symbol	Abundance Ra	Adj. p-value
Q92567	Protein FAM168A	FAM168A	0.01	5.57427E-17
Q9HAV0	Guanine nucleotide-binding protein subunit beta-4	GNB4	0.01	5.57427E-17
P13671	Complement component C6	C6	0.01	5.57427E-17
Q9H7D0	Dedicator of cytokinesis protein 5	DOCK5	0.01	5.57427E-17
Q5W111	SPRY domain-containing protein 7	SPRYD7	0.01	5.57427E-17
P0DUB6	Alpha-amylase 1A	AMY1A	0.01	5.57427E-17
Q9H972	Uncharacterized protein C14orf93	C14orf93	0.01	5.57427E-17
Q9UDY2	Tight junction protein ZO-2	TJP2	0.01	5.57427E-17
Q9C000	NACHT, LRR and PYD domains-containing protein 1	NLRP1	0.01	5.57427E-17
Q96T58	Msx2-interacting protein	SPEN	0.01	5.57427E-17
Q9H8M9	Protein eva-1 homolog A	EVA1A	0.01	5.57427E-17
Q9Y4C0	Neurexin-3	NRXN3	0.01	5.57427E-17
O95715	C-X-C motif chemokine 14	CXCL14	0.01	5.57427E-17
P02461	Collagen alpha-1(III) chain	COL3A1	0.01	5.57427E-17
Q8IUK5	Plexin domain-containing protein 1	PLXDC1	0.01	5.57427E-17
Q13201	Multimerin-1	MMRN1	0.01	5.57427E-17
Q9NT68	Teneurin-2	TENM2	0.01	5.57427E-17
P06744	Glucose-6-phosphate isomerase	GPI	0.01	5.57427E-17
P51452	Dual specificity protein phosphatase 3	DUSP3	0.01	5.57427E-17
A1L4H1	Soluble scavenger receptor cysteine-rich domain-containing protein SSC5D	SSC5D	0.01	5.57427E-17
Q9NS15	Latent-transforming growth factor beta-binding protein 3	LTBP3	0.01	5.57427E-17
Q9BQ16	Testican-3	SPOCK3	0.01	5.57427E-17
Q96BP3	Peptidylprolyl isomerase domain and WD repeat-containing protein 1	PPWD1	0.01	5.57427E-17
Q9UKS6	Protein kinase C and casein kinase substrate in neurons protein 3	PACSIN3	0.01	5.57427E-17
Q6UX71	Plexin domain-containing protein 2	PLXDC2	0.01	5.57427E-17
Q969X1	Protein lifeguard 3	TMBIM1	0.01	5.57427E-17
Q63HQ2	Pikachurin	EGFLAM	0.01	5.57427E-17
P07358	Complement component C8 beta chain	C8B	0.01	5.57427E-17
Q13188	Serine/threonine-protein kinase 3 STK3	STK3	0.01	5.57427E-17
P80404	4-aminobutyrate aminotransferase, mitochondrial	ABAT	0.01	5.57427E-17
Q8WWI5	Choline transporter-like protein 1	SLC44A1	0.01	5.57427E-17
P01040	Cystatin-A	CSTA	0.01	5.57427E-17
P04275	von Willebrand factor	VWF	0.01	5.57427E-17
Q5VW32	BRO1 domain-containing protein BROX	BROX	0.01	5.57427E-17
Q00796	Sorbitol dehydrogenase	SORD	0.01	5.57427E-17
Q8NDC0	MAPK-interacting and spindle-stabilizing protein-like	MAPK1IP1L	0.01	5.57427E-17
Q96MM7	Heparan-sulfate 6-O-sulfotransferase 2	HS6ST2	0.01	5.57427E-17
O95196	Chondroitin sulfate proteoglycan 5	CSPG5	0.01	5.57427E-17
P23471	Receptor-type tyrosine-protein phosphatase zeta	PTPRZ1	0.01	5.57427E-17
Q9P2S2	Neurexin-2	NRXN2	0.01	5.57427E-17
Q9NRX4	14 kDa phosphohistidine phosphatase	PHPT1	0.01	5.57427E-17
O15554	Intermediate conductance calcium-activated potassium channel protein 4	KCNN4	0.01	5.57427E-17
Q9H4A4	Aminopeptidase B	RNPEP	0.01	5.57427E-17
Q96FV2	Secernin-2	SCRN2	0.01	5.57427E-17
P22694	cAMP-dependent protein kinase catalytic subunit beta	PRKACB	0.01	5.57427E-17
Q07092	Collagen alpha-1(XVI) chain COL16A1	COL16A1	0.01	5.57427E-17
P06727	Apolipoprotein A-IV	APOA4	0.01	5.57427E-17
Q9BTV5	Fibronectin type III and SPRY domain-containing protein 1	FSD1	0.01	5.57427E-17
P83110	Serine protease HTRA3 HTRA3	HTRA3	0.01	5.57427E-17

P05455	Lupus La protein SSB	SSB	0.01	5.57427E-17
Q9H7P6	Multivesicular body subunit 12B	MVB12B	0.01	5.57427E-17
Q86Y38	Xylosyltransferase 1	XYLT1	0.01	5.57427E-17
Q6PCB5	Lysine-specific demethylase RSBN1L	RSBN1L	0.01	5.57427E-17
Q16787	Laminin subunit alpha-3	LAMA3	0.01	5.57427E-17
P60983	Glia maturation factor beta	GMFB	0.01	5.57427E-17
P02748	Complement component C9	C9	0.084	1.3078E-05
P34741	Syndecan-2	SDC2	0.076	1.3942E-05
O43854	EGF-like repeat and discoidin I-like domain-containing protein 3	EDIL3	0.05	3.62962E-05
P01591	Immunoglobulin J chain	JCHAIN	0.086	8.36146E-05
Q9HCE0	Ectopic P granules protein 5 homolog	EPG5	0.058	9.44348E-05
Q3V6T2	Girdin	CCDC88A	0.071	0.000284263
A5D8V6	Vacuolar protein sorting-associated protein 37C VPS37C	VPS37C	0.077	0.000426182
Q9NRX1	RNA-binding protein PNO1	PNO1	0.137	0.000734713
Q08380	Galectin-3-binding protein	LGALS3BP	0.088	0.000887162
Q96M89	Coiled-coil domain-containing protein 138	CCDC138	0.159	0.000953549
P35052	Glypican-1	GPC1	0.092	0.001121408
Q8TBG4	Ethanolamine-phosphate phospho-lyase	ETNPPL	0.124	0.001252771
Q13361	Microfibrillar-associated protein 5	MFAP5	0.133	0.001445265
O94766	Galactosylgalactosylxylosylprotein 3-beta-glucuronosyltransferase 3	B3GAT3	0.134	0.001581765
Q08431	Lactadherin	MFGE8	0.107	0.002286175
P19827	Inter-alpha-trypsin inhibitor heavy chain H1	ITIH1	0.108	0.002443918
O00629	Importin subunit alpha-3	KPNA4	0.179	0.002485969
P00441	Superoxide dismutase [Cu-Zn]	SOD1	0.177	0.003191099
Q96KG7	Multiple epidermal growth factor-like domains protein 10	MEGF10	0.184	0.003745577
Q01469	Fatty acid-binding protein 5 FABP5	FABP5	0.2	0.004607682
Q8NBF6	Late secretory pathway protein AVL9 homolog	AVL9	0.127	0.005136572
B9A064	Immunoglobulin lambda-like polypeptide 5	IGLL5	0.185	0.005466488
P10915	Hyaluronan and proteoglycan link protein 1	HAPLN1	0.13	0.005759431
O95965	Integrin beta-like protein 1	ITGBL1	0.167	0.006167816
Q92783	Signal transducing adapter molecule 1 STAM	STAM	0.205	0.00638456
O95630	STAM-binding protein	STAMBP	0.183	0.007466142
P00439	Phenylalanine-4-hydroxylase	PAH	0.2	0.007928364
Q9Y5Y7	Lymphatic vessel endothelial hyaluronic acid receptor 1	LYVE1	0.198	0.012714385
Q9UL42	Paraneoplastic antigen Ma2	PNMA2	0.236	0.01416803
Q96DD7	Protein shisa-4 SHISA4	SHISA4	0.232	0.014171174
P20742	Pregnancy zone protein	PZP	0.161	0.01422887
Q9Y6K1	DNA (cytosine-5)-methyltransferase 3A	DNMT3A	0.223	0.014733384
Q14624	Inter-alpha-trypsin inhibitor heavy chain H4	ITIH4	0.252	0.014911689
P61964	WD repeat-containing protein 5	WDR5	0.24	0.0154672
P19022	Cadherin-2	CDH2	0.213	0.016395571
Q9NRY6	Phospholipid scramblase 3	PLSCR3	0.219	0.016593789
Q9H313	Protein tweety homolog 1	TTYH1	0.252	0.01912309
Q15036	Sorting nexin-17	SNX17	0.178	0.021178079
Q7RTS7	Keratin, type II cytoskeletal 74	KRT74	0.226	0.021627794
O00560	Syntenin-1	SDCBP	0.186	0.025208457
C9J7I0	UBAP1-MVB12-associated (UMA)-domain containing protein 1	UMAD1	0.271	0.026054822
O43657	Tetraspanin-6	TSPAN6	0.282	0.031306988
Q9NZ53	Podocalyxin-like protein 2	PODXL2	0.29	0.033896222
Q63ZY3	KN motif and ankyrin repeat domain-containing protein 2	KANK2	0.292	0.033936148

O00468	Agrin	AGRN	0.204	0.035842268
P39656	Dolichyl-diphosphooligosaccharide--protein glycosyltransferase 48 kDa subunit	DDOST	0.276	0.036187228
Q6PCE3	Glucose 1,6-bisphosphate synthase	PGM2L1	0.263	0.038031247
Q9Y625	Glypican-6	GPC6	0.208	0.038257444
Q02413	Desmoglein-1	DSG1	0.287	0.038342484
Q9UN86	Ras GTPase-activating protein-binding protein 2	G3BP2	0.294	0.039486773
P07148	Fatty acid-binding protein, liver	FABP1	0.211	0.039759287
Q92954	Proteoglycan 4	PRG4	0.296	0.040148506
Q08629	Testican-1	SPOCK1	0.322	0.040790951
P20908	Collagen alpha-1(V) chain	COL5A1	0.213	0.041540991
P30566	Adenylosuccinate lyase	ADSL	0.271	0.041710761
P19883	Follistatin	FST	0.214	0.041892057
Q9GZM7	Tubulointerstitial nephritis antigen-like	TINAGL1	0.217	0.043599737
Q6ZMW3	Echinoderm microtubule-associated protein-like 6	EML6	0.294	0.043660212
Q96A37	E3 ubiquitin-protein ligase RNF166 RNF166	RNF166	0.304	0.047761077
Q06033	Inter-alpha-trypsin inhibitor heavy chain H3	ITIH3	0.223	0.047968176
A1L390	Pleckstrin homology domain-containing family G member 3	PLEKHG3	0.274	0.050764801
P13611	Versican core protein	VCAN	0.312	0.051782868
Q69YN4	Protein virilizer homolog VIRMA	VIRMA	0.303	0.052649228
Q9H4B7	Tubulin beta-1 chain	TUBB1	0.282	0.053312888
O15230	Laminin subunit alpha-5	LAMA5	0.23	0.053388621
Q03692	Collagen alpha-1(X) chain	COL10A1	0.298	0.053533771
P18827	Syndecan-1	SDC1	0.231	0.053898096
P29590	Protein PML	PML	0.311	0.054538175
O75954	Tetraspanin-9	TSPAN9	0.311	0.055181375
P02765	Alpha-2-HS-glycoprotein	AHSG	0.234	0.05645323
Q9P265	Disco-interacting protein 2 homolog B	DIP2B	0.315	0.05663651
P16112	Aggrecan core protein	ACAN	0.239	0.060544213
P02452	Collagen alpha-1(I) chain	COL1A1	0.244	0.065097473
Q9BUT1	3-hydroxybutyrate dehydrogenase type 2	BDH2	0.344	0.06639463
O14817	Tetraspanin-4	TSPAN4	0.333	0.070896006
P07477	Trypsin-1	PRSS1	0.252	0.07301708
Q9C0H2	Protein tweety homolog 3 TTYH3	TTYH3	0.255	0.075138443
O15260	Surfeit locus protein 4	SURF4	0.322	0.081662729
Q5VIR6	Vacuolar protein sorting-associated protein 53 homolog	VPS53	0.361	0.084291645
P04114	Apolipoprotein B-100	APOB	0.267	0.086964253
P05090	Apolipoprotein D	APOD	0.339	0.089009734
Q01105	Protein SET	SET	0.33	0.089174481
P15169	Carboxypeptidase N catalytic chain	CPN1	0.366	0.090134088
Q6PKG0	La-related protein 1 LARP1	LARP1	0.323	0.090331275
P21810	Biglycan	BGN	0.352	0.09236924
P02768	Albumin	ALB	0.275	0.095961339
Q8NES3	Beta-1,3-N-acetylglucosaminyltransferase lunatic fringe	LFNG	0.277	0.097466681
P21926	CD9 antigen	CD9	0.283	0.104253146
P19823	Inter-alpha-trypsin inhibitor heavy chain H2	ITIH2	0.283	0.104979409
P36871	Phosphoglucomutase-1	PGM1	0.398	0.107806301
Q14254	Flotillin-2	FLOT2	0.379	0.113821022
P02462	Collagen alpha-1(IV) chain	COL4A1	0.297	0.120981953
Q13093	Platelet-activating factor acetylhydrolase	PLA2G7	0.39	0.127757375
O75487	Glypican-4	GPC4	0.302	0.128022604

Q99436	Proteasome subunit beta type-7	PSMB7	0.391	0.129134452
P28072	Proteasome subunit beta type-6	PSMB6	0.372	0.131017693
Q07021	Complement component 1 Q subcomponent-binding protein, mitochondrial	C1QBP	0.397	0.133231784
O15162	Phospholipid scramblase 1	PLSCR1	0.398	0.134914031
P08476	Inhibin beta A chain	INHBA	0.361	0.136093846
A6NK89	Ras association domain-containing protein 10	RASSF10	0.398	0.139186042
Q9H2M9	Rab3 GTPase-activating protein non-catalytic subunit	RAB3GAP2	0.391	0.141881921
Q9NWX6	Probable tRNA(His) guanylyltransferase	THG1L	0.383	0.144153636
Q92828	Coronin-2A	CORO2A	0.408	0.144733185
P01042	Kininogen-1	KNG1	0.38	0.144733185
P58397	A disintegrin and metalloproteinase with thrombospondin motifs 12	ADAMTS12	0.322	0.144733185
Q15198	Platelet-derived growth factor receptor-like protein	PDGFRL	0.318	0.144733185
O94851	[F-actin]-monooxygenase MICAL2	MICAL2	0.399	0.146234063
P02649	Apolipoprotein E	APOE	0.391	0.147560096
Q96JB6	Lysyl oxidase homolog 4	LOXL4	0.326	0.148549677
P63151	Serine/threonine-protein phosphatase 2A 55 kDa regulatory subunit B alpha isoform	PPP2R2A	0.397	0.151111131
P28070	Proteasome subunit beta type-4	PSMB4	0.394	0.155503635
Q8WUA4	General transcription factor 3C polypeptide 2	GTF3C2	0.431	0.155793332
A9Z1Z3	Fer-1-like protein 4	FER1L4	0.424	0.156347702
P02788	Lactotransferrin	LTF	0.396	0.157343365
P36955	Pigment epithelium-derived factor SERPINF1	SERPINF1	0.335	0.160186051
Q9BYK8	Helicase with zinc finger domain 2	HELZ2	0.44	0.160748582
P35443	Thrombospondin-4	THBS4	0.431	0.164814041
P98160	Basement membrane-specific heparan sulfate proteoglycan core protein	HSPG2	0.34	0.16602047
P02749	Beta-2-glycoprotein 1	APOH	0.408	0.16629195
P53041	Serine/threonine-protein phosphatase 5	PPP5C	0.428	0.169841164
Q86SF2	N-acetylgalactosaminyltransferase 7	GALNT7	0.448	0.171338307
Q92747	Actin-related protein 2/3 complex subunit 1A	ARPC1A	0.429	0.171528146
P69905	Hemoglobin subunit alpha	HBA1; HBA2	0.351	0.180744148
P35030	Trypsin-3	PRSS3	0.434	0.182322206
Q13907	Isopentenyl-diphosphate Delta-isomerase 1 IDI1	IDI1	0.414	0.182476207
Q12834	Cell division cycle protein 20 homolog	CDC20	0.456	0.183431286
Q9H4G4	Golgi-associated plant pathogenesis-related protein 1	GLIPR2	0.455	0.189210338